NOTE TO USERS

This reproduction is the best copy available.

UMI®

"I will lift up my eyes to the hills--from whence comes my help?
My help comes from the LORD, Who made heaven and earth.
He will not allow your foot to be moved; He who keeps you will not slumber.
Behold, He who keeps Israel shall neither slumber nor sleep.
The LORD is your keeper; The LORD is your shade at your right hand.
The sun shall not strike you by day, nor the moon by night.
The LORD shall preserve you from all evil; He shall preserve your soul.
The LORD shall preserve your going out and your coming in from this time forth, and even forevermore."

Psalm 121, Old Testament, The Bible

University of Alberta

Adaptation of Intermittent Contact Modes to Inverted Atomic Force Microscopy

By

Sandra Suk Fung Chan ©

A thesis submitted to the Faculty of Graduate Studies and Research in partial fulfillment of the requirements for the degree of *Master of science*

Department of *Chemistry*

Edmonton, Alberta
Fall 2005

0-494-09137-1

Library and Archives Canada

Published Heritage Branch

395 Wellington Street
Ottawa ON K1A 0N4
Canada

Bibliothèque et Archives Canada

Direction du Patrimoine de l'édition

395, rue Wellington
Ottawa ON K1A 0N4
Canada

Your file *Votre référence*
ISBN:
Our file *Notre référence*
ISBN:

NOTICE:
The author has granted a non-exclusive license allowing Library and Archives Canada to reproduce, publish, archive, preserve, conserve, communicate to the public by telecommunication or on the Internet, loan, distribute and sell theses worldwide, for commercial or non-commercial purposes, in microform, paper, electronic and/or any other formats.

The author retains copyright ownership and moral rights in this thesis. Neither the thesis nor substantial extracts from it may be printed or otherwise reproduced without the author's permission.

AVIS:
L'auteur a accordé une licence non exclusive permettant à la Bibliothèque et Archives Canada de reproduire, publier, archiver, sauvegarder, conserver, transmettre au public par télécommunication ou par l'Internet, prêter, distribuer et vendre des thèses partout dans le monde, à des fins commerciales ou autres, sur support microforme, papier, électronique et/ou autres formats.

L'auteur conserve la propriété du droit d'auteur et des droits moraux qui protège cette thèse. Ni la thèse ni des extraits substantiels de celle-ci ne doivent être imprimés ou autrement reproduits sans son autorisation.

In compliance with the Canadian Privacy Act some supporting forms may have been removed from this thesis.

While these forms may be included in the document page count, their removal does not represent any loss of content from the thesis.

Conformément à la loi canadienne sur la protection de la vie privée, quelques formulaires secondaires ont été enlevés de cette thèse.

Bien que ces formulaires aient inclus dans la pagination, il n'y aura aucun contenu manquant.

Canada

This thesis is dedicated to my parents, Pui Hing Lee and Hon Chun Chan.

ABSTRACT

This work is aimed at evaluating the plausibility of using atomic force microcopy (AFM) instrumentation and techniques for the measurement of interaction force and surface characterization in a high throughput manner. Investigations of the feasibility of combining tapping mode (TM) AFM and pulsed-force mode (PFM) AFM with an inverted AFM (i-AFM) design were carried out. Conventional AFM requires a cantilever with an integrated tip to image a substrate-supported sample, whereas i-AFM, uses one of tens of thousands of substrate-supported tips to image a cantilever-supported sample. Microcontact printed and dip-pen nanolithographyically modified silicon chip and tipless cantilevers were characterized by both conventional and inverted AFM in contact mode (CM), TM, force volume (FV) and PFM.

We have demonstrated for the first time that iTM-AFM and iPFM-AFM are capable of differentiating chemical heterogeneity of a patterned surface by phase contrast and adhesive force measurement, respectively.

ACKNOWLEDGEMENTS

I would like to take this opportunity to thank those who have been helping me out, guiding me, encouraging me and making my life much easier throughout the course of my study in the past two and a half years. Without your support and encouragement, I would not have a chance to type out this passage. There are so many people I want to thank and I'm sure I will forget to mention some of them. If I do, please accept my apologies.

First of all, I'd like to thank Dr. J.-B. Green, my supervisor, for letting me join his group. Thank you for being patient with me, a student who repeatedly saying *"I don't know"*, and guiding me through this mysterious path. Thank you for treating us chocolate-fondue, which simply reflects my life in the past two and a half years: bitter and sour, but most of all, it was sweet.

Members in the green group: Ademola, Nirala, Tayo, Sulayman, Katie, Ran, Shiau-yin, Andrea and Rick, and also friends from the Department of Chemistry, you guys have filled my memory with joy and laughter. I wish you all the best and success in your future career.

John, what a friend you are. Thank you for proof-reading this thesis since the early stage. I appreciate your presence at the times I felt frustrated and down, as well as joyous and cheerful.

Thank brothers and sisters from The Assembly of God in Edmonton for giving me spiritual support. Your prayers and caring means a lot to me.

Uncle Hon and Auntie Eva, thank you for taking care of me since I was 14. You allowed me to concentrate on my studies without worrying about doing daily chores. I am going to miss the food and desserts made by Auntie Eva, and the bbq steaks by Uncle Hon, they are always delicious (um… yummy).

Lastly, I would like to thank my family. Simon ("ah orange"), it's a disaster to have you as a brother (heehee j/k). Thank you for your love and care, and the rides to and from school once in a while. You have motivated me to finish this thesis as soon as I could so that I could escape from you (heehee kidding again. Oops, someone will beat me up tonight). Mom, Dad and Albert, though we

are far apart, you are always in my heart. Mom and Dad, how blessed I am to be your daughter. You have always provided me with more than I need. Thank you for letting me choose my path and being there when I needed you. Your love, support and encouragement have given me strength to face whatever problem I encountered and whatever task I needed to go through.

TABLE OF CONTENT

CHAPTER 1.....1

1.1 BACKGROUND..... 1
1.2 ATOMIC FORCE MICROSCOPY..... 3
1.2.1 CONTACT MODE..... 6
1.2.1.1 Friction Force Microscopy..... 9
1.2.1.2 Force Modulation Microscopy..... 9
1.2.2 INTERMITTENT CONTACT MODE..... 10
1.2.2.1 Tapping Mode..... 10
1.2.2.2 Force Volume..... 13
1.2.2.3 Pulsed-Force Mode..... 13
1.2.3 NON-CONTACT MODE..... 14
1.2.3.1 Magnetic Force Microscopy..... 16
1.2.4 INVERTED AFM..... 16
1.3 SELF-ASSEMBLED MONOLAYERS..... 17
1.3.1 MICROCONTACT PRINTING..... 19
1.3.2 DIP-PEN NANOLITHOGRAPHY..... 19
1.4 COMBINATORIAL INVERTED AFM..... 21
1.5 RESEARCH OBJECTIVES..... 23
1.6 REFERENCES..... 23

CHAPTER 2..... 29

2.1 INTRODUCTION..... 29
2.2 EXPERIMENTAL..... 32
2.2.1 CHEMICALS..... 32
2.2.2 CANTILEVERS AND TIP ARRAYS..... 33
2.2.3 INSTRUMENTATION..... 36
2.2.4 MICROCONTACT PRINTING OF CANTILEVER..... 38
2.2.5 MICROCONTACT PRINTING OF TIP ARRAY..... 40
2.2.6 DPN PATTERNING OF CANTILEVERS..... 40

2.2.7 IMAGING..... 42
2.2.7.1 Conventional..... 42
2.2.7.2 Inverted..... 42
2.2.8 AMPLITUDE DISTANCE..... 43
2.3 RESULTS AND DISCUSSION..... 44
2.3.1 MICRO CONTACT PRINTING..... 44
2.3.2 DPN PATTERNING OF CANTILEVERS..... 49
2.3.3 EFFECT OF TIP HEIGHT..... 49
2.3.4 AMPLITUDE-DISTANCE CURVES..... 52
2.4 CONCLUSIONS..... 60
2.5 REFERENCES..... 62

CHAPTER 3..... 64

3.1 INTRODUCTION..... 64
3.2 EXPERIMENTAL..... 68
3.2.1 CHEMICALS..... 68
3.2.2 SILICON CHIP, CANTILEVERS AND TIP ARRAYS..... 69
3.2.3 INSTRUMENTATION.....72
3.2.4 MICROCONTACT PRINTING OF CANTILEVER..... 73
3.2.5 MICROCONTACT PRINTING OF AU-COATED SI CHIP..... 73
3.2.6 IMAGING.....73
3.2.6.1 Conventional Orientation.....73
3.2.6.2 Inverted Orientation.....74
3.3 RESULTS AND DISCUSSION.....74
3.4 CONCLUSION..... 95
3.5 REFERENCES..... 97

CHAPTER 4..... 99

4.1 CONCLUSIONS..... 99
4.2 FUTURE PROSPECTS..... 100
4.3 REFERENCES..... 101

APPENDIX A 103

APPENDIX B 104

LIST OF TABLES

Table 2.1. Characteristics of the cantilevers that were used in this project. Cantilever geometries are adopted from manufacturer's specification..... 35

Table 2.2. Characteristics of tips from different batches of arrays obtained by SEM..... 37

Table 3.1. Characteristics of the cantilevers that were used in this project. Cantilever geometries were adapted from manufacturer's specification..... 70

Table 3.2. Average adhesion measured by PFM (oscilloscope) and FV in 1mm and 5mm of modified cantilever in inverted orientation..... 96

LIST OF FIGURES

Figure 1.1. Schematic diagram of an AFM. The laser beam coming out from the laser source is bounced off the back of the cantilever, which scans over the sample in a raster pattern, and the mirror onto the position-sensitive photodiode detector. The piezoelectric transducer is made of electrical sensitive material. It is responsible for the lateral (xy plane) movement of the sample and the vertical (z direction) movement in the feedback mechanism.....4

Figure 1.2. Schematic illustration of a cantilever exhibits (left) deflection perpendicular to the surface and (right) torsion parallel to the surface plane.....5

Figure 1.3. Typical force-distance curve observed in AFM. A Si tip probing a Si surface.....7

Figure 1.4. Typical TM AFM amplitude vs. z distance curve. A Si tip probing a Si surface.....12

Figure 1.5. Typical force curve shown on an oscilloscope in PFM experiment. The dark solid line traces the cantilever deflection and the dashed line represents the sine wave that drives the z-piezo to oscillate. The schematic figures on the bottom depict the movements of the z-piezo and the response of the cantilever....15

Figure 1.6. (A) Scanning electron micrograph of a tip array and (B) optical micrograph of a sub-array with 100 tips. (Bottom) Inset of a schematic illustration of i-AFM.....18

Figure 1.7. Schematic illustration of procedures for mCP of alkylthiol on a transition metal substrate.....20

Figure 1.8. Illustration of molecules being transfer from an AFM tip to a substrate surface through the water meniscus between the tip and the substrate. The molecules then undergo self-organization to form SAMs.....22

Figure 2.1. Illustration of a tipless cantilever addressing one of the tips from a tip array.....30

Figure 2.2. Scanning electron micrograph of a Si chip with three tipless cantilevers attached to one end.....34

Figure 2.3. Scanning electron micrographs of substrate-supported tips and a tip-integrated cantilever.....37

Figure 2.4. Optical micrograph of the patterning setup.....39

Figure 2.5. Optical micrograph of the position of the PDMS stamp relative to the cantilever.....41

Figure 2.6. (A) Topography and (B) friction (trace minus retrace) image of cantilever 1a by AFM in conventional orientaion. The scan size is 20mm x 20mm. Cross-sectional profiles correspond to (A) height and (B) friction on horizontal line as shown in the images.....45

Figure 2.7. (A) Topography and (B) phase image of cantilever 1a by AFM in conventional orientation. The scan size is 10mm x 10mm. Cross-sectional profiles correspond to (A) height and (B) phase lag on horizontal line as shown in the images.....46

Figure 2.8. (A) Topography and (B) phase image of cantilever 1a by AFM in inverted orientation. The scan size is 10mm by 10mm. Cross-sectional profiles correspond to (A) height and (B) phase lag on horizontal line as shown in the images.....48

Figure 2.9. (A) Topography and (B) friction image of cantilever 1b by AFM in conventional orientation. The scan size is 2mm x 2mm. Cross-sectional profiles correspond to (A) height and (B) friction on horizontal line as shown in the images.....50

Figure 2.10. (A) Topography and (B) phase image of cantilever 1b by AFM in inverted orientation. Probed by tip array A. The scan size is 2mm x 2mm. Cross-sectional profiles correspond to (A) height and (B) phase lag on horizontal line as shown in the images.....51

Figure 2.11. (A) Topography and (B) phase image of cantilever 1b by AFM in inverted orientation. Probed by tip array B. The scan size is 2mm x 2mm. Cross-sectional profiles correspond to (A) height and (B) phase lag on horizontal line as shown in the images.....53

Figure 2.12. (A) Topography and (B) phase image of cantilever 1b by AFM in inverted orientaion. Probed by tip array O. The scan size is 2mm x 2mm. Cross-sectional profiles correspond to (A) height and (B) phase lag on horizontal line as shown in the images.....54

Figure 2.13. Illustration of the edge of a tipless cantilever bumping into the base of the substrate.....55

Figure 2.14. Amplitude-distance curves captured in different cantilever-tip combinations and different orientations.....57

Figure 2.15. Illustrations of the model described in squeeze-film damping (left) and i-AFM (right).....59

Figure 2.16. (A) Theoretical fitting (dotted line) over the experimentally captured (solid line) spectrum of an oscillating tipless cantilever. (B) Theoretical fitting (dotted line) over experimentally captured (solid line) amplitude-distance curve.....61

Figure 3.1. Front panel of a PFM unit.....66

Figure 3.2. Typical force-versus-time curve obtain in PFM measurement and the corresponding positions of the triggers. The dotted line represents the output voltage from PFM that modulates the z-piezo and the solid line represents the response of the cantilever.....67

Figure 3.3. Scanning electron micrograph of a representative tip from a tip array. Image was taken at 87° from the plane normal.....71

Figure 3.4. (A) Topography and (B) friction image of the patterned Au-coated chip imaged by AFM in conventional orientation. Friction image was generated by trace minus retrace. Scan size is 15mm x 15mm. Dark contrast in (B) represents lower friction and bright contrast represents higher friction. Cross-sectional profiles correspond to the average (A) height and (B) friction calculated within the box shown in the images.....75

Figure 3.5. (A) Topography and (B) FV adhesion image of the patterned Au-coated chip imaged by AFM in conventional orientation. Scan size is 14.8mm x 14.8mm. Adhesion image is composed by 4096 force curves. Dark contrast in (B) represents higher adhesion and bright contrast represents lower adhesion.....77

Figure 3.6. Force-distance curves obtained from FV adhesion measurements of the patterned chip inside (A) stamped region and (B) backfilled region with 100 nm scan area. Each plot is composed of 256 (retract) force curves and each force curve has 512 data points.....79

Figure 3.7. Histograms generated from FV measurements inside modified region (diamond) and backfilled region (triangle) of the patterned Si chip. Each histogram is composed of 256 force measurements. The measured average adhesion inside the modified region and the backfilled region are 5.1nN and 14.0nN, respectively.....80

Figure 3.8. (A) Topography and (B) PFM adhesion image of the patterned Au-coated chip imaged by AFM in conventional orientation. Scan size is 15mm x 15mm. Dark contrast in (B) represents lower adhesion and bright contrast represents higher adhesion. Cross-sectional profiles represent average (A) height and (B) adhesion calculated within the box shown in the images.....81

Figure 3.9. (A) Topography and (B) PFM adhesion image within the backfilled area of patterned chip by AFM in conventional orientation. The scan size is 100nm. The adhesion image (B) is composed of ~600,000 force measurements. Cross-sectional profiles correspond to the horizontal line shown on the topography (dashed line) and adhesion (solid line) image.....84

Figure 3.10. Histograms generated from PFM adhesion measurements inside modified region (diamond) and backfilled region (triangle) of the patterned chip. Each histogram is composed of ~600,000 force measurements. The measured average adhesion inside the modified region and the backfilled region are 2.5nN and 3.2nN, respectively.....85

Figure 3.11. Force-time curves generated from oscilloscope during PFM adhesion measurements within 100nm scan area of the (A) modified region and (B) backfilled region of the patterned chip.....86

Figure 3.12. Histograms generated from oscilloscope captured PFM adhesion measurements inside modified region (diamond) and backfilled region (triangle) of the patterned Si chip. Each histogram is composed of 50 force measurements. The measured average adhesion inside the modified region and the backfilled region are 6.9nN and 11.6nN, respectively.....88

Figure 3.13. (A) Topography and (B) friction (trace) image of patterned cantilever by AFM in conventional orientation. Scan size is 15mm x 15mm. Dark contrast in (B) represents lower friction and bright contrast represents higher friction. Cross-sectional profiles correspond to the average (A) height and (B) friction calculated within the box shown in the images.difference indicate that PFM i-AFM is capable of differentiating surface compositions.....89

Figure 3.14. (A) Topography and (B) PFM adhesion image of patterned cantilever by AFM in inverted orientation. Scan size is 10mm x 10mm. The adhesion image is composed of ~600,000 force measurements. Dark contrast in (B) represents lower adhesion and bright contrast represents higher adhesion. Cross-sectional profiles correspond to average (A) height and (B) friction calculated within the box shown in images.....90

Figure 3.15. (a) Topography and (B) PFM adhesion image of modified cantilever by AFM in inverted orientation. Scan size is 1mm x 1mm. The adhesion image is composed of ~600,000 force measurements. Dark contrast in (B) represents lower adhesion and bright contrast represents higher adhesion.Cross-sectional profiles represent horizontal lines shown on images.....92

Figure 3.16. Force-distance curves generated from measurements of a modified cantilever and a modified tip array by AFM in inverted orientation. (A) 20 force-distance curves generated by oscilloscope captured PFM measurements. (B) 256 force-distance curves (retract) generated by FV measurements.....93

Figure 3.17. Histograms generated from FV (cross) and oscilloscope captured PFM (circle) adhesion measurements of modified cantilever by AFM in inverted orientation. FV generated histogram is composed of 256 force measurements and the PFM generated histogram is composed of 70 force measurements.....94

LIST OF SYMBOLS

F	Force exerted on the sample by a tip
k	Spring constant
x	Deflection of a cantilever
ϕ	Phase angle
m	Effective mass
ω	Drive frequency
ω_o	Resonance frequency
Q	Quality factor
σ	Sum of force derivatives
$\Delta\phi_o$	Phase angle shift
A	Oscillating amplitude
A_o	Drive amplitude
b	Damping coefficient
b_∞	damping coefficient when cantilever is far from surface
d	cantilever-tip separation
a	Area of cantilever
μ	Gas viscosity
Å	Distance unit (angstroms)
F_{max}	Most repulsive force experienced by cantilever in PFM

LIST OF ABBREVIATIONS

μCP	Micro-contact printing (printed)
μm	Distance unit (micrometers)
AFM	Atomic force microscopy (microscope)
Au	Gold
CCD	Charge-coupled device
CH_3-	Methyl group
CM	Contact mode
cm	Distance unit (centimeters)
COOH-	Carboxylic acid group
Cr	Chromium
DPN	Dip-pen nanolithography
FFM	Friction force microscopy (microscope)
FV	Force volume
HF	Hydrogen fluoride
Hz	Frequency unit (hertz)
i-AFM	Inverted-atomic force microscopy (microscope)
iPFM-AFM	Inverted pulsed-force mode atomic force microscopy
iTM-AFM	Inverted tapping mode atomic force microscopy
kHz	Frequency unit (kilohertz)
m	Distance unit (meters)
mbar	Pressure unit (millibar)
mM	Concentration unit (millimolar)
mm	Distance unit (millimeters)
MUA	11-Mercaptoundecanoic acid
N	Force unit (newtons)
N_2	Nitrogen
nm	Distance unit (nanometers)
nN	Force unit (nanonewtons)
ODT	Octadecanethiol

PDMS	polydimethylsiloxane
Piezo	Piezoelectric transducer
PFM	Pulsed-force mode
S	Sensitivity
s	Time unit (seconds)
SAM	Self-assembled monolayer
SCEM	Scanning electrochemical microscopy (microscope)
SEM	Scanning electron microscopy (microscope)
SNOM	Scanning near-field optical microscopy (microscope)
Si	Silicon
Si_3N_4	Silicon nitride
SiO_2	Silicon dioxide
SPM	Scanning probe microscopy
STM	Scanning tunneling microscopy (microscope)
t	Time
Ti	Titanium
TEM	Transmission electron microscopy (microscope)
TM	Tapping mode
V	Cantilever deflection
v	volume
w	weight

CHAPTER 1

INTRODUCTION

1.1 Background

Scientists are interested in studying the microscopic properties of materials since a lot of fundamental interactions between objects are dependent on their microscopic natures. Amongst these properties, scientists are curious about *what is it*, *how much is it*, and *where is it*. In order to answer these questions, different instrumentation techniques were developed. First there were wave microscopies such as optical microscopy and electron microscopy. Optical microscopy uses visible light and lenses to obtain information. However, the resolution of using such a method is limited by diffraction effects to approximately half of the wavelength of light [1]; for example, light with a wavelength of 500 nm would have a diffraction limited resolution of ~250 nm. This resolution is increased by changing the waves from electromagnetic (optics) to DeBroglie (electrons). The DeBroglie wavelength of an electron can be made arbitrarily small by accelerating it to a high kinetic energy, for example, an electron accelerated to 30keV would have a DeBroglie wavelength of 0.007 nm, resulting in a substantially higher resolution than can be obtained with light. This led to the development of techniques such as scanning electron microscopy (SEM) [2] and transmission electron microscopy (TEM) [3], which have demonstrated atomic resolution [4,5]. The drawbacks for these techniques, however, are the high-energy electrons can easily damage the sample, and these techniques must be performed in vacuum.

The last three decades have witnessed the development of scanning probe microscopies (SPM), which in some cases boast atomic resolution and are less destructive to the samples than the corresponding electron microscopies. Each one of these SPM methods scans a probe of some kind over the sample surface, to produce an image of the surface, in a three-dimensional manner. Several different kinds of probes have been developed, based on electron tunneling (scanning tunneling microscopy), mechanical forces (scanning force microscopy),

electrochemical current (scanning electrochemical microscopy), and even optics (scanning near-field optical microscopy). Each of these methods employ piezoelectric transducers [6] (hereafter referred to as piezos) to control the xyz coordinates of the sample relative to the probe. By scanning the position of the sample relative to the probe in a raster manner, images of the properties can be produced. The research presented herein is concerned with the development of novel SPM instrumentation.

In scanning tunneling microscopy (STM) [7,8], the probe is a metallic tip, and when a bias voltage is applied between the tip and the sample a tunneling current is produced which depends exponentially on the tip-sample separation. Therefore, small changes in the surface topography can alter the current greatly, allowing STM to achieve a very high sensitivity to height differences (0.01 Å) [9]. This scanning method has the best lateral resolution among all of the SPM techniques and the reproducibility of atomic resolution images can be obtained day after day [10,11].

The probe used in atomic force microscopy (AFM) [12] often has very small radius of curvature (<30 nm) because the observed topography and the measured force are largely dependent on the contact area and the shape of the AFM tip. The system detects the cantilever deflection which is related to the sample topography [13] as well as sample properties such as elasticity [14] and compositional chemistry [15,16]. Reports of atomic resolution acquired by AFM have been published [17,18]. There are different operating modes in AFM for measurements of different properties of interest.

SECM [19,20] is in fact the combination of probe microscopy and ultramicro size electrode electrochemistry [21]. The probe is an ultramicroelectrode and the experiment is performed in an electrolytic solution. A constant potential difference verses a reference electrode is applied to both the tip and the sample substrate. The system detects the Faradaic current from the electrolysis of the solution species, which changes depending upon the tip-sample separation, the local electrical conductivity of the sample and other variables. Like other SPMs, there are different operating modes based on different feedback

mechanisms in SECM. One of them is the monitoring of the distance-dependent electrochemical reaction of the electrolyte to obtain surface topography [22].

The following section will introduce the basic principles of AFM and a few of the commonly used AFM operating modes, strengths and weaknesses, and some examples of applications will be discussed.

1.2 Atomic Force Microscopy

Since its introduction in 1986, AFM has found wide application in many fields of study such as pharmacology [23,24], polymer sciences [25,26], biology [27,28], chemistry [29,30] and various surface characterization studies [31,32]. AFM often requires little sample preparation and it can be used to image many different types of surfaces under many different kinds of conditions [33,34]. It allows direct measurements of insulating materials, and can provide atomic-resolution data [17,18].

Figure 1.1 illustrates the principle of an AFM using the optical-lever deflection method. In this case, the sample is mounted on a xyz-piezo for three-dimensional translation. A laser beam is focused on the back of a microfabricated cantilever. The laser beam is then reflected by the cantilever, depending on the cantilever's deflection, and directed by a mirror onto a quadrant photodiode detector. There are usually two photodiodes on top and two at the bottom to form a quadrant detector. The laser beam reflects to the bottom two photodiodes when the cantilever bends upward, while it is reflected on the top two photodiodes when it bends downward. The advantage of having four photodiodes over two is that not only the deflection of the cantilever, but also the torsion of the cantilever can be detected, as illustrated in Figure 1.2. When the sample scans the tip in direction that is perpendicular to the cantilever's side, the tip-sample interaction causes the cantilever to tilt parallel to the sample plane. Therefore, information about the adhesion between the tip and the sample can be obtained (details of friction force microscopy (FFM) will be described in section 1.2.1.1).

An AFM cantilever can be considered as a spring with a spring constant k. The force, F, exerted on the sample by the tip can be calculated using Hooke's Law if k is known [35,36]

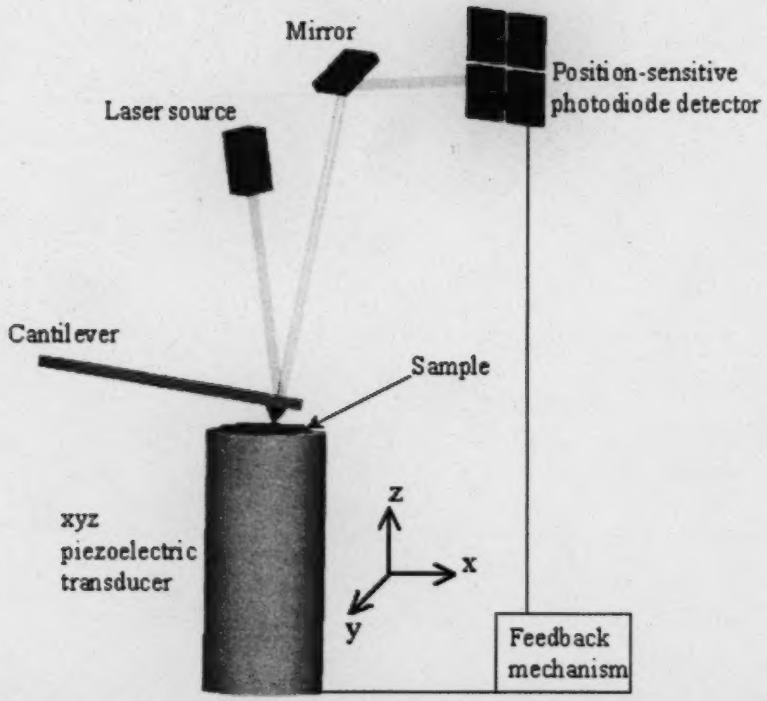

Figure 1.1. Schematic diagram of an AFM. The laser beam coming out from the laser source is bounced off the back of the cantilever, which scans over the sample in a raster pattern, and the mirror onto the position-sensitive photodiode detector. The piezoelectric transducer is made of electrical sensitive material. It is responsible for the lateral (xy plane) movement of the sample and the vertical (z direction) movement in the feedback mechanism.

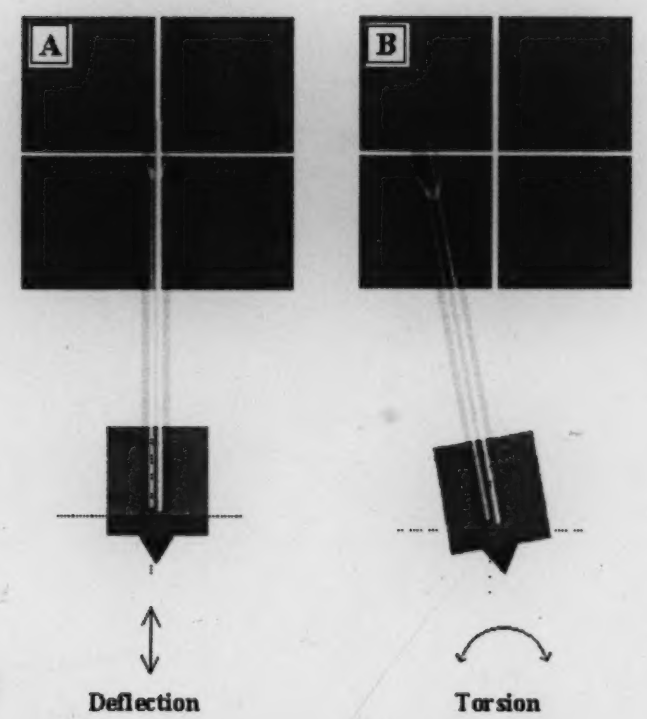

Figure 1.2. Schematic illustration of a cantilever exhibits (left) deflection perpendicular to the surface and (right) torsion parallel to the surface plane.

$$F = -k\Delta z, \tag{1.1}$$

where Δz is the deflection of the cantilever from its equilibrium position.

In a typical force-distance curve (Figure 1.3), the cantilever deflection is recorded as a function of the tip-sample separation as the tip approaches and retracts from the sample. The tip starts far from contact with the sample at (A). When tip-sample separation is large, there are no substantial interaction forces between the tip and the sample, and the cantilever is not deflected from its equilibrium position. As the tip-sample separation is decreased, by moving the z-piezo in the z direction, eventually the tip-sample interaction will result in a force being applied to the cantilever which in turn causes the cantilever to bend from its equilibrium position (position when the tip is not in contact with the sample). In this force-distance curve, the force is attractive; the tip "jumps" to contact with the sample at (B). As the tip-sample separation continues to decrease, the interaction forces between them become repulsive which causes the cantilever to deflect away from the sample at (C). When the tip is retracted from the sample, the cantilever slowly moves back to its equilibrium position and the tip-sample adhesion forces causing the tip to bind with the sample. As the sample continues to move away from the cantilever, eventually the restoring force of the cantilever overcomes the adhesion force between the tip and the sample and the tip is detached from the sample at (D).

The AFM uses feedback mechanisms to perform imaging and measurements. According to the different operating modes, various feedback mechanisms can be used. The two most commonly used operating modes are *contact mode* (CM) and *tapping mode* (TM), while other modes such as adhesion mapping, pulsed-force mode (PFM) and non-contact mode (NCM) are also available.

1.2.1 Contact Mode

As the name implies, the tip and the sample are in contact during the imaging process in CM. Before going into contact with the sample, i.e. far above the sample, the cantilever is at its equilibrium position. The deflection set point is

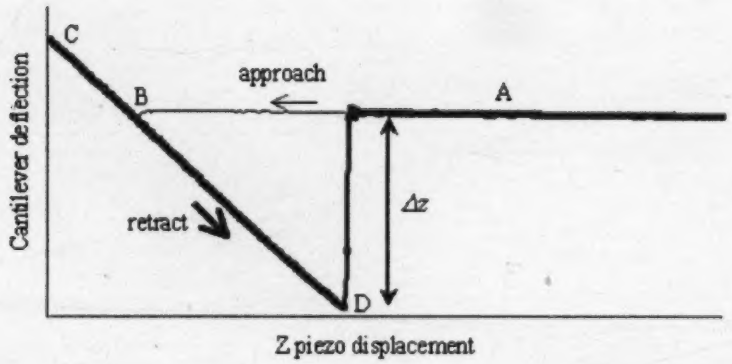

Figure 1.3. Typical force-distance curve observed in AFM. A Si tip probing a Si surface.

externally adjusted so that during imaging, the cantilever is allowed to deflect from its equilibrium position. Before the tip and the sample are engaged (*engage* is a term commonly used in AFM to describe the satisfaction of the feedback set point by the cantilever deflection), the tip continues to approach the sample until the deflection of the cantilever reaches the deflection set point. Once the tip has engaged it starts to scan in the x and y directions. Within CM two surface imaging options can be chosen: "constant height" and "constant force". The former is good when the surface is relatively flat. The feedback loop is turned off, thus, the vertical position of the sample is fixed. The cantilever deflection as a result of tiny changes in surface roughness is monitored. Since the output signal for this imaging method is collected directly from the cantilever deflection, inaccurate data acquisition arising from slow electronic communication and slow piezo response that might occur in the feedback loop can be eliminated. Therefore, high vertical resolution images can be obtained. However, the draw back for this imaging method is that it prevents the control over the imaging force, which can easily lead to sample or tip destruction. Hence, it is not commonly practised in our group.

In constant force imaging, a feedback mechanism is employed to ensure that the force being exerted on the sample by the tip is kept constant. A feedback loop is connected between the detector and the z-piezo. By monitoring the deflection of the cantilever, the feedback signals the z-piezo to retract or extend in order to maintain the cantilever deflection at a constant level as the tip is scanning in the lateral direction. For instance, if the tip scans over a tall feature, which causes the cantilever to deflect above the set point, the feedback mechanism will signal the z-piezo to retract the sample to return the cantilever deflection to its set point value. As mentioned above, the tip is continuously touching the surface in CM, which happens in both constant height and constant force imaging; thus, when the tip is scanning in the lateral direction, a shear force (force that is induced by the dragging motion of the tip on the sample which could cause sample destruction) is introduced. In general, CM imaging is not ideal for soft and delicate samples as it tends to damage the sample surface.

1.2.1.1 Friction Force Microscopy

Mate *et al.* [28] at the IBM research center in Almaden made use of this shear force and invented the friction force microscope (FFM). We learnt from a famous artist, Leonardo da Vinci, that friction is proportional to the applied load and that friction is independent of the apparent contact area [37,38]. However, this is only true for macroscopic objects. Kendall [39,40] and many other scientists [41,42,43] believed that for small length scale objects where the true area of contact is small, such as an AFM tip and sample, friction is dependant on the applied load, interaction (adhesion) and the contact area between the two objects. If we assumed the AFM tip as a sphere with a certain radius of curvature, which probes an atomically flat surface, and the tip-sample contact area and the applied force are constant throughout the friction force measurement, the observed friction contrast must be due to the tip-sample interaction (adhesion). By monitoring the degree of torsion of a cantilever, the interaction between the tip and the sample can be determined, i.e. higher friction results in higher torsion of the cantilever. Local properties such as elasticity [44] and chemical heterogeneity [45] on a surface can also be revealed. In fact, surface roughness also contributes to the tilting of the AFM cantilever [46]. Nevertheless, by examining the friction image against the topographic image, one can still extract qualitative properties of the surface.

Due to FFM's ability to differentiate chemical heterogeneity at high scan rates, and the ease of preparation, this surface characterization technique was used for verification of the chemical patterning on Au-covered microscopic slides and Au-coated cantilevers in the projects that will be presented in Chapter 2 and Chapter 3.

1.2.1.2 Force Modulation Microscopy

In a typical force modulation microscopy (FMM) [47,48], either the tip or the sample is oscillated at hundreds of kiloHertz with an amplitude of a few nanometers [49] while the sample is scanned in contact with the tip. The amplitude of the cantilever is monitored and is associated with the local elastic properties of the sample in such a way that the amplitude is directly related to the

stiffness of the sample. For instance, if the tip scans over a soft material, more indentation is forced into the sample and results in a smaller oscillation amplitude. The drawback for this operating mode, however, is that tip and sample destruction could result from the sample indentation. Some applications of the FMM include the analyses of automotive brake pads [50], carbon nanotubes [51] and polyester films [52].

1.2.2 Intermittent Contact Mode

Three main operating modes fall under this category, TM, force volume (FV) and PFM.

1.2.2.1 Tapping Mode

In contrast to the CM, the tip in the TM-AFM is not constantly in contact with the sample, but rather striking on it intermittently at a very high frequency [53,54]. Up to date, there are two excitation modes that have been developed to excite the tip-integrated cantilever: the magnetic mode [55] and the acoustic mode [53,54]. The former mode excites the magnetized cantilever directly by applying an oscillating magnetic field [55,56], whereas in the latter mode an oscillating voltage is applied to a piezoelectric actuator which is assembled inside the cantilever holder, causing the cantilever to oscillate [53,54,56]. The advantage of the magnetic mode over the acoustic mode is that when imaging under fluid, undesired resonances associated with the acoustic excitation in the liquid medium can be eliminated [55]. However, since the magnetic excitation mode was not used in our lab and none of the experiments that will be presented in the following chapters were performed in fluid, the description of the magnetic mode will not be covered here, and I will focus mainly on the TM with the acoustic excitation mode.

In TM-AFM the cantilever is excited to oscillate at or near its resonant frequency, which is usually between 50-500kHz depending on the type of cantilever being used, with an oscillation amplitude in the range of 10-100nm. It uses a feedback mechanism to obtain topographical data and other useful information of a surface. The amplitude of an oscillating cantilever is monitored as a function of distance, and the signal triggers the z-piezo to retract or extend

depending on the surface topography. If the amplitude of the cantilever is damped below the pre-defined amplitude set point, then the feedback loop will signal the z piezo to retract so that the set point amplitude is maintained [53,54].

Figure 1.4 is a typical amplitude-distance curve obtained in a TM experiment. Before the tip-sample engagement, the amplitude set point is defined as some voltage below the free oscillating amplitude, which is determined by viscous damping of the cantilever in air [57] when it is far from the sample at (A). As the tip is approaching the sample, the attractive interaction acts on the tip and the sample causes the amplification of oscillations [57]. Eventually the tip "jumps" to contact with the sample, and the amplitude is reduced as the tip continues to approach the sample at (B). Since the cantilever is oscillating at a high amplitude, it has sufficient energy to break free from the capillary attraction (a layer of water formed between the tip and the sample which draws the tip and the sample together), the electrostatic, magnetic and van der Waals interactions that are binding it to the sample [46]. As the tip-sample distance decreases, the tip-sample contact time increases. Once the damped amplitude reaches the pre-set set point, the z-approach stops and the tip starts to scan in the lateral direction at (B). During the imaging process the tip continues to oscillate at the excitation frequency (usually a few hundred kiloHertz). Since the tip "jumps" in and out of contact with the sample at a high frequency in the TM, the shear force acting on the sample can be greatly reduced, and it is reasonable to assume that no friction force is induced. Furthermore, since TM-AFM can operate in a wide range of conditions (ambient, fluid and vacuum), it is an ideal scanning probe method for a large diversity of samples such as biomolecules and living cells [58-59--60].

It is unlikely that the amplitude of the cantilever will reduce to zero ((C) in Figure 1.4) in a TM experiment because the cantilever is no longer tapping in this region but is constantly touching the surface, which will exert a great amount of force on the sample. By adjusting the amplitude set point, one has the control over the force applied to the sample.

Although the TM-AFM does not have the ability for friction imaging, phase imaging in TM can map out surface compositions and differentiate local

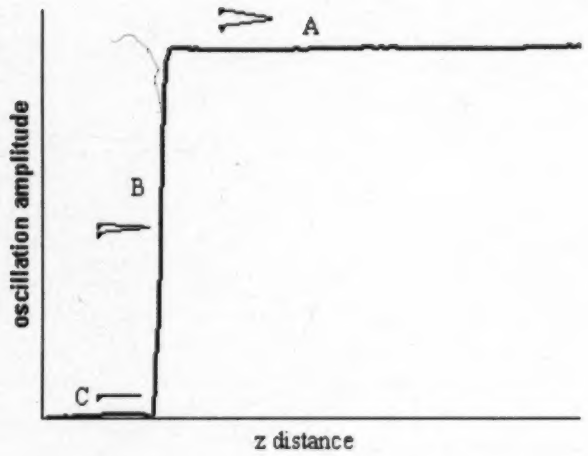

Figure 1.4. Typical TM AFM amplitude vs. z distance curve. A Si tip probing a Si surface.

properties of a sample [61,62]. Phase imaging is the detection of the difference between the measured cantilever oscillation phase angle and the one that is driving it. Since the degree of phase lag is correlated to the energy being dissipated into the sample and maybe the surrounding medium [63,64], phase imaging is capable of providing quantitative analysis in surface characterization [65-666768].

1.2.2.2 Force Volume

This imaging mode is mostly used for measurements of elasticity [69,70], magnetic and chemical properties of a sample [71-7273]. Basically force volume (FV) includes the measurements of force-distance curves in a two-dimensional scanning area. At each unique xy position in the image, a force-distance curve is obtained. By combining the measured force-distance curves within an image, a three-dimensional force data can be acquired. Extension of this mode to measure interactions between two distinct functional groups has been made by Lieber and co-workers [74], in which chemically modified AFM tips and substrates were used.

1.2.2.3 Pulsed-Force Mode

Although not as commonly used as adhesion mapping (section 1.2.2.2), PFM [75] is a useful and rapid force-measuring device. PFM is an external z-piezo modulator that can be connected to many commercially available AFM instruments, allowing them to measure the local stiffness and adhesion, and obtain the topographic information without introducing a shear force on the sample [75,76-777879]. In contrast to the triangular wave in FV, an AC current with a sinusoidal waveform is applied to the z-piezo of an AFM unit, which causes the z-piezo to oscillate vertically in a frequency of 100 Hz to 2 kHz with the amplitude in the range of 10-500nm. The purpose of controlling the oscillating frequency below 2kHz is to prevent any disturbing resonance from the cantilever, cantilever holder and the z transducer tube [75]. Similar to the TM, the amplitude of the z-piezo must be large enough to avoid the tip-sample adhesion binding them throughout the oscillation cycle as the adhesion is measured at the points where the tip breaks free from the sample (Figure 1.5). An oscilloscope in conjunction

with the PFM unit is used to monitor the behavior of the cantilever and to set several parameters in accordance. The principle of PFM can be better illustrated by Figure 1.5 which shows a typical force curve observed in a PFM measurement as well as the corresponding responses of the tip with respect to the z-piezo.

The dark solid line in Figure 1.5 refers to the cantilever's response (cantilever deflection) while the dashed line represents the sine wave that drives the z-piezo to oscillate. The tip is at its equilibrium position at (A) where the sample is withdrawn from the tip. As the sample moves toward the tip, driven by the sine wave modulation of the z piezo, the attractive force between them causes the tip to sanp into contact with the sample at (B). The tip and the sample experience the largest repulsive force at (C) when the driving sine wave reaches its maximum, and here is where the topographic data is obtained. Then the z-piezo, i.e. sample, retracts from the tip until it is far enough to overcome the adhesion at (D) and is completely free from the sample. Finally the subsequent free oscillation of the cantilever is damped to the baseline at (E). The cycle repeats from (A) to (E) at a rate of 100 to 2,000 cycles per second according to the pre-defined frequency. The detection of the maximum repulsive force value and the adhesion peak is achieved by connecting a peak-picker circuit and a sample-and-hold circuit [80] to the unit. The peak-picker follows the original force signal and picks up the maximum value in the case of maximum force detection and the minimum value for adhesion [75,80]. At the end of each cycle, the peak-picker is read out by a sample-and-hold circuit and then reset to the original value. The advantage of PFM over force-volume is that PFM provides high-speed and high-resolution force measurements by collecting only a few well-chosen data points [75] instead of recording the complete force-distance curve.

1.2.3 Non-Contact Mode

This imaging mode is good for soft samples [81,82] because the tip will not cause damage to the sample due to the fact that they are not in contact. In addition, if one is concerned about contamination introduction from the tip to the sample, this mode of operation can certainly deal with the problem. This imaging mode is designed for monitoring the cantilever response due to the van der Waals

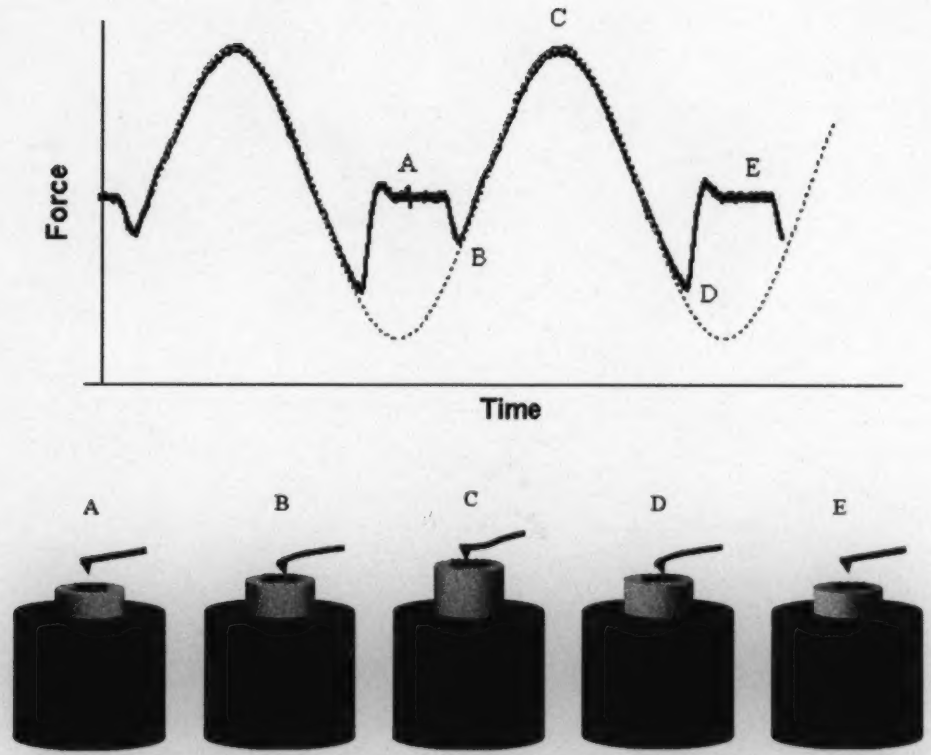

Figure 1.5. Typical force curve shown on an oscilloscope in PFM experiment. The dark solid line traces the cantilever deflection and the dashed line represents the sine wave that drives the z-piezo to oscillate. The schematic figures on the bottom depict the movements of the z-piezo and the response of the cantilever.

interaction between the tip and the sample. The tip is excited to vibrate above the sample, i.e. tens to hundreds of angstroms. Since the resonant frequency of a cantilever is dependent on the distance-related force gradient it experiences, the system detects the changes in the amplitude, phase or frequency of the oscillating cantilever in order to feedback to the z-piezo. For example, when a tip experiences an attractive force from the sample, its oscillation amplitude increases; the feedback then increase the tip-sample separation to return the amplitude to its set point value. Unfortunately, the fluid contaminant layer on the sample surface is often thicker than the van der Waals force gradient. Therefore, NCM is not as sensitive to the surface topography as CM unless the fluid contaminant layer is eliminated.

1.2.3.1 Magnetic Force Microscopy

The tip and the sample are operated in the non-contact domain in magnetic force microscopy (MFM) and this operating mode can be used to collect information of the topography and the magnetic properties of a sample [83,84]. First, the tip is coated with a ferromagnetic thin film and oscillated near the sample. The tip-sample separation dependent magnetic field induced by the tip and the sample causes changes of the cantilever resonant frequency. The system keeps the amplitude, phase or frequency of the cantilever at a constant value by monitoring one of these variables and feedback to the z piezo. Note that the topographic information and the magnetic properties of the sample are both contained in a MFM obtained image. In order to determine which property contributes more to the image, one must image the same area with the same tip at various tip-sample separations. This is because van der Waals interaction, which allows detection of the topography (as described in section 1.2.3), is predominate at small tip-sample separation, whereas magnetic effect is more significant at greater tip-sample separation.

1.2.4 Inverted AFM

Inverted AFM (i-AFM) [85] is simply the inverted design of the conventional AFM. Instead of having a cantilever integrated tip probing a substrate, one substrate-supported tip from a tip array is used to probe a

cantilever-supported sample at a time. Our custom-built 1 cm x 1 cm tip array [86] is composed of 90,000 tips and two adjacent tips are 25μm apart. Each $1cm^2$ tip array is divided into 9 squares and each square has 100 sub-arrays, each of which having an index marker and 100 tips, as illustrated in Figure 1.6. The index marker serves as the tip identification of different tip sub-arrays.

It is important to understand that AFM topographic image is a convolution of the tip shape. The actual shape of the sample being probed and the measured force are significantly dependent on the area of contact between the tip and sample. Therefore, it is desirable to probe a sample with an ultra-sharp tip (e.g. carbon nanotube tip [87]) to achieve higher lateral resolution images or with various tips to obtain more precise results. However, the development for carbon nanotubes as AFM tips is not yet mature and the commercial tip-integrated cantilevers are costly. Note that in i-AFM switching from one tip to another simply moves the cantilever. Thus, the enhanced availability of tips for topographic imaging and force measurements in i-AFM can greatly increase the speed of data collection and reduce the research cost from the economical point-of-view.

Since i-AFM is a newly developed extension to the AFM, not much study or application of such technique has been published. In this work, I aimed to investigate the plausibility of operating TM and PFM in the i-AFM design.

1.3 Self-Assembled Monolayers

The applications of self-assembled monolayers (SAMs) have grown extensively since the discovery of these structures due to their ability to modify the physical and chemical properties of a surface [88-8990]. The formation of self- assembled alkanethiol monolayers is spontaneous self-organization of functionalized, long chain alkanethiol molecules onto the surface of appropriate substrates (e.g. Au, Ag) by physisorption without external aid [91-9293]. This process can be achieved by the exposure of a substrate to the alkanethiol-contained media for various times. Once the molecules have adsorbed to the substrate, they begin to organize themselves so that the closely packed hydrocarbon tails are mainly in trans configuration and are tilted at approximately

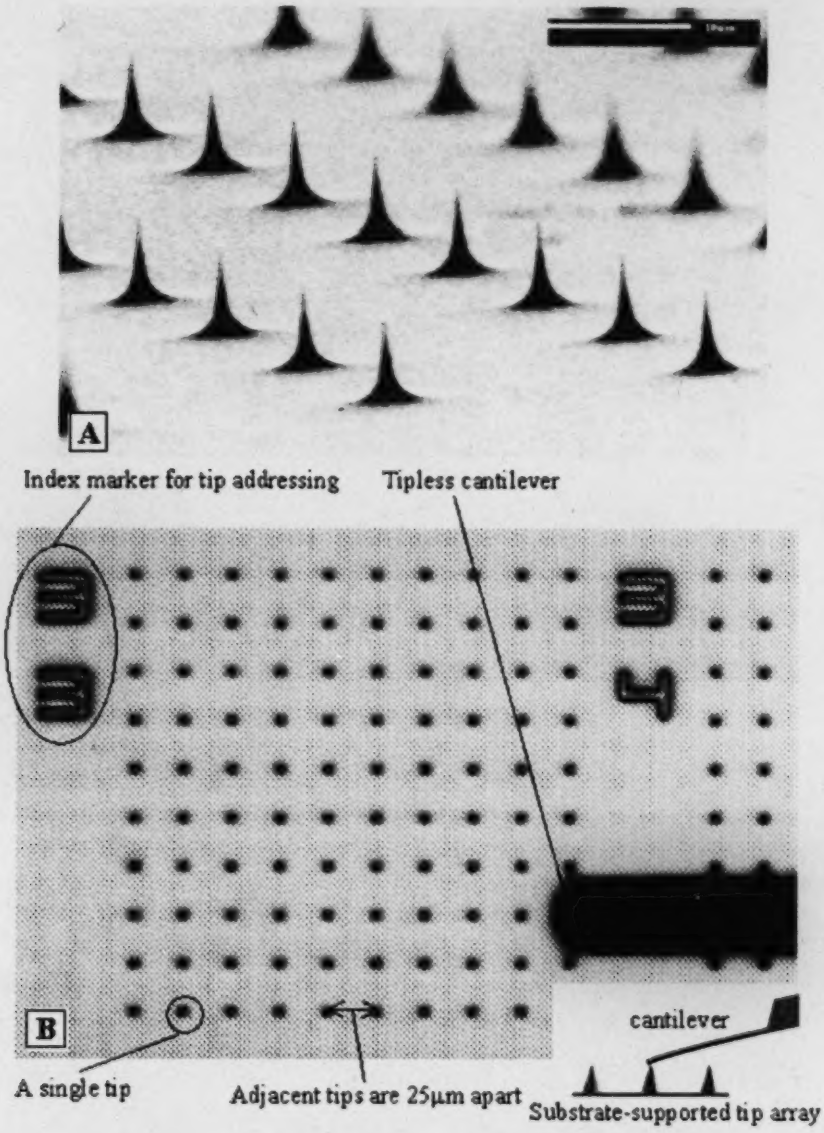

Figure 1.6. (A) Scanning electron micrograph of a tip array and (B) optical micrograph of a sub-array with 100 tips. (Bottom) Inset of a schematic illustration of i-AFM.

30° from the surface normal to maximize the van der Waals interaction between the adjacent methylene groups [88,93,94].

An alkanethiol molecule consists of a sulfur atom at one end (called the head group), which bonds to the substrate, and any type of functional groups at the other end (called the end group) connected by a methylene chain. The end group serves to provide different properties to the SAM surface. For example the surface becomes hydrophilic if a carboxyl group is used as the end group, while the surface becomes hydrophobic if a methyl group is attached instead. By choosing alkanethiols with different terminal functional groups, one can adjust the lubrication, adhesion and friction of the surface [91-9293,95]. There are several methods to pattern SAMs, such as microcontact printing (μCP) [95] and dip-pen nanolithography (DPN) [96] (readers are directed to an excellent review of SAM by Smith *et al.*, Ref. [88]).

1.3.1 Microcontact Printing

Microcontact printing is a technique in which an elastomeric polymer, usually polydimethylsiloxane (PDMS) is used to transfer thiol molecules to a substrate surface [88,95]. Figure 1.7 depicts the procedure for μCP of alkanethiol molecules on a transition metal substrate. A PDMS stamp with predefined pattern acts as a sponge and absorbs the alkanethiol after immersion into alkanethiol solution and dried (Step i). Then the molecules are transferred to the substrate through the direct contact of the inked PDMS stamp and the substrate (Step ii).

After removing PDMS, the alkanethiol molecules order themselves in a spontaneous fashion to form a uniform SAM (Step iii). The unstamped regions on the substrate can be modified with different molecules by immersing the substrate into another dilute solution [93]. Hence, a surface composed of binary chemistries can be easily produced.

1.3.2 Dip-Pen Nanolithography

In DPN, the AFM tip and the substrate can be considered as a nib of a dip-pen and paper, respectively. The tip is inked by immersion into a saturated solution of interest (alkanethiol) or by other spotting methods such as non-contact robotic spotting. The molecules from the "ink"-coated AFM tip are directly

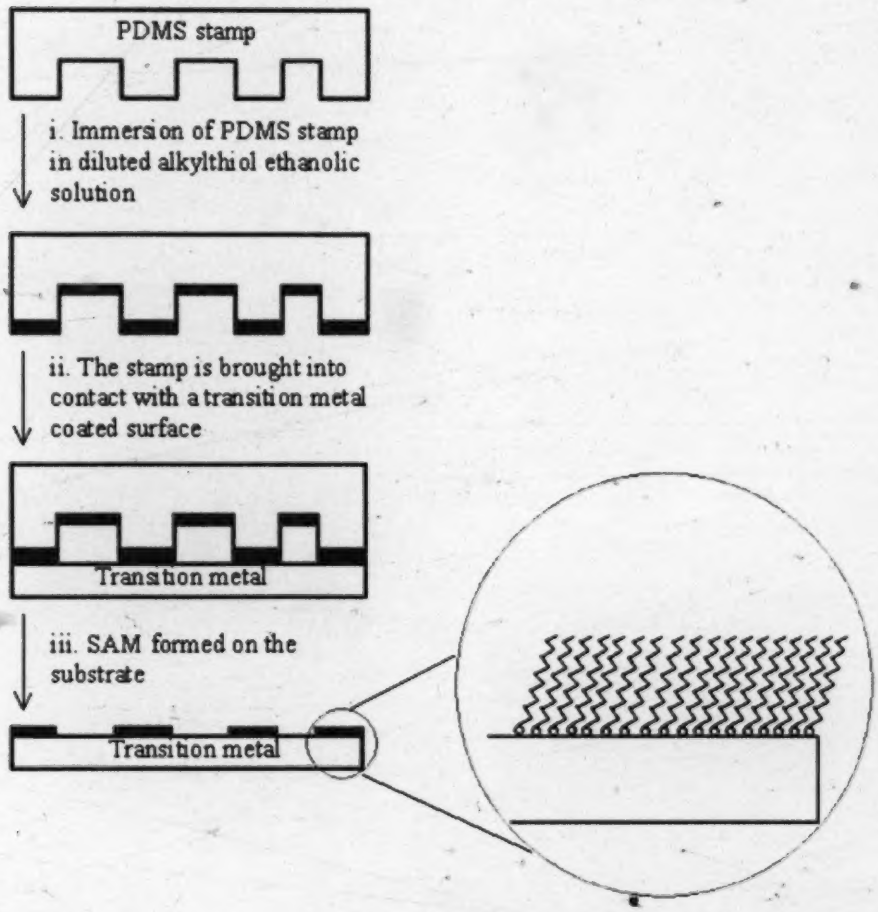
PDMS stamp
i. Immersion of PDMS stamp in diluted alkylthiol ethanolic solution
ii. The stamp is brought into contact with a transition metal coated surface
Transition metal
iii. SAM formed on the substrate
Transition metal

Figure 1.7. Schematic illustration of procedures for μCP of alkylthiol on a transition metal substrate.

deposited onto the substrate of interest [97]. Some researchers believe that the transfer of the molecules from the tip to the substrate depends on the water meniscus formed between the two [96,98], while others propose that in some cases water plays no role in the transport process [99,100].

There are possibly two basic steps involved in the patterning process in a DPN experiment if we assume that the transfer of the molecules is water-related: i) molecular transport from the tip to the substrate, and ii) "ink" adsorption onto the surface and monolayer formation [97], as illustrated in Figure 1.8. The first step is achieved by the dissolution of "ink" (alkanethiol) into the water meniscus, while the second step is a spontaneous self-organization process. Nonetheless, the mechanisms for both the "ink" transportation and adsorption are complicated and are dependent on a number of variables such as temperature, humidity and the writing speed (i.e. scan rate of the AFM tip) [97].

In this work, SAMs formed by μCP and DPN were used to modify the cantilever surface and some gold-coated macro-substrates in order to prevent any contamination and to provide a heterogeneous surface.

1.4 Combinatorial inverted AFM

Some of the early AFM studies revealed that the measured adhesion, friction and other tip-sample interactions are correlated to the tip and the sample surface chemistries [101,102]. By altering the surface functional groups of a tip, one can enhance the interaction selectivity between the tip and the sample.

Lieber and co-workers [74] were the first group which applied SAMs to both the AFM tip and the surface that was studied. They measured the interaction between the CH_3- and COOH- modified tip and the CH_3- and COOH- modified surfaces. Despite the fact that they did not take into account the tip radii, which affect the degree of interaction, they were able to distinguish the adhesive forces between CH_3/CH_3, CH_3/COOH, and COOH/COOH functional groups.

One of the benefits of the i-AFM is that there are tens of thousands of tips that are available for modification. By modifying the tipless cantilever and the tip arrays with different chemistries or biomaterials, one can obtain a series of distinct force measurements between different chemistries or biochemical

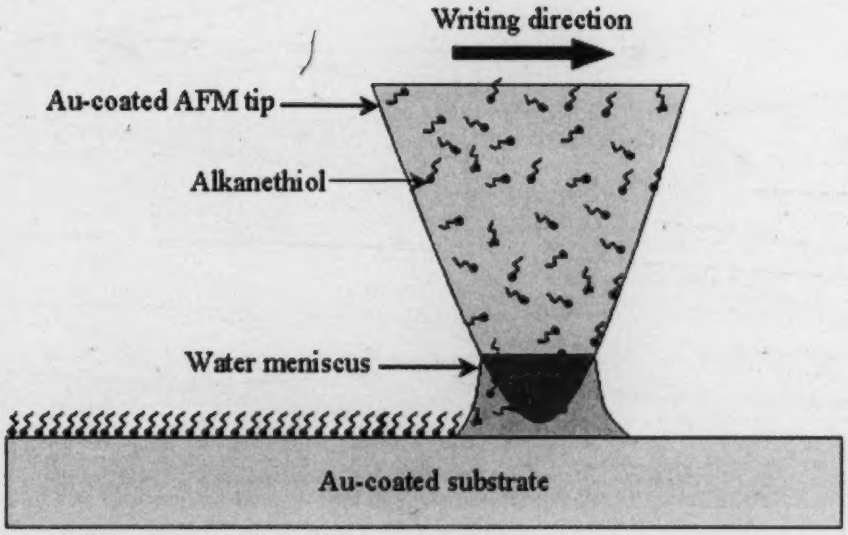

Figure 1.8. Illustration of molecules being transfer from an AFM tip to a substrate surface through the water meniscus between the tip and the substrate. The molecules then undergo self-organization to form SAMs.

combinations in a relatively short period of time [103]. The modification of the cantilevers and the tip arrays can be achieved by employing different surface modification techniques such as robotic spotting [104] and the ones mentioned in section 1.3.

1.5 Research Objectives

This work is aimed at evaluating the plausibility of performing TM with i-AFM and also PFM with i-AFM in order to achieve high-speed and high lateral-resolution force measurements. Surface modification techniques like μCP and DPN were employed to modify the tipless cantilevers and the tip arrays. The ability to differentiate different chemically modified areas by phase imaging in the iTM-AFM, and adhesion force measurement in the iPFM-AFM were examined. Experimental setup, results and discussions, as well as the directions of future developments of these methods will also be addressed.

1.6 References

1 Abbe, M. Archiv. Mikroscop. Anat. Entwicklungsmech. **1873**, 9, 431.

2 Zworykin, V. K.; Hiller, J. and Snyder, R. L. *ASTM Bull.* **1942**, *117*, 15.

3 Knoll, M.; Ruska, E. *Z. Phys.* **1932**, *78*, 318.

4 Batson, P. E. *Nature* **1993**, *366*, 727.

5 Williams, D. B.; Michael, J. R., Goldstein, J. I., Romig Jr, A. D. *Ultramicroscopy* **1992**, *47*, 121.

6 Jaffe, H.; Berlinco, D. A. *Pr. Inst. Electr. Elect.* **1965**, *53*, 1372.

7 Binnig, G.; Rohrer, H.; Gerber, C.; Weibel, E. *Phys. Rev. Lett.* **1982**, *49*, 57.

8 Binnig, G.; Rohrer, H.; Gerber, C.; Weibel, E. *Phys. Rev. Lett.* **1983**, *50*, 120.

9 Woodward, J. T.; Zasadzinski, J. A. *Biophys. J.* **1997**, *72*, 964.

10 Brause, R.; Moltgen, H.; Kleinermanns, K. *Appl. Phys. B-Lasers O.* **2002**, *75*, 711.

11 Vonau, F.; Aubel, D.; Gewinner, G.; Pirri, C.; Peruchetti, J. C.; Bolmont, D.; Simon, L *Phys. Rev. B* **2004**, *69*, Art. No. 081305.

12 Binnig, G.; Quate, C. F.; Gerber, C. *Phys. Rev. Let.* **1986,** *56*, 930.

13 Maye, M. M.; Lim, I. I. S.; Luo, J.; Rab, Z.; Rabinovich, D.; Liu, T. B.; Zhong, C. J. *J. Am. Chem. Soc.* **2005**, *127*, 1519.

14 Shi, W. Q.; Wang, Z. Q.; Cui, S. X.; Zhang, X.; Bo. Z. S. *Macromolecules* **2005**, *38*, 861.

15 Tan, S. S.; Sherman, R. L.; Qin, D. Q.; Ford, W. T. *Langmuir* **2005**, *21*, 43.

16 Najman, M. N.; Kasrai, M.; Bancroft, G. M. *Tribo. Lett.* **2004**, *17*, 217.

17 Holscher, H.; Allers, W.; Schwarz, U. D.; Schwarz, A.; Wiesendanger, R. *Phys. Rev. B* **2000**, *62*. 6967

18 Hirai, N.; Okada, H.; Hara, S. *ISIJ Int.* **2000**, *40*, 702.

19 Bard, A. J.; Fan, F. R. F.; Pierce, D. T.; Unwin, P. R.; Wipf, D. O.; Zhou, F. *Science* **1991**, *254*, 68.

20 Bard, A. J.; Fan, F. R. F.; Kwak, J.; Lev, O. *Anal. Chem.* **1989**, *61*, 132.

21 Nagy, G.; Nagy, L. Fresenisu J. *Anal. Chem.* **2000**, *366*, 735.

22 Tsionsky, M.; Cardon, Z. G.; Bard, A. J.; Jackson, R. B. *Plant Physiol.* **1997**, *113*, 895.

23 Mao, G. Z.; Chen, D. Z.; Handa, H.; Dong, W. F.; Kurth, D. G.; Mohwald, H. *Langmuir* **2005**, *21*, 578.

24 Mu, L.; Seow, P. H.; Ang, S. N.; Feng, S. S. *Colloid Polym. Sci.* **2004**, *283*, 58.

25 Kwon, S.; Han, S.; Ihm, D.; Kim, E.; Kim, J. *Mol. Cryst. Liq. Cryst.* **2004**, *425*, 355.

26 Sun, G. X.; Kappl, M.; Butt, H. J. *Colloid. Surface A* **2004**, *250*, 203.

27 Toca-Herrera, J. L.; Moreno-Flores, S.; Friedmann, J.; Pum, D.; Sleytr, U. B. *Microsc. Res. Techniq.* **2004**, *65*, 226.

28 Obataya, I.; Nakamura, C.; Han, S.; Nakamura, N.; Miyake, J. *Nano. Lett.* **2005**, *5*, 27.

29 Najman, M. N.; Kasrai, M.; Bancroft, G. M.; Frazer, B. H.; De Stasio, G. *Tribol. Lett.* **2004**, *17*, 811.

30 Li, J.; Cui, Z.; Baker, M. A. *Surf. Interface Anal.* **2004**, *36*, 1254.

31 Wang, Y.; Yang, W. *Langmuir* **2004**, *20*, 6225.

32 Wang, H.; Bash, R.; Yodh, J. G.; Hager, G.; Lindsay, S. M.; Lohr, D. *Biophys. J.* **2004**, *87*,1964.

33 Rossell, J. P.; Allen, S.; Davies, M. C.; Roberts, C. J.; Tendler, S. J. B.; Williams, P. M. *Ultramicroscopy* **2003**, *96*, 37.

34 Gotzinger. M.; Peukert, W. *Langmuir* **2004**, *20*, 5298.

35 Shakesheff, K. M.; Davies, M.C.; Roberts, C. J.; Tendler, S. J. B.; Williams, P. M. *Crit. Rev. Therap. Drug Carr. Syst.* **1996**, *13*, 225.

36 Heinz, W. F.; Hoh, J. H. *Nanotechnology* **1999**, *17*, 143.

37 Dowson, D. *History of Tribology*, Longman, London, **1979**.

38 Bowden, F. P.; Tabor, D. *The Friction and Lubrication of Solids*, Clarendon Press, Oxford, **1950**.

39 Johnson, K. L.; Kendall, K.; Roberts, A. D. *Proc. R. Soc. London* **1971**, *Ser. A 324*, 301.

40 Kendall, K. *Nature* **1986**, *319*, 203.

41 Johnson, K. L. *Langmuir* **1996**, *12*, 4510.

42 Carpick, R. W.; Ogletree, D. F.; Salmeron, M. *Appl. Phys. Lett.* **1997**, *70*, 1548.

43 Schwarz, U. D.; Zworner, O.; Koster, P.; Wiesendanger, R. *Phys. Rev. B* **1997**, *56*, 6987.

44 Resch, R.; Friedbacher, G.; Grasserbauer, M.; Kanniainen, T.; Lindroos, S.; Leskela, M. Niinisto, L. *Appl. Surf. Sci.* **1997**, *120*, 51.

45 Kuutti, L.; Peltonen, F.; Myllarinen, P.; Teleman, O.; Forssell, P. *Carbohyd. Polym.* **1998**, *37*, 7.

46 Bhushan, B.; Fuchs, H.; Hosaka, S. *Applied Scanning Probe Methods*; Springer-Verlag Berlin Heidelburg: NY, **2004**, Chapter 1.

47 Haga, H.; Nagayama, M.; Kawabata, K.; Ito, E.; Ushiki, T.; Sambongi, T. *J. Electron Microsc.* **2000**, *49*, 473.

48 Fritz, M.; Radmacher, M.; Petersen, N.; Gaub, H. E. *J. Vac. Sci. Technol. B* **1994**, *12*, 1526.

49 Lin, H.-N.; Hung, T.-T.; Chang, E.-C.; Chen, S.-A. *Appl. Phys. Lett.* **1999**, *74*, 2785.

50 Munz, M.; Schulz, E.; Sturm, H. *Surf. Interface Anal.* **2002**, *33*, 100.

51 Volodin, A.; Ahlskog, M.; Seynaeve, E.; Van Haesendonck, C.; Fonseca, A.; Nagy, J. B. *Phys. Rev. Lett.* **2000**, *84*, 3342.

52 Beake, B. D.; Leggett, G. J.; Shipway, P. H. *Surf. Interface Anal.* **1999**, *27*, 1084.

53 Zhong, Q.; Inniss, D.; Kjoller, K.; Elings, V. B. *Surf. Sci.* **1993**, *290*, L688.

54 Martin, Y,; Williams, C. C.; Wickramasinghe, H. K. *J. Appl. Phys.* **1987**, *61*, 4723.

55 Han, W.; Jing, T.; Lindsay, S. M. *Appl. Phys. Lett.* **1996**, *69*, 4111.

56 Garcia, R,; Perez, R. *Surf. Sci. Rep.* **2002**, *47*, 197.

57 Sheiko, S. S. *Adv. Polym. Sci.* **2000**, *151*, 61.

58 Bolshakova, A. V.; Kiselyova, O. I.; Yaminsky, I. V. *Biotechnol. Progr.* **2004**, *20*, 1615.

59 Han, D.; Ma, W. Y.; Liao, F. L.; Yeh, M. L.; Ouyang, Z. G.; Sun, Y. X. *Phys. Med. Biol.* **2003**, *48*, 3897.

60 Howard, A.J.; Rye, R. R.; Houston, J. E. *J. Appl. Phys.* **1996**, *79*, 1885.

61 Magonov, S. N.; Elings, V. B.; Whangbo, M.-H. *Surf. Sci.* **1997**, *375*, L385.

62 Finot, M. O. and McDermott, M. T. *J. Am. Chem. Soc.* **1997**, *119*, 8564.

63 Cleveland, J. P.; Anczykowski, B.; Schmid, A. E.; Elings, V. B. *Appl. Phys. Lett.* **1998**, *72*, 2613.

64 Whangbo, M.-H.; Bar, G.; Brandsch, R. *Surf. Sci.* **1998**, *411*, L794.

65 Finot, M. O. and McDermott, M. T. *J. Am. Chem. Soc.* **1997**, *119*, 8564.

66 Feng, J. Y.; Weng, L. T.; Chan, C. M.; Xhie, J.; Li, L. *Polymer* **2001**, *42*, 2259.

67 Howard, A.J.; Rye, R. R.; Houston, J. E. *J. Appl. Phys.* **1996**, *79*, 1885.

68 Lysetska, M.; Knoll, A.; Boehringer, D.; Hey, T.; Krauss, G.; Krausch, G. *Nucleic Acids Res.* **2002**, *30*, 2686.

69 Schaer-Zammaretti, P.; Ubbink, J. *Ultramicroscopy* **2003**, *97*, 199.

70 Parbhu, A. N.; Bryson, W. G.; Lal, R. *Biochemistry* **1999**, *38*, 11755.

71 Gad, M, Itoh. A.; Ikai, A. *Cell Biol. Int.* **1997**, *21*, 697.

72 Kim, D. T.; Blanch, H. W.; Radke, C. J. *Langmuir* **2002**, 18, 5841.

73 Tan, S. S.; Sherman, R. L.; Ford, W. T. *Langmuuir* **2004**, *20*, 7015.

74 Frisbie, C. D.; Rozsnyai, L. F.; Noy, A.; Wrighton, M. S.; Lieber, C. M. *Science* **1994**, *265*, 2071.

75 Rosa, A,; Weilandt, E.; Hild, S.; Marti, O. *Meas. Sci. Technol.* **1997**, *8*, 1333.

76 Miyatani, T.; Horii, M.; Rosa, A,; Fujihira, M.; Marti, O. *Appl. Phys. Lett.* **1997**, *71*, 2632.

77 Krotil, H.-U.; Stifter, T.; Waschipky, H. Weishaupt, K.; Hild, S.; Marti, O. *Surf. Interface Anal.* **1999**, *27*, 336.

78 Okabe, Y.; Furugori, M.; Tani, Y.; Akiba, U.; Fujihira, M. *Ultramicroscopy* **2000**, *82*, 203.

79 Schneider, M.; Zhu, M,; Papastavrous, G.; Akari, S.; Mohwald, H. *Langmuir* **2001**, *18*, 602.

80 Analog Devices 1992 *Special Linear Reference Manual* (Norwood: Analog Devices).

81 Zimmermann, H.; Hagedorn, R.; Richter, E.; Fuhr, G. *Eur. Biophys. J.* **1999**, *28*, 516.

82 Yamashina, S.; Shigeno, M. *J. Electron Micros.* **1995**, *44*, 462.

83 Szmafa, W.; Grobelny, J.; Cichomski, M.; Makita, K. *Vacuum* **2004**, *74*, 297.

84 Winzer, M.; Kleiber, M.; Dix, N.; Wiesendanger, R. *Appl. Phys. A* **1996**, *63*, 617.

85 Green, J.-B. D.; Novoradovsky, A.; Park, D.; Lee, G. U. *Appl. Phys. Lett.* **1999**, *74*, 10.

86 Mabry, J. C.; Yau, T.; Yap, H.-W.; Green, J.-B. D. *Ultramicroscopy* **2002**, *91*, 73.

87 Wong, S. S.; Harper, J. D.; Lansbury, Jr. P. T.; Lieber, C. M. *J. Am. Chem. Soc.* **1998**, *120*, 603.

88 Smith, R. K.; Lewis, P. A.; Weiss, P. S. *Prog. Surf. Sci.* **2004**, *75*,1.

89 Pernstich, K. P.; Haas, S.; Oberhoff, D.; Goldmann, C.; Gundlach, D. J.; Batlogg, B.; Rashid, A. N.; Schitter, G. *J. Appl. Phys.* **2004**, *96*, 6431.

90 Nakamura, F. Ito, E.; Sakao, Y.; Ueno, N.; Gatuna, I. N.; Ohuchi, F. S.; Hara, M. *Nano Lett.* **2003**, *3*, 1083.

91 Nuzzo, R. G.; Allara, D. L. *J. Am. Chem. Soc.* **1983**, *105*, 4481.

92 Bhushan, B.; Fuchs, H.; Hosaka, S. *Applied Scanning Probe Methods*; Springer-Verlag Berlin Heidelburg: NY, **2004**, Chapter 10.

93 Xia, Y.; Whitesides, G. M.; *Angew. Chem., Int. Ed.* **1998**, *37*, 551.

94 Porter, M. D.; Bright, T. B.; Allara, D. L.; Chidsey, C. E. D. *J. Am. Chem. Soc.* **1987**, *109*, 3559.

95 Kumar, A. Whitesides, G. M. *Appl. Phys. Lett.* **1993**, *63*, 2002.

96 Piner, R. D.; Zhu, J.; Xu, F.; Hong, S. H.; Mirkin, C. A. *Science* **1999**, *283*, 661.

97 Rozhok, S.; Piner, R.; Mirkin, C. A. *J. Phys. Chem. B* **2003**, *107*, 751.

98 Jang, J.; Hong, S.; Schatz, G. C.; Ratner, M. A. *J. Chem. Phys.* **2001**, *115*, 2721.

99 Sheehan, P. E.; Whiteman, L. *J. Phys. Rev. Lett.* **2002**, *88*, 156104.

100 Schwartz, P. V. *Langmuir* **2002**, *18*, 4041.

101 Burnham, N. A.; Dominguez, D. D.; Mowery, R. L.; Colton, R. *J. Phys. Rev. Lett.* **1990**, *64*, 1931.

102 Overney, R. M.; Meyer, E.; Frommer, J.; Brodbeck, D.; Luthi, R.; Howald, L.; Guntherodt, H.-J.; Fujihira, M.; Takano, H.; Gotoh, Y. *Nature* **1992**, *359*, 133.

103 Green, J. B. D.; Lee, G. U. *Langmuir* **2000**, *16*, 4009.

104 Zubritsky, E. *Anal. Chem.* **2000**, *72*, 761A.

CHAPTER 2

TAPPING MODE INVERTED ATOMIC FORCE MICROSCOPY

2.1 Introduction

Over the years, atomic force microscopy (AFM) [1] has been utilized to measure the forces between molecules and to study surface properties [2-3-4]. In conventional AFM, a cantilever-supported tip is used to probe a surface. If the tip gets destroyed, or if one wants to replace the tip with a different chemically modified tip, the time it required for replacement and the pre-experimental alignment is unnecessarily long. The solution to this tedious task was given by the invention of the inverted-AFM (i-AFM) [5]. A schematic diagram of an i-AFM is shown in Figure 0.1.

In i-AFM, a substrate-supported tip from a tip array is used to probe a cantilever-supported sample. Since the area for imaging on a tipless cantilever (35 μm x ~15 μm) is much smaller than the sample size (1 cm x 1 cm) often used in conventional AFM, the limited scan size in i-AFM makes it much easier for experimentalist to locate the same spot on a sample substrate for imaging over and over again with different tips. In our 1 cm x 1 cm custom-built tip array, there are 90,000 tips and each adjacent tip is 25 μm apart from the others. Since they are sufficiently far apart, only one tip probes the tipless cantilever at a time. With the aid of modern spotting technology [6], it is possible to modify a 1 cm x 1 cm tip array with hundreds or even thousands of distinct chemistries or biomolecules. Similarly, a tipless cantilever can theoretically be modified with tens or hundreds of different chemistries or biomolecules. Therefore, a large number of combinations of interactions could in principle be measured. With new modes these measurements may be made in a relatively short period of time [7].

As it is becoming more important in pharmaceutical and drug industries to examine cell-chemistry, virus-antibody and ligand-receptor interactions in a fast and convenient way, a soft imaging tool with high throughput force measurement

Figure 2.1. Illustration of a tipless cantilever addressing one of the tips from a tip array.

is essential. Hence, in this project we will examine the plausibility of performing TM in the inverted AFM design and to investigate the optimal conditions for such performance.

In TM-AFM, the cantilever is excited to oscillate at or near its resonant frequency, the amplitude and phase of the oscillating cantilever are measured, and used to create images of the sample. The cantilever is allowed to oscillate freely at a drive amplitude when it is far from the sample where there is no tip-sample interaction. When the tip is approaching the sample surface, the oscillation amplitude is monitored as a function of z distance (tip-sample separation). As the tip gets closer to the sample, the interactions between them, for example, long-range electromagnetic interactions and van der Waals interaction, reduce the cantilever oscillation amplitude. Once the amplitude is reduced to the preset set point, usually 50-80% of the free oscillation amplitude, the tip starts to scan in both x and y directions, and the feedback loop keeps a constant amplitude by adjusting the tip-sample distance. If the amplitude drops below the amplitude set point, then the feedback loop signals the z-piezo to retract, moves away from the tip, and in such manner the topography in the x and y plane is obtained. Since the tip is tapping on the sample at high frequency instead of dragging along the sample during imaging, the shear force acting on the sample is minimized [8,9]. As a result of the relatively small forces applied to the sample, TM-AFM can yield a more accurate representation of the actual sample topography. The oscillating tip together with the feedback loop makes TM-AFM an ideal imaging tool for soft and fragile samples.

As mentioned the actual data recorded is the amplitude of cantilever oscillation, but by comparing the amplitude of cantilever oscillation to the drive signal we can also measure the phase lag of the cantilever with respect to the drive signal. This phase signal can be used for imaging chemical sensitive samples [10], biomaterial [11] and nanoparticles [12]. This phase data can be correlated with the chemical heterogeneity [13], viscosity and local elasticity of a surface [14,15]. Such detection is simultaneously performed as the topographical data is generated. If we consider the AFM cantilever as a damped harmonic

oscillator, then the resonance frequency, ω_o, of the cantilever is related to its spring constant, k, and effective mass, m, by $k=m\omega_o^2$ [15]. The phase angle, ϕ (in radians), as a function of a driving frequency, ω, of a freely oscillating cantilever can be expressed as [15]

$$\phi = \tan^{-1}\left(\frac{m\omega\omega_o}{Q\left(k - m\omega^2\right)}\right), \tag{2.1}$$

where Q is the quality factor. The phase angle is at $\pi/2$ when the driving frequency is equal to the resonance frequency. When the tip is brought relatively close to the sample, the phase angle will change due to the interaction between the tip and the sample. Thus equation (2.1) becomes [15]

$$\phi = \tan^{-1}\left(\frac{m\omega\omega_o}{Q\left(k + \sigma - m\omega^2\right)}\right), \tag{2.2}$$

where σ is the sum of force derivatives that are acting on the cantilever. Assuming that σ is very small compared to k, then the phase angle shift, $\Delta\phi_o$, of the free oscillating and interacting cantilever is defined as [15]

$$\Delta\phi_o = \frac{\pi}{2} - \tan^{-1}\left(\frac{k}{Q\sigma}\right) \approx \frac{Q\sigma}{k}. \tag{2.3}$$

It can be seen from this equation that phase shift is dependent on the degree of tip-sample interaction. The stronger interaction between the tip and the sample produces more phase angle shift. Thus, by probing a surface with a well-characterized tip in TM-AFM, it is possible to extract qualitative (i.e. compositional chemistry) and quantitative (i.e. adhesion force) information on a surface [16-171819].

2.2 Experimental

2.2.1 Chemicals

Octadecanethiol (ODT) and 11-mercaptoundecanoic acid (MUA) (Sigma-Aldrich) were used for cantilevers and tip arrays modification. Anhydrous ethanol (Commercial Alcohols Inc.) was used in all chemical ethanolic solution and for rinsing. Distilled and deionized 17.4 MΩ cm water from a water purificatoin system (Barnstead) was used throughout the experiment. 49% hydrofluoric acid

aqueous solution (Fisher Scientific Company) was used for stripping off SiO_2 layer on the tip arrays. Sylgard 184 silicone elastomer and sylgard 184 curing agent (Dow Corning) were used for the fabrication of polydimethylsiloxane (PDMS) stamp. Hexane (EMD Chemicals Inc., Germany) was used for the cleaning and purification of the PDMS stamp. Purified N_2 gas for drying was used throughout the experiment.

2.2.2 Cantilevers and tip arrays

These experiments make use of 3 different kinds of cantilevers and 3 different kinds of tip arrays. Figure 2.2 shows a scanning electron micrograph (SEM) of a representative Si chip supporting 3 tipless cantilevers. The assigned names for the cantilevers, their manufacturer specified characteristics, chemical modification and the types of experiments they were involved in this work are presented in Table 2.1. The cantilevers that were used in the imaging were 1a, 1b, 2b and 3. Cantilever 2b was Au-coated and chemically modified by immersion into 0.1 mM of MUA ethanolic solution. Cantilevers 1a and 1b were also Au-coated and were chemically modified by μCP and DPN (details of the chemical modification are covered in section 2.2.4 and section 2.2.6, respectively). The patterns on cantilevers 1a and 1b were verified by cantilever 3 in conventional friction force microscopy (FFM) imaging (i.e. cantilever 3 on top and cantilevers 1a and 1b on bottom). After verification of the patterning, cantilever 1a was imaged in TM in the conventional and inverted orientations, and cantilever 1b was imaged in TM in the inverted orientation. Cantilever 2b was used to image cantilever 1a in conventional TM. Cantilevers 1c and 2a were used for the measurements of the amplitude-distance curves in both conventional and inverted orientations, and the cantilevers were used as received.

All of the tip arrays were microfabricated by Dr. J.-B. Green (as described in Ref. [20]) at the Cornell Nanofabrication Facility. The silicon dioxide (SiO_2) layer (~2 μm thick), which was remained on the tip arrays after the fabrication to protect the tips from being damaged, was removed by the immersion of the tip

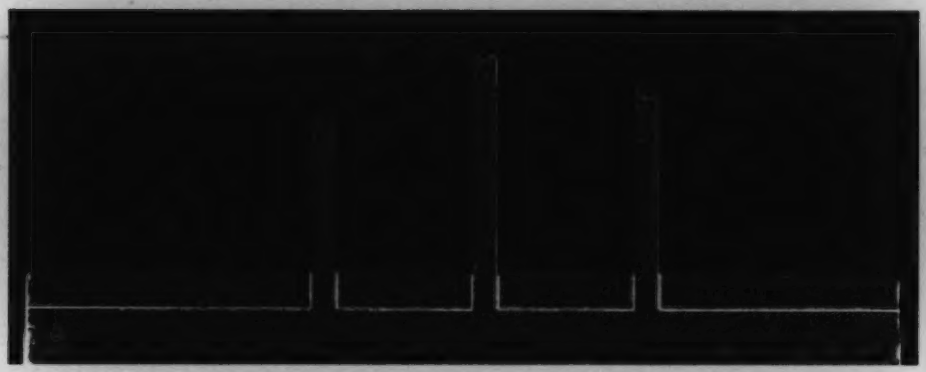

Figure 2.2. Scanning electron micrograph of a Si chip with three tipless cantilevers attached to one end.

Assigned name[1,2]	Tipped or tipless	Material and shape	Length and thickness	Resonant frequency	Spring constant	Chemical modification	Experiment
1a	Tipless	Si Rectangular	90 μm 2 μm	256 kHz	14 N/m	Au-coated μCP	Conventional FFM, TM and inverted TM imaging
1b	Tipless	Si Rectangular	110 μm 2 μm	203 kHz	7.5 N/m	Au-coated DPN	Conventional FFM and inverted TM imaging
1c	Tipless	Si Rectangular	110 μm 2 μm	194 kHz	7.5 N/m	N/A	Conventional and inverted A(d) curves
2a	Tipped	Si Rectangular	125 μm 4 μm	325 kHz	40 N/m	N/A	Conventional and inverted A(d) curves
2b	Tipped	Si Rectangular	125 μm 4 μm	325 kHz	40 N/m	Au-coated Immersion in MUA	Conventional TM imaging
3	Tipped	Si_3N_4 V-shaped	90 μm 0.4 μm	34 kHz	0.08 N/m	N/A	Conventional FFM imaging

Table 2.1. Characteristics of the cantilevers that were used in this project. Cantilever geometries are adopted from manufacturer's specification.

[1] Cantilevers 1a, 1b, 1c, 2a and 2b purchased from MicroMash.
[2] Cantilever 3 was purchased from Veeco Intruments Inc.61

arrays in HF for more than 20 minutes, followed by rinsing with water and dried under a stream of N_2 before they were used.

Representative tips from the same batch of tips as the ones that were used in this experiment were characterized by SEM, as shown in Figure 2.3. The images were captured at 87° to the plane normal. A commercially available Si tapping tip (cantilever 2a) was also characterized. The assigned names for the substrate-supported tips, the geometries of the tips and cantilever 2a, and the experiments they were involved are tabulated in Table 2.2.

The SEM micrographs reveal that the tip radius of curvature and the tip height from different batches of tip array vary greatly. The radii of curvature of the tips were measured to be in the range of 30 nm to 300 nm, and the tip height varied from 2 μm to 7 μm. The tallest tip (7 μm) among the substrate-supported tips is one third of the tapping tip and the shortest one is only one tenth of the tapping tip. The SEM images also reveal that the substrate-supported tips are cylindrically symmetric and the tapping tip is octagonal pyramidal.

It should be obvious to the readers that all of the tip arrays were only used in the inverted orientation. Tip array X was Au-coated and chemically modified, which was used for phase imaging of cantilever 1a, and tip arrays A, B and O were used for phase imaging of cantilever 1a. Tip arrays A, B and O were also used to obtain amplitude-distance curves with cantilever 1c.

Au deposition on cantilevers 1a, 1b, 2b and tip array X was achieved by gold sputtering using Kurt J. Lesker DC sputtering system (Nanofab, University of Alberta) under vacuum (below 10^{-6} torr). Ti worked as an adhesive layer between the substrate and Au and the deposition rates for Ti and Au are ~5 nm and ~40 nm, respectively.

2.2.3 Instrumentation

All topographic, phase and friction images for the DPN and μCP modified tipless cantilevers were obtained using Nanoscope IV controller equipped with a Dimension 3100 scanning probe microscope (Veeco Inc.). Amplitude-distance curves were obtained with a Multimode scanning probe microscope and Nanoscope IIIa controller (Veeco Inc.).

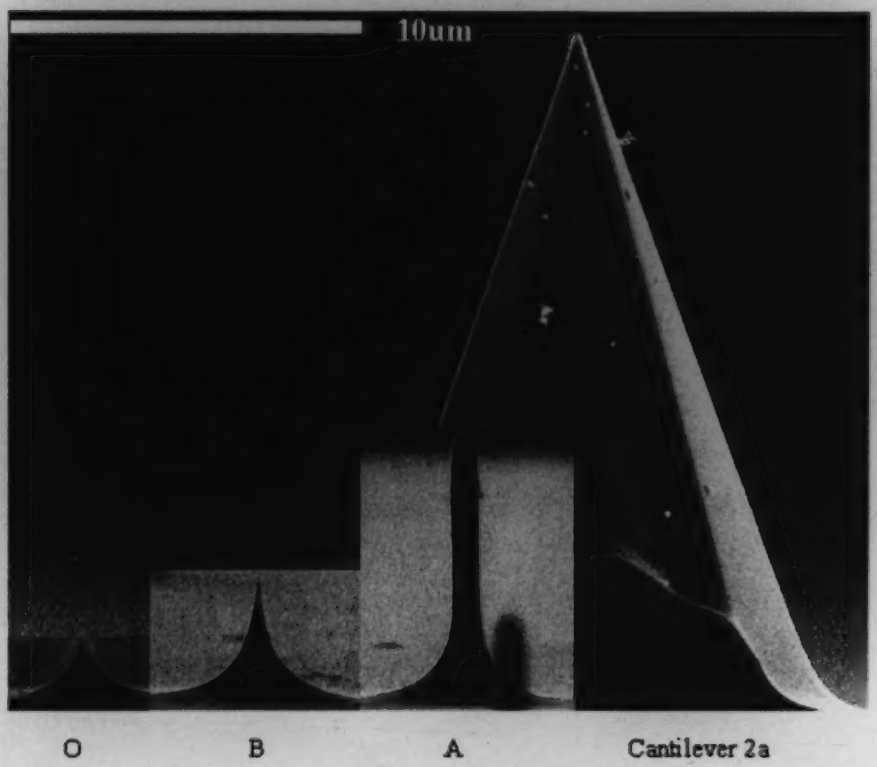

Figure 2.3. Scanning electron micrographs of substrate-supported tips and a tip-integrated cantilever.

Assigned name	Tip radius of curvature	Tip height	Experiment
A	~300 nm	~7 μm	Inverted TM and A(d) curve
B	~30 nm	~3 μm	Inverted TM and A(d) curve
O	~50 nm	~2 μm	Inverted TM and A(d) curve
X	N/A	N/A	Inverted TM
Cantilever 2a	~150 nm	~20 μm	Conventional and inverted A(d) curves

Table 2.2. Characteristics of tips from different batches of arrays obtained by SEM.

All scanning electron micrographs were obtained from the scanning electron microscope (SEM) laboratory in the department of earth and atmospheric sciences in the University of Alberta (X-vision, JSM-6301 FXV, JEOL).

2.2.4 Microcontact printing of cantilever

Cantilever 1a was modified by μCP. A patterned polydimethylsiloxane (PDMS) stamp was fabricated by mixing 10 parts of sylgard 184 silicone elastomer with 1 part of sylgard 184 curing agent w/w, and then poured onto a Si master (the Si master was made by Ademola Idowu at the University of Alberta NanoFab). The PDMS was left to cure on the Si overnight. After the removal from the Si master, the PDMS underwent cycles of purification and cleaning before it was ready to use. Prior to usage, the PDMS stamp was cleaned in accordance with the protocol suggested by Ratner *et al.* [21]. Briefly, the stamp was immersed in hexane overnight; the next morning the stamp was removed and dried inside a vacuum dessicator for 4 hours. This was followed by sonication in 1:1 anhydrous ethanol and deionized water v/v for 15 minutes and dried under a stream of N_2. After completion of the cleaning procedure, the PDMS stamp was immersed into a 1 mM ethanolic solution of ODT for 1 minute and then removed from solution and dried under a stream of N_2.

Figure 2.4 illustrates the patterning setup for the μCP on cantilever 1a. First attaching the bottom side (side without pattern) of the PDMS on a microscopic glass slide and having the pattern facing down. Then the glass slide was lifted up by two small glass vials and was placed under a microscope (10x magnification, Nikon, Japan) equipped with a CCD camera (Sony, Japan), which allowed precise positioning of the PDMS and the cantilever. The cantilever chip was cleaned in ozone (UVO-Cleaner®, Jetlight Company Inc.) for 40 minutes and was adhered on one end of a homemade cantilever holder using double-sided tape. The other end of the cantilever holder was attached to an xyz translator (model mmn-1, Nirishige, Japan). The microscope was adjusted to focus on the PDMS pattern, and the cantilever was slowly moved up using the z translator until it was relatively close to the surface of the stamp. Then the xy translator was utilized to align the end of the cantilever to the pattern. After the alignment was

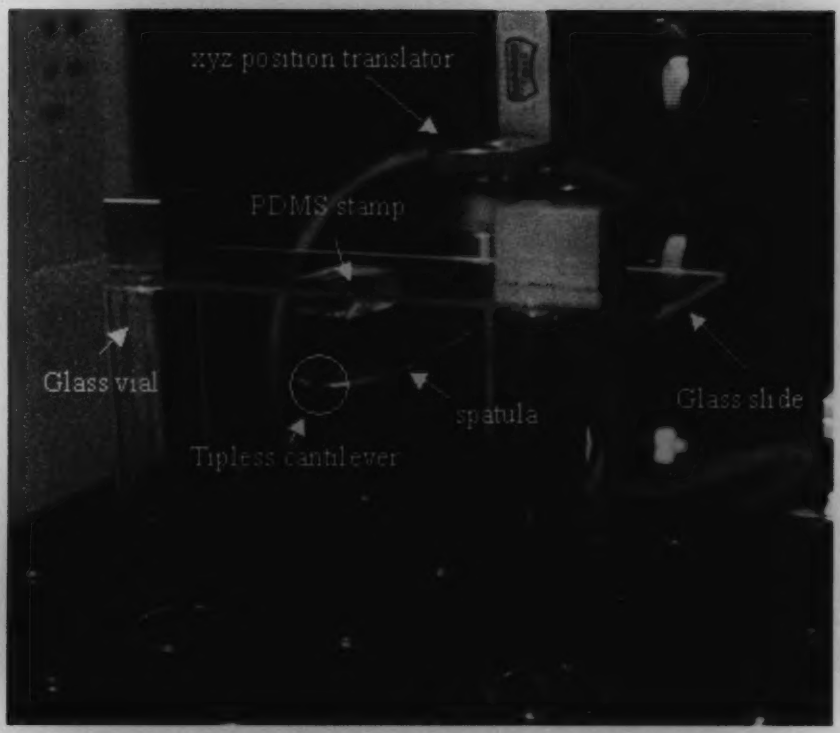

Figure 2.4. Optical micrograph of the patterning setup.

done, the cantilever was brought into contact, using the z translator, with the PDMS stamp. The cantilever remained in contact for 5 minutes, at which time it was separated from the stamp. Figure 2.5 is the optical micrograph captured while the PDMS stamp and the cantilever were in contact.

To avoid contamination from tape residue, the back of the cantilever chip was gently abraded with a piece of filter paper that was wet with ethanol. Then the cantilever chip was immersed into a 1 mM ethanolic solution of MUA for 2 minutes. After immersion in MUA, the cantilever was rinsed by ethanol, followed by drying under a stream of N_2.

2.2.5 Microcontact printing of tip array

Chemical modification of tip array X was also achieved with the contact printing technique. A small piece of PDMS, without any pattern on it, was cut from the piece of PDMS that was prepared from section 2.2.4. The same cleaning procedure mentioned in that section was applied to this PDMS. After the completion of the cleaning procedure, the PDMS was immersed into a 1 mM ethanolic solution of ODT for 1 minute and then dried under a stream of N_2. Tip array X was cleaned in an ozone cleaner for 30 minutes prior for stamping. The stamp was placed on top of tip array X, covering half of the surface, for 3 minutes. It was then immersed in a 1 mM ethanolic solution of MUA for 4 minutes. Upon removal from the MUA solution, the tip array was rinsed with ethanol and dried under a stream of N_2. By doing this half of the tips on the array were ODT modified while the other half were MUA modified.

2.2.6 DPN patterning of cantilevers

The modification of the cantilever 1b was done in an inverted AFM design where a substrate-supported tip was used to modify a tipless cantilever (performed by Shiau-Yin Wu, University of Alberta). To briefly describe the DPN process, a non-contact robotic spotting system (OmniGrid 100, Genomic Solutions) was used to modify the tips of a tip array with 0.1 mM ethanolic ODT. Then the cantilever and the ODT modified tip were brought into close proximity in iCM-AFM.

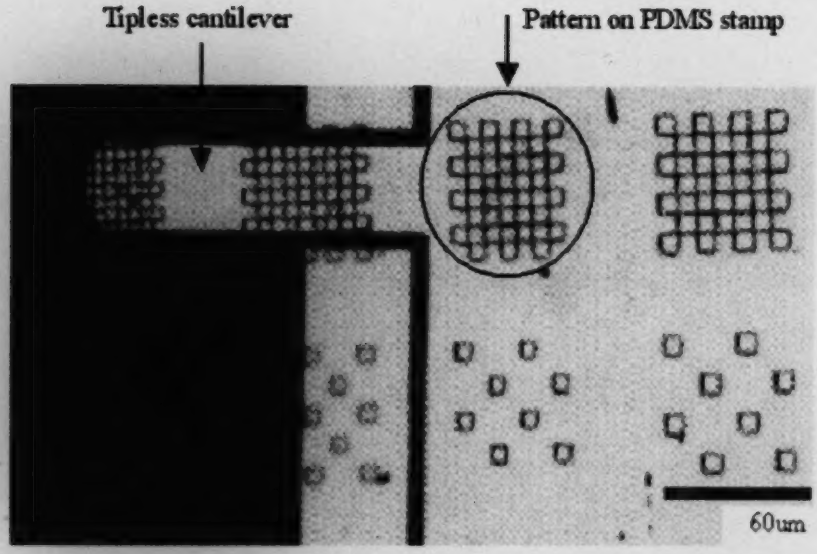

Figure 2.5. Optical micrograph of the position of the PDMS stamp relative to the cantilever.

The humidity of the DPN experiment was controlled by pumping N_2 gas through water into the AFM chamber. The relative humidity and the temperature were between 80 % and 90 %, and about 23 °C, respectively. The tip was scanned at a rate of 2 μm/s and had scanned over the same area (1 μm^2) for 26 times continuously. The cantilever was then immersed into a 1 mM ethanolic solution of MUA for 5 minutes, followed by rinsing with ethanol and dried under a stream N_2.

2.2.7 Imaging

Note: all of the AFM images in the results and discussion section have been plane fitted and flattened by the Nanoscope software to remove imaging artifacts, care was taken not to introduce additional flattening artifacts. Flattening the images renders the average and the slope of each scan line equal to zero.

2.2.7.1 Conventional

Friction: Cantilever 3 was used in the friction force microscopy (FFM) to verify the patterning on cantilevers 1a and 1b in the conventional orientation (i.e. cantilever 3 on top and cantilevers 1a and 1b on bottom). The tip was scanned at a rate of 5 Hz and the images were composed of 512 x 512 data points. Topography, friction images of the tip scanned in the trace and retrace directions were captured. The friction images that present in section 2.3.1 and section 2.3.2 had been modified by the trace minus retrace function from the Nanoscope software in order to remove topographic artifacts, i.e. change in slope, and light interference in the images.

Tapping Mode: Cantilever 2b was excited to oscillate at its resonant frequency and the phase shift was set to 0° when the cantilever was freely oscillating. The free amplitude was 2.25 V (rms volts) and the amplitude set point was 1.5 V. The scan rate of the cantilever was 1.4 Hz and the number of data points for the topographic and phase images were 512 x 512.

2.2.7.2 Inverted

Cantilever 1a and 1b were excited to oscillate at their resonant frequencies and the free amplitude was 1.9 V (rms volts). Phase shift was set to 0° when the cantilever was freely oscillating. The scan rate of the cantilevers was 0.9 Hz and

the amplitude set points varied when different tip arrays and cantilever 2b were used. The number of data points for the topographic and phase images were also 512 x 512.

2.2.8 Amplitude distance

Amplitude-distance, A(d), curves were acquired in both conventional and inverted orientations. In the conventional orientation, cantilever 2a was positioned above cantilever 1c so that the imaging tip was located ~2 μm from the end of the tipless cantilever. In the inverted orientation, the same Si tipless cantilever was used with the 4 different kinds of tips (3 tip arrays and 1 cantilever as mentioned in section 2.2.2). The tipped cantilever is now mounted as a substrate. The end of the cantilever was aligned in a manner similar to in the conventional case. The tip was centered under the cantilever and ~1-2 μm from the end of the tipless cantilever.

The remaining steps are identical whether the measurements were in the conventional or inverted orientation. The top cantilever oscillated at its resonant frequency, and the free oscillation amplitude of the cantilever was set to 2 V (rms volts) when the tip-cantilever separation was ~40 μm. After the tip had engaged in TM, the operating mode was switched to *force calibration mode* and the amplitude-distance and deflection-distance plots were obtained. The number of data points for the approach and retract plots was 8192. The ramp size of the z-piezo excursion was set to 5 μm at a rate of 35 μm/s. No triggering was used, there were no pauses between the approach and the retract cycles, and the cycles were continuously repeated. The stepper motor was used to adjust the z distance between the cantilever and the tip until the cantilever oscillation was reduced to zero. Automate 5 Professional®, an automation software (Network Automation Inc., CA) was used to automatically and repeatedly increment the stepper motor to increase the z distance. The software also allowed the automated capture of the corresponding amplitude-distance and deflection-distance plots after each increment. The automation macro is included in Appendix A for reference.

2.3 Results and Discussion

2.3.1 Micro Contact Printing

Conventional FFM was used to verify the patterning on the μCP tipless cantilever (cantilever 1a). FFM has demonstrated sensitivity to chemical and material properties [22-232425], and it is recognized as a fast and reliable method to examine surface heterogeneity [26]. The conventional topography and friction images are shown in Figure 2.6. The friction image clearly displays a checkerboard pattern similar to the pattern on the PDMS stamp. This supports the assertion that we have modified the cantilever, and that the regions on the cantilever are distinguishable. The chain length of ODT is ~1nm longer than MUA due to the seven extra methylene groups. Therefore, regions modified by ODT should be noticeably higher than the regions modified by the MUA in the topography image. Nevertheless, the topography does not show an agreement with the expectation. At the time of these experiments, the cantilever handling and patterning had not yet developed into reliable routine procedures. Thus, although the friction image confirmed that there was a chemical heterogeneity on the cantilever, it might not necessarily correspond to ODT and MUA, and it is more appropriate to address the lower friction region as the PDMS stamped region, and the higher friction region as the backfilled region. This assignment was based on the pattern, which uniquely identified which region was under the stamp.

After frictional verification of the patterning, the cantilever was probed by a MUA modified tapping tip (cantilever 2b), in conventional TM-AFM to obtain the topography and phase image shown in Figure 2.7. The phase angle was at 0^{o} when the cantilever was freely oscillating.

The bright area in Figure 2.7B corresponds to the backfilled regions. The phase contrast between the modified and backfilled regions is most likely due to the change of tip-sample interactions in the different regions as equation (2.3) shows that the phase shift is proportional to the force derivatives acting on the tip. Although the contrast in the phase image is not as obvious as it is in the friction

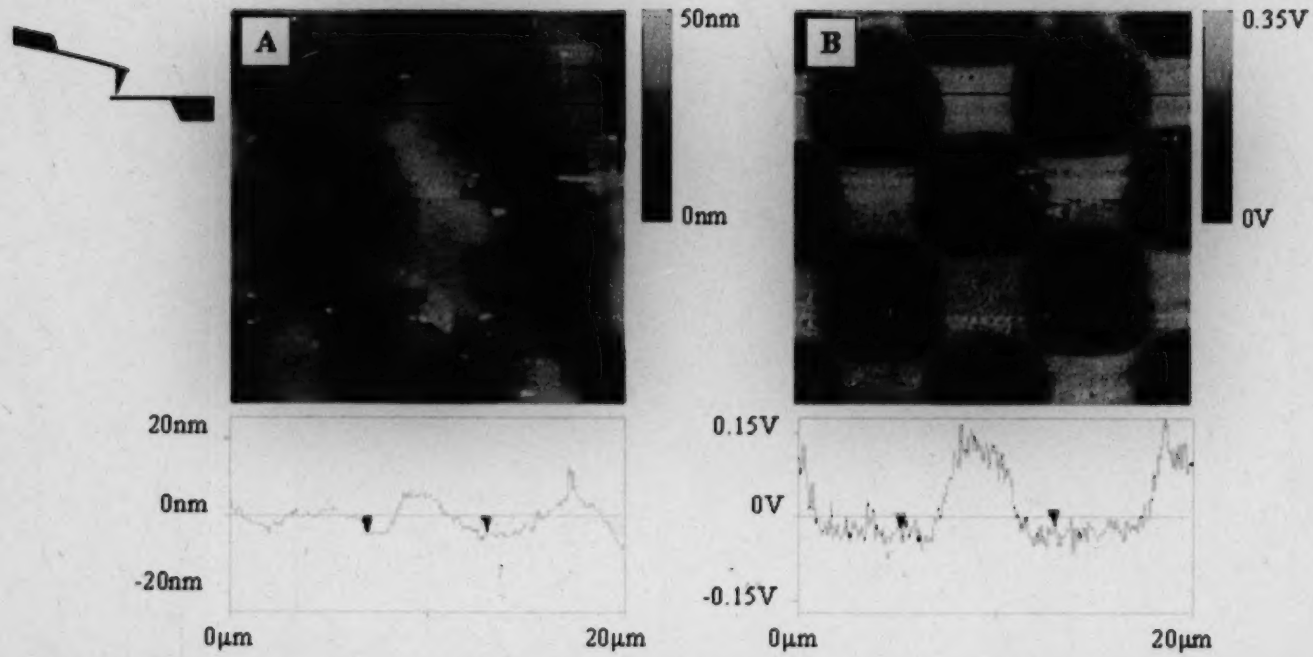

Figure 2.6. (A) Topography and (B) friction (trace minus retrace) image of cantilever 1a by AFM in conventional orientaion. The scan size is 20μm x 20μm. Cross-sectional profiles correspond to (A) height and (B) friction on horizontal line as shown in the images.

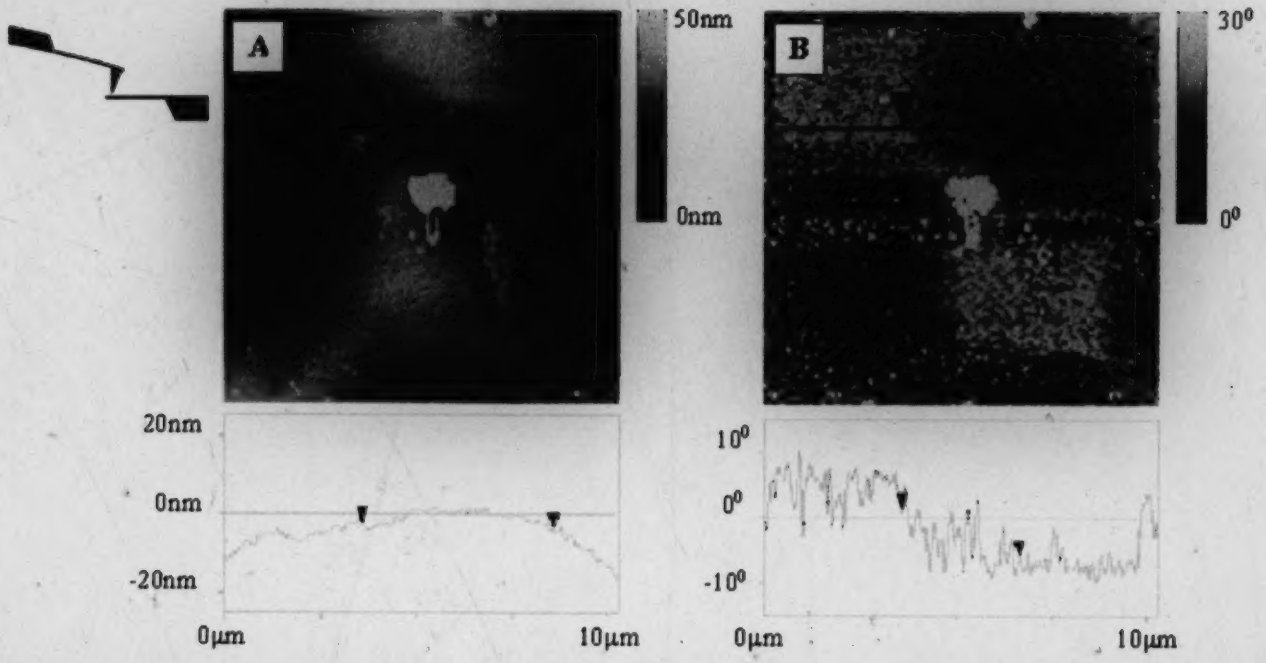

Figure 2.7. (A) Topography and (B) phase image of cantilever 1a by AFM in conventional orientation. The scan size is 10μm x 10μm. Cross-sectional profiles correspond to (A) height and (B) phase lag on horizontal line as shown in the images.

image, the phase difference between the modified and backfilled regions is still observable and measurable. The phase difference between the modified and backfilled regions was found to be about 10^{o} according to the section analysis provided in the Nanoscope software.

Note that the topography (Figure 2.7A) does not correlate to the phase image except for the tall feature at the centre of the image which is consistent with the assertion that the phase contrast in Figure 2.7B is due to the chemical inhomogeneity on the surface.

The results that will be shown in this section were performed in the inverted orientation, where the tipless cantilever was mounted to the cantilever holder and was probed by substrate-supported tips. Figure 2.8 shows the corresponding topography and phase image. Note that Figure 2.8 is the mirror image of Figure 2.6 and Figure 2.7 because the left-right orientation on a surface is reversed when it is changed from the conventional design to the inverted design.

Also note that the phase contrast on the top part of Figure 2.8B does not resemble the pattern. We hypothesize that this is due to a change in the tip chemistry, perhaps the tip temporarily picked up some particles in the beginning and lost them during the scanning process. When a particle is stuck on the tip, it alters the tip properties, making it difficult to distinguish the chemical composition on a surface. However, when the tip was scanning over that tall feature in the middle of the image, the particle that was attached to the tip was removed, leaving a more stable, possibly MUA modified tip imaging the cantilever.

Experiments using ODT modified tip and ODT modified substrate-supported tip to probe the patterned tipless cantilever in conventional AFM and i-AFM were also performed. However, such experiments did not produce a noticeable contrast in the phase images. Rationale for this observation could be the relatively small interaction of ODT modified tip to either regions in air. Thus, AFM images obtained from those experiments will not be presented here

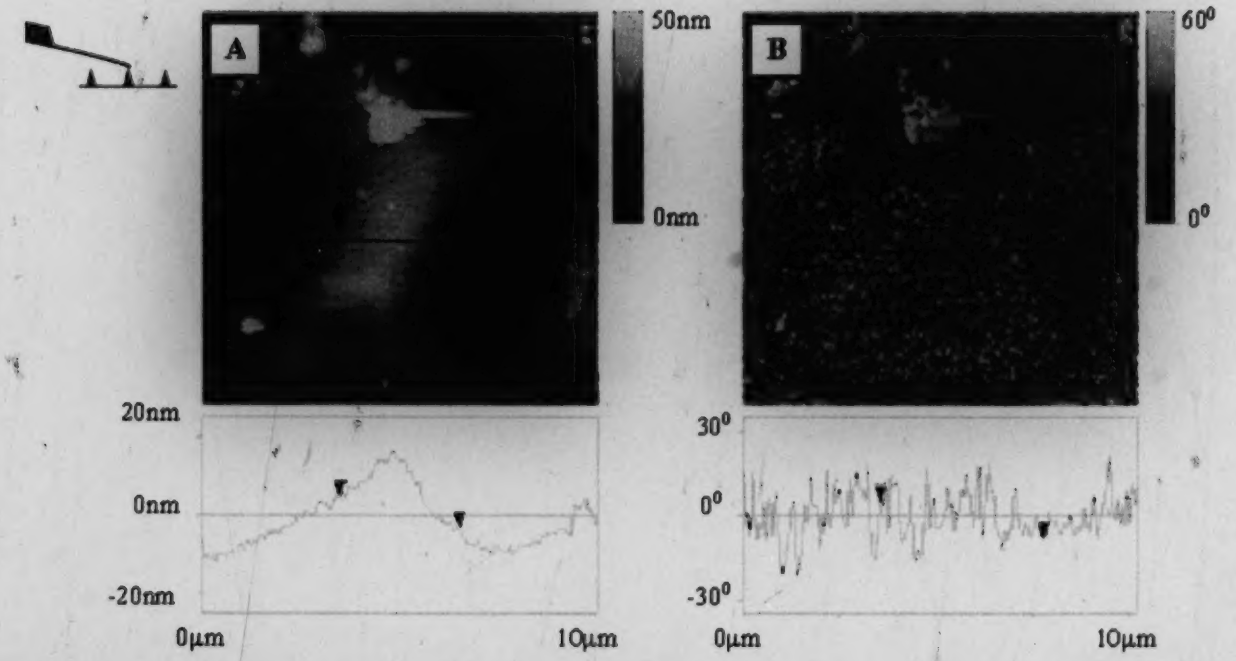

Figure 2.8. (A) Topography and (B) phase image of cantilever 1a by AFM in inverted orientation. The scan size is 10μm by 10μm. Cross-sectional profiles correspond to (A) height and (B) phase lag on horizontal line as shown in the images.

2.3.2 DPN patterning of cantilevers

A DPN patterned tipless cantilever (cantilever 1b) was used to conduct more iTM-AFM experiments. The cantilever was probed by a Si_3N_4 tip (cantilever 3) prior to patterning to ensure that the surface was clear of undesired particles. Then it was patterned using ODT modified tip in contact mode in the inverted design, and backfilled with MUA. After patterning, the cantilever was characterized by the same Si_3N_4 tip (cantilever 3) that was used in the verification of the μCP cantilever, to verify the pattern using FFM. Figure 2.9 is the topography and friction image of the DPN patterned cantilever.

The square is clearly shown in the friction image but not in the topography with 20 nm scale. However, the average section shows that the area inside the square is lower than its surrounding. This observation contradicted the expectation that the ODT modified square should appear higher than the MUA backfilled region. As discussed above, at the time when this experiment was conducted, the surface modification technique had not yet been fully developed, and surface contamination led to unpredictable and irreproducible patterning. Nevertheless, contrast in friction image shows heterogeneity on the cantilever surface. Thus, although the surface might not be ODT and MUA modified, the presence of surface heterogeneity was good enough for demonstration purposes.

2.3.3 Effect of Tip Height

Sputtered gold-coated tips with various tip heights (section 2.2.2) were used to probe the cantilever in iTM-AFM after the pattern had been verified. The topography and phase image obtained by imaging the DPN patterned cantilever with tip A are shown in Figure 2.10. Once again, images captured in i-AFM are mirror image of the ones captured in the conventional AFM. The fact that topography of AFM image is a convolution of the tip shape and the surface is clearly illustrated in Figure 2.10A, where the wide radius of curvature of tip array A broadened the surface structure or the particles that lie on the cantilever in the topography and the phase image. Therefore, it is important to have the knowledge of the tip geometry in order to accurately extract information from AFM images; otherwise it might lead to a false interpretation of the actual surface.

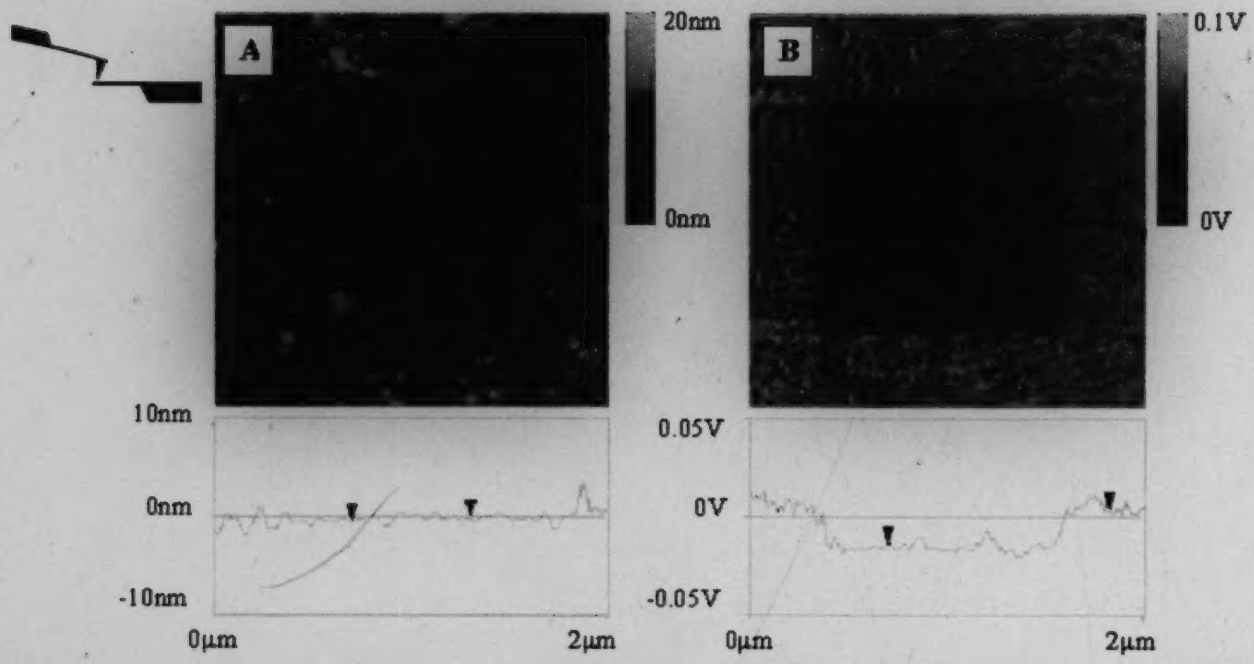

Figure 2.9. (A) Topography and (B) friction image of cantilever 1b by AFM in conventional orientation. The scan size is 2µm x 2µm. Cross-sectional profiles correspond to (A) height and (B) friction on horizontal line as shown in the images.

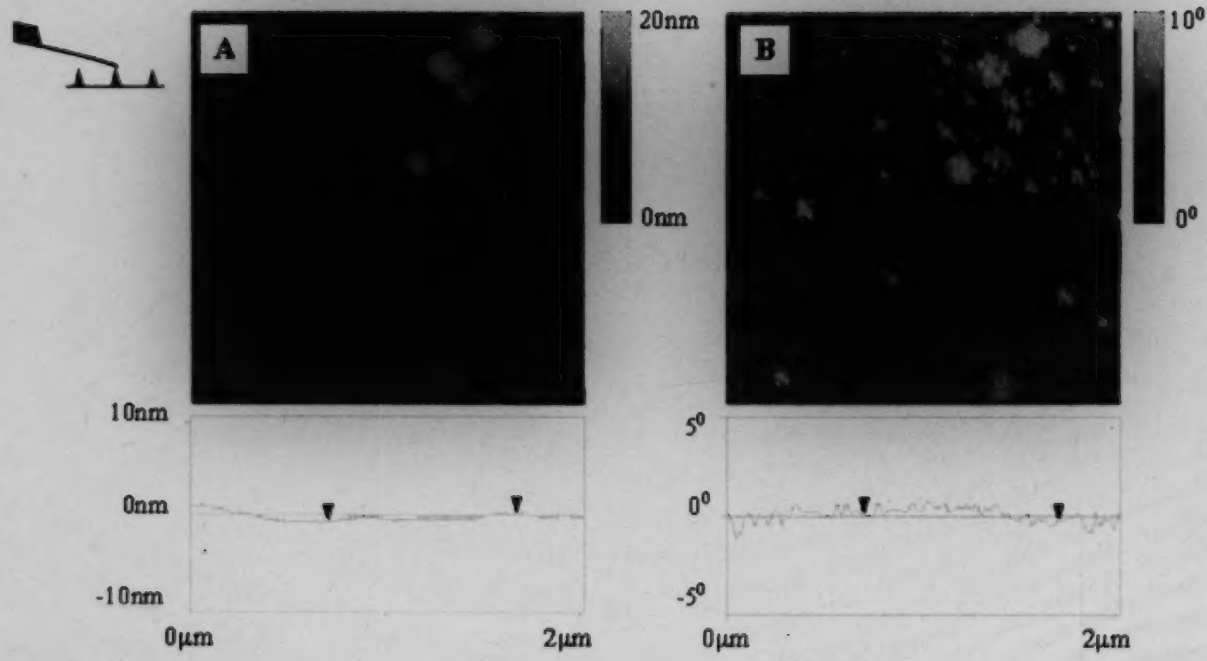

Figure 2.10. (A) Topography and (B) phase image of cantilever 1b by AFM in inverted orientation. Probed by tip array A. The scan size is 2μm x 2μm. Cross-sectional profiles correspond to (A) height and (B) phase lag on horizontal line as shown in the images.

Figure 2.11 shows the topography and phase image captured from tip array B imaging the DPN patterned cantilever. Among all of the substrate-supported tips, tip array B has the smallest tip radius of curvature (~30 nm). It is obvious that the features shown in Figure 2.11A are smaller than those appear in Figure 2.10A. This observation also supports the statement made earlier: dull tip makes a surface looks broader than it actually is.

Figure 2.11A shows that the surface is more uniform within the modified area compared to the backfilled area. Section analysis of the topography shows that the height difference between the modified region and the backfilled region is about 1 nm. Clearly the inverted TM-AFM is capable of differentiating the two regions on the cantilever, and can be used for compositional mapping.

Next, the tip with tip height of ~2 μm (tip array O) was used to image the DPN patterned cantilever. The topography and phase image are shown in Figure 2.12. These images look similar to the ones in Figure 2.11 except that the features in Figure 2.12 appear to be broader. This is again due to the larger radius of curvature of tip O. Notice that the bottom part of Figure 2.12 does not seem to be continuous from the upper part of the image because the tip was too short. As the tip was moving towards the base of the cantilever, the end of the cantilever touched the surface of the substrate and lifted the cantilever above the tip. Instead of the tip imaging the cantilever, the end of the cantilever began imaging the substrate. This phenomenon is illustrated schematically in Figure 2.13.

Due to the fact that the chip holder tilts the cantilever at 10° from the horizontal surface, it is not possible to obtain image with a scan size greater than 12 μm when a short tip, less than 2 μm, is used. The end of the cantilever would eventually bump into the base of the array. Fortunately this problem can be overcome by using taller tips.

2.3.4 Amplitude-distance curves

The difference between the rate of the amplitude-distance curves and the rate of capturing was such that about every third amplitude-distance curves was captured. This allowed the system to briefly equilibrate after each motor step,

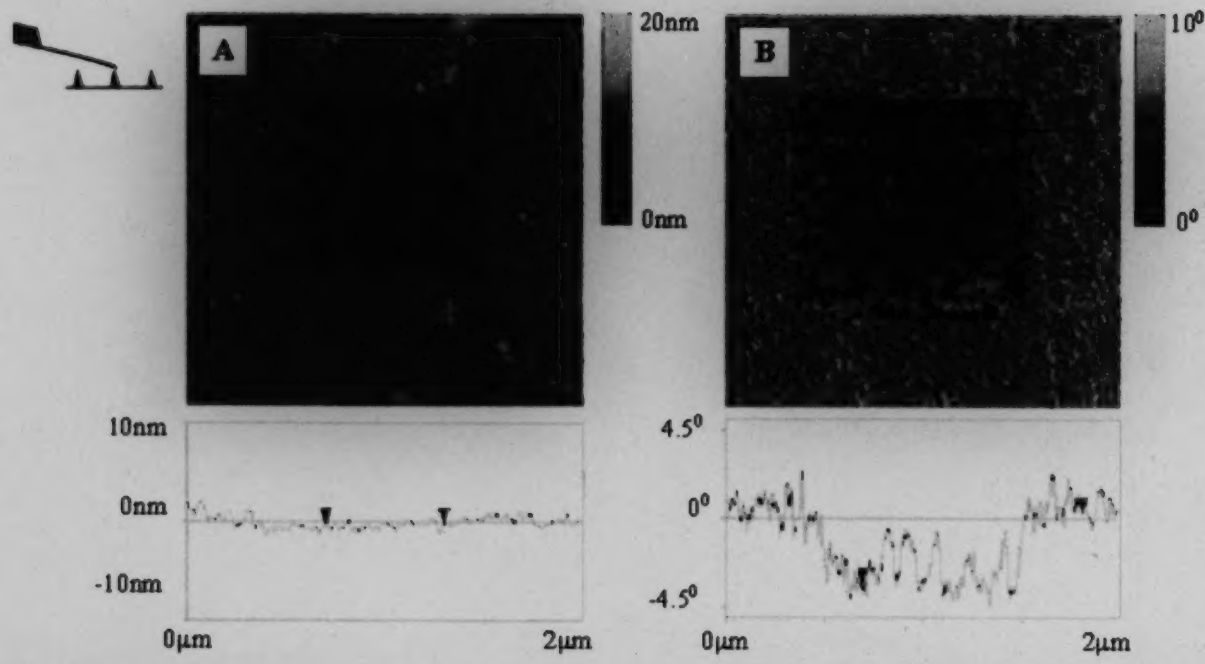

Figure 2.11. (A) Topography and (B) phase image of cantilever 1b by AFM in inverted orientation. Probed by tip array B. The scan size is 2μm x 2μm. Cross-sectional profiles correspond to (A) height and (B) phase lag on horizontal line as shown in the images.

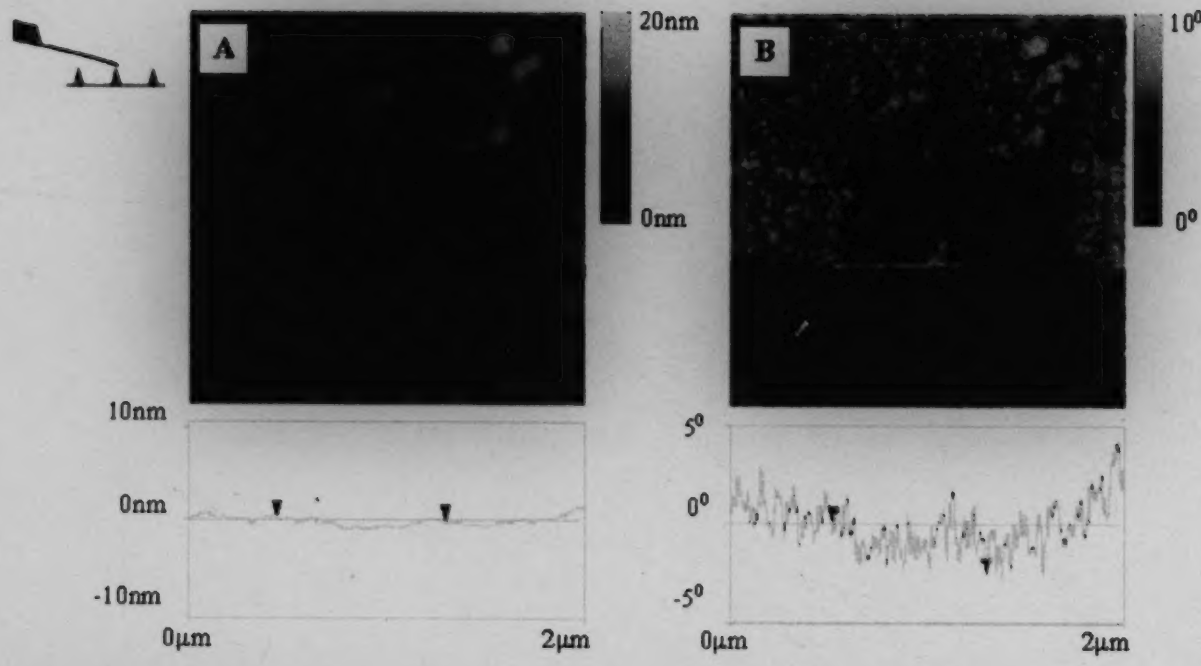

Figure 2.12. (A) Topography and (B) phase image of cantilever 1b by AFM in inverted orientaion. Probed by tip array O. The scan size is 2μm x 2μm. Cross-sectional profiles correspond to (A) height and (B) phase lag on horizontal line as shown in the images.

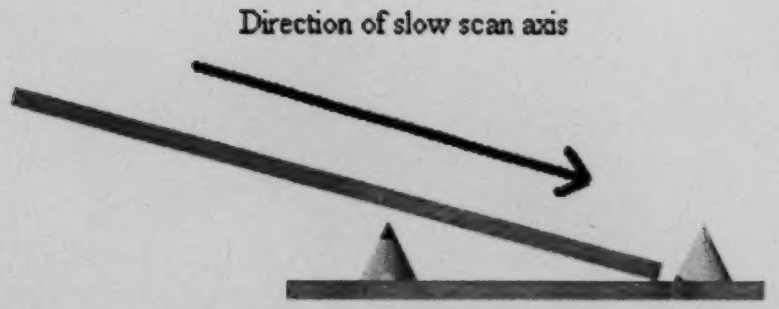

Figure 2.13. Illustration of the edge of a tipless cantilever bumping into the base of the substrate.

ensuring that the amplitude-distance curve was not distorted. Amplitude-distance curves were captured in both conventional and inverted TM experiments. The curves were then processed in Microsoft® Excel to create a continuous and complete amplitude curve from z = 0 μm to z = 50 μm. Figure 2.14 displays a set of amplitude-distance curves measured over tips with different tip heights. For comparison purposes, the y-axes for these plots have all been normalized to the free oscillation amplitude. To understand these curves we should briefly review the behavior of driven and damped harmonic oscillators. The displacement of the oscillator from equilibrium (z) can be expressed by the differential equation:

$$m\frac{d^2z}{dt^2} + b\frac{dz}{dt} + kz = F_o \sin(\omega t). \tag{2.4}$$

The solution to this differential equation can be expressed in terms of the amplitude of the cantilever oscillation as a function of frequency, where the cantilever oscillating amplitude, A, is defined as [27]

$$A = A_0\omega_0^2\left(\frac{1}{\left(\omega_0^2 - \omega^2\right)^2 + \frac{b^2\omega^2}{m^2}}\right)^{1/2}, \tag{2.5}$$

and where A_0, ω_0, ω, b and m are the cantilever amplitude at zero frequency, the resonance frequency of the cantilever, the drive frequency, the damping coefficient and the effective mass of the cantilever, respectively. The amplitude at zero frequency will depend on the amplitude of the drive force F_o. The damping coefficient, b, originates from the sum of all of the dissipating processes that oppose oscillation of the cantilever. In this case that will include the intra-cantilever friction, but at atmospheric pressures, this term will be dominated by fluid dynamic viscous drag of the atmosphere surrounding the cantilever. When the cantilever is far from any other surfaces, this damping will be a constant value; however, as the cantilever approached other surfaces, the extent of the fluid damping will change. Several models have been developed to study these phenomena, known as "squeeze-film damping". In principle one could solve the

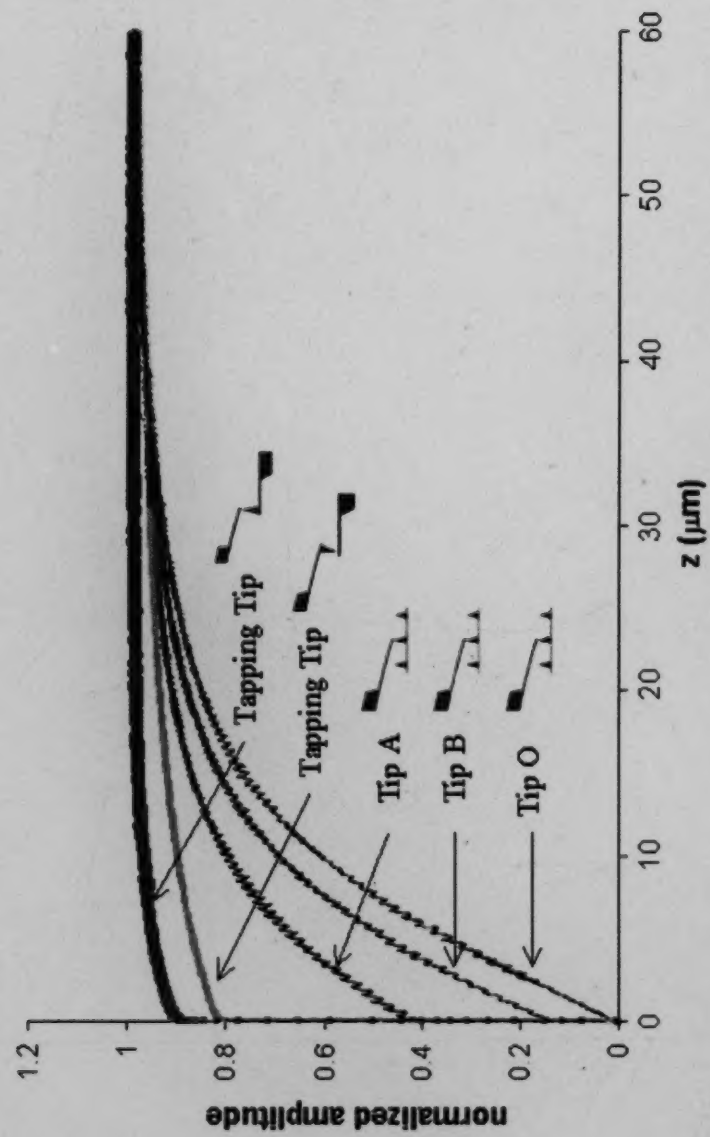

Figure 2.14. Amplitude-distance curves captured in different cantilever-tip combinations and different orientations.

Navier-Stokes differential equations for the appropriate geometry, and determine the effects that the fluid dynamics would have on the oscillating cantilever. However, in practice, approximations and numerical simulations are the methods of choice. Based on some initial investigations into software capabilities and our system geometry, we concluded that the simulation of this oscillating cantilever in close proximity to the tip array is beyond the scope of this thesis. However, there are some models (based on approximations) for simplified geometries that might be instructive for comparison. One such model involves equal sized parallel plates that are driven to oscillate [27-29]. Approximate solutions for this model suggest that the damping coefficient is inversely proportional to the third power of the separation between the plates [27-29]. The cantilever used in iTM-AFM acts very similarly to this squeeze-film damping model except (i) the cantilever is tilted at 10°, (ii) there are tips on the substrate, and (iii) the "plates" are not equal in size. Schematic diagrams of the two models are described in Figure 2.15. Fitting of the theoretical curves over the experimental amplitude-distance curves was attempted. According to this model of squeeze-film damping, the damping coefficient is related to the area of the cantilever, a^2, gas viscosity, μ, and the separation between the cantilever and the base of the tip array, d, in the form of [27]

$$b = \frac{b_0}{d^3} + b_\infty \quad , \quad b_0 = 0.42a^2\mu . \tag{2.6}$$

Here b_∞ is the damping coefficient when the cantilever is far away from the tip array. In order to examine how A is related to d experimentally, equations (2.5) and (2.6) are combined to form a new expression

$$A = A_0\omega_0^{\,2}\left(\frac{1}{\left(\omega_0^{\,2}-\omega^2\right)^2+\left(\frac{b_0}{d^n}+b_\infty\right)^2\frac{\omega^2}{m^2}}\right)^{1/2}, \tag{2.7}$$

where a new term n defines the order of dependence of A on the distance between the cantilever and the tip array. Three parameters b_0, b_∞ and n were adjusted by

Figure 2.15. Illustrations of the model described in squeeze-film damping (left) and i-AFM (right).

regression analysis to find the best-fit to the experimental curve. The drive frequency was the experimental value. The A_0, ω_0 and Q were derived from the fitting of the cantilever spectrum, when it was far from the surface, using the following equation

$$A = \frac{A_0 \omega_0^{\,2}}{\left[\left(\omega_0^{\,2} - \omega^2\right)^2 + \frac{\omega_0^{\,2}\omega^2}{Q^2}\right]^{1/2}}. \qquad (2.8)$$

The results are shown in Figure 2.16. The fitting result shows that b is inversely proportional to one and a half power of distance, which is in variation with the suggested mathematical solutions for the parallel plates model, to the third power. Thus, the observed damping of the cantilever is not well modeled by the parallel plate model for squeeze-film damping. Although the solutions to the parallel plates model does not solely fit our experimental data, the cantilever damping is believed to be related to the separation between the cantilever and the base of the tip arrays. This is illustrated in Figure 2.14, where the shortest tip demonstrates the greatest reduction of oscillation amplitude, and the tallest tip shows little reduction.

2.4 Conclusions

This study shows that chemically heterogeneous samples positioned on a tipless cantilever can be imaged with tapping mode in the inverted orientation. Unfortunately patterning procedures and sample handling issues remain problematic and need to be improve of. Patterning efforts are still too unpredictable and irreproducible for routine operation.

Scanning electron micrographs reveal that the tip heights range from 2 μm to 7 μm for the substrate-supported tips and 20 μm for the tapping tip. The amplitude-distance curves indicate that there was severe damping of the oscillating cantilever even when it was far above the substrate. The reduction of the cantilever's oscillation amplitude is related to the tip height in a way that the shortest tip showed the most severe damping. Fitting of the experimental amplitude-distance curves resulted in a $1/d^{1.5}$ dependence to the damping

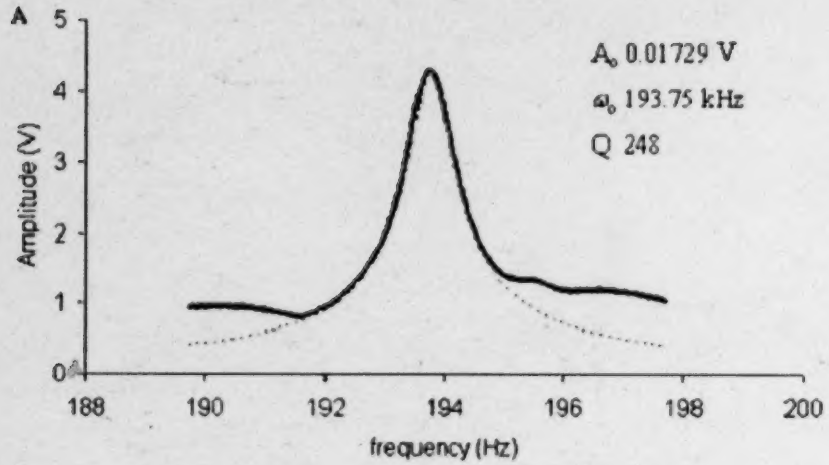
A
Amplitude (V)
frequency (Hz)
A_o 0.01729 V
ω_o 193.75 kHz
Q 248

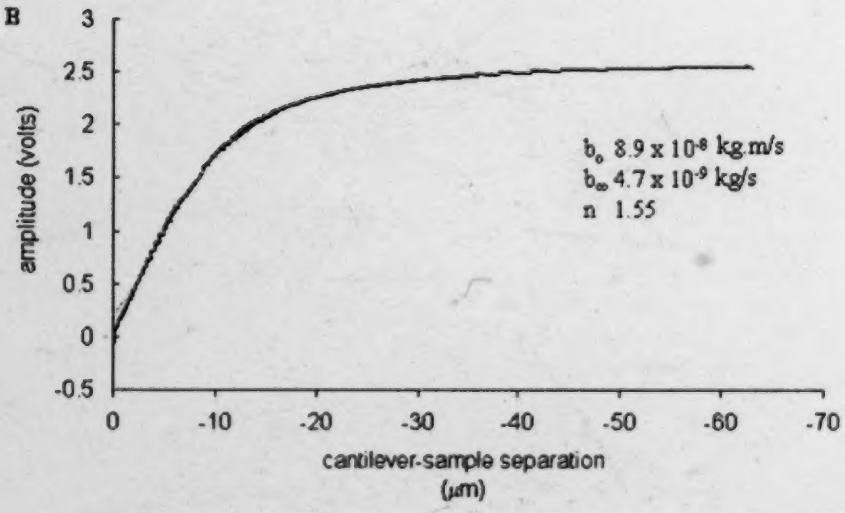
B
amplitude (volts)
cantilever-sample separation (μm)
b_o 8.9 x 10^{-8} kg.m/s
b_∞ 4.7 x 10^{-9} kg/s
n 1.55

coefficient. This is not consistent with the parallel plate model for squeeze-film damping, which predicted a $1/d^3$ dependence. The reason for this disparity is as yet unknown, but we think that this may be the result of our more complicated geometry. Investigations on the oscillation damping are still ongoing by other group members. Increasing tip heights clearly minimizes the magnitude of the damping, so tapping mode AFM is completely accessible to the inverted AFM orientation, and while taller tips are likely to produce identical results to the conventional design, smaller tips still allow routine imaging of the sample.

2.5 References

1 Binnig, G.; Quate, C. F.; Gerber, C. *Phys. Rev. Lett.* **1986**, *56*, 930.

2 Ramana, C. V.; Smith, R. J.; Hussain, O. M.; Julien, C. M. *J. Vac. Sci. Technol. A* **2004**, *22*, 2453.

3 Blach, J. A.; Watson, G. S.; Busfield, W. K.; Myhra, S. *Polym. Int.* **2002**, *51*, 12.

4 Vezenov, D. V.; Noy, A.; Lieber, C. M. *J. Adhes. Sci. Technol.* **2003**, *17*, 1385.

5 Green, J. B. D.; Novoradovsky, A.; Park, D.; Lee, G. U. *Appl. Phys. Lett.* **1999**, *74*, 1489.

6 Zubritsky, E. *Anal. Chem.* **2000**, *72*, 761A.

7 Green, J. B. D.; Lee, G. U. *Langmuir* **2000**, *16*, 4009.

8 ThermoMicroscopes

9 Elings, V.;Gurley, J. US Patents Nos. 5412980 and 5519212, **1995**.

10 Noy, A.; Sanders, C. H.; Vezenov, D. V.; Wong. S. S.; Lieber, C. M. *Langmuir* **1998**, *14*, 1508.

11 Lysetska, M.; Knoll, A.; Boehringer, D.; Hey, T.; Krauss, G.; Krausch, G. *Nucleic Acids Res.* **2002**, *30*, 2686.

12 Feng, J. Y.; Weng, L. T.; Chan, C. M.; Xhie, J.; Li, L. *Polymer* **2001**, *42*, 2259.

13 Finot, M. O. and McDermott, M. T. *J. Am. Chem. Soc.* **1997**, *119*, 8564.

14 Howard, A.J.; Rye, R. R.; Houston, J. E. *J. Appl. Phys.* **1996**, *79*, 1885.

15 Magonov, S. N.; Elings, V. B.; Whangbo, M.-H. *Surf. Sci.* **1997**, *375*, L385.

16 Zhong, Q.; Inniss, D.; Kjoller, K.; Elings, V. B. *Surf. Sci.* **1993**, *290*, 1.

17 Yu, M.; Ivanisevic, A. *Biomaterial* **2004**, *108*, 4289.

18 Rogers, B.; Manning, L.; Sulchek, T. Adams, J. D. *Ultramicroscopy* **2004**, *100*, 267.

19 Khaget, M.; Khulbe, K. C.; Matsuura, T. *J. Membrane Sci.* **2004**, *238*, 199.

20 Mabry, J. C.; Yau, T.; Yap, H.-W.; Green, J.-B. *Ultramicroscopy* **2002**, *91*, 73.

21 Graham, D. J.; Price, D. D.; Ratner, B. D. *Langmuir* **2002**, *18*, 1518.

22 Mate, C. M.; McClelland, G. M.; Erlandsson, R.; Chiang, S. *Phys. Rev. Lett.* **1987**, *59*, 1942.

23 Moon, S. H.; Swearingen, S.; Foster, M. D. *Polymer* **2004**, *45*, 5951.

24 Brewer, N. J.; Leggett, G. J. *Langmuir* **2004**, *20*, 4109.

25 Ara, M.; Tada, H. *Appl. Phys. Lett.* **2003**, *83*, 578.

26 Gnecco, E.; Bennewitz, R.; Meyer, E. *Phys. Rev. Lett.* **2002**, *88*, Art. No. 215501.

27 Andrews, M.; Harris, I.; Turner, G. *Sensors and Actuators A* **1993**, *36*, 79.

28 Blech, J. J. *J. of Lubrication Tech.* **1983**, *105*, 615.

29 Serry, F. M.; Neuzil, P.; Vilasuso, R.; Maclay, G. J. *Electrochem. Soc. Proc.* **1995**, *95*, 83.

CHAPTER 3

PULSED FORCE MODE INVERTED ATOMIC FORCE MICROSCOPY

3.1 Introduction

Pulsed-force mode (PFM) [1,2] has been recently developed as an add-on module for the commercially available atomic force microscope (AFM). The main functions of PFM are to (i) determine the adhesion between the tip and the sample, (ii) map the sample stiffness and (iii) simultaneously collect the topographical data [1-3]. There are a numerous ways to measure the adhesive force between the tip and the sample using AFM. For instance, force verses distance curves [4-6], force volume (FV) [7-9] and phase imaging in tapping mode (TM) [10]. However, these methods have some limitations, such as poor lateral resolution, slow data acquisition, a large amount of required memory space for data storage, and the complication of the quantitative extraction of the adhesion force [1,2,11]. The newly developed PFM has the capability to overcome these limitations by employing the sample-and-hold circuit in which the most useful data is acquired and analyzed [1]. In addition, PFM can acquire thousands of force curves per second, which is hundred times faster than the conventional force-distance curve measurements.

Despite being newly (1997) developed, the PFM-AFM, possessing the advantages of the contact mode (high scan speed), the force-distance curve (mapping adhesion), and the tapping mode (elimination of the lateral shear force), has found its applications in many research fields [12-15]. Fujihira and his co-workers have performed a substantial amount of studies on surface characterization using the PFM-AFM [2,16-23]; many of these studies focused on interactions between self-assembled monolayers (SAM) of COOH- and CH_3-functionalized tip and surface [17-20]. They have demonstrated that the adhesive force mapping by PFM-AFM has the ability to discriminate different functional groups of a surface both in ambient air and in pure water [17], and that the

and that the adhesion measured between a tip and a surface is dependent on the chemistry and the contact area [18,20].

As it has been mentioned in chapter two that the inverted AFM (i-AFM) [24] has the capability for high-speed imaging between different chemistry combinations with the modified tips and tipless cantilever. The aim for this research project is to investigate the plausibility of combining the PFM with the i-AFM to develop an instrumentation method that is competent to perform ultra high-speed force measurements.

In PFM-AFM, a function generator sends out a sinusoidal voltage to the z piezoelectric transducer (z-piezo) which causes vibration of the z-piezo at a variable frequency of 100 Hz to 2 kHz with an adjustable amplitude of 10 nm to 500 nm [1,2,25]. The z modulation is chosen to oscillate below 2 kHz because the scanning system, i.e. the piezo and the cantilever, can be excited to produce disturbing resonance at higher frequency, which might interfere with the topography and adhesion data [25]. The PFM-AFM is also connected to an oscilloscope that is used to monitor the response of the cantilever during the experiment. By observing the cantilever deflection (force signal) as a function of time on the oscilloscope, one can select the points-of-interest from the trace, which later defines the topography and adhesion. A picture of the front panel of the PFM modulator is shown in Figure 3.1. The top and the bottom displays on the left hand side of the unit show the z modulation frequency in Hertz and the percentage of the maximum amplitude, respectively, and the knobs beside them are used to adjust their values.

The knobs in the *Trigger Module* are triggers for the sample-and-hold circuits at the points-of-interest. The positions of the triggers are indicated in a typical force-versus-time curve shown in Figure 3.2. The curve simply reflects the response of the cantilever in each of the modulation cycle. Because the PFM unit modulates the z-piezo and in turn the sample stage, it is more appropriate to describe the tip-sample distance as the sample moves towards and away from the tip rather than the tip moving towards and away from the sample. When the sample is far from the tip, the cantilever is at its equilibrium position, as denoted

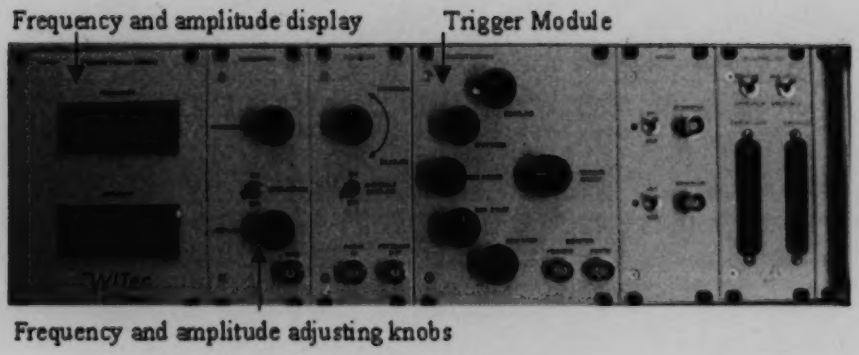

Figure 3.1. Front panel of a PFM unit.

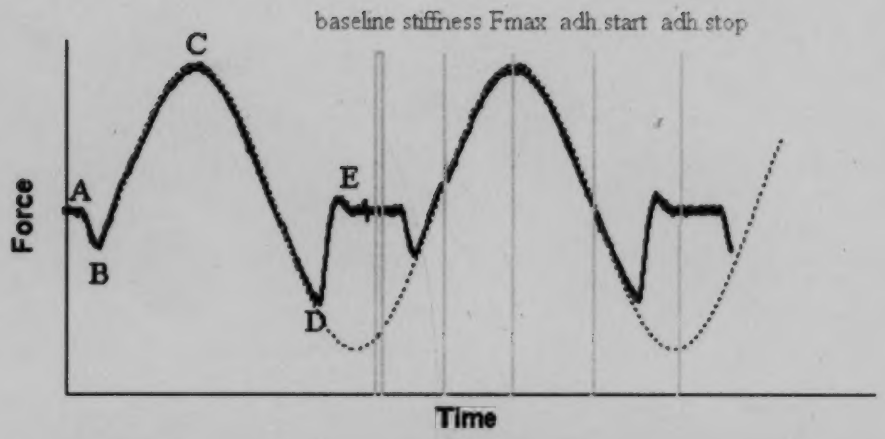

Figure 3.2. Typical force-versus-time curve obtain in PFM measurement and the corresponding positions of the triggers. The dotted line represents the output voltage from PFM that modulates the z-piezo and the solid line represents the response of the cantilever.

by (A) in Figure 3.2, where the cantilever is bending neither upward or downward. As the sample moves closer to the tip, long-range electromagnetic interactions between them cause the cantilever to bend towards the sample and eventually snap into contact with it at (B). At (C), the sample and the tip experience the most repulsive force, F_{max}. The F_{max} is used in the feedback loop to maintain a constant applied force on the sample by adjusting the z-piezo, and give the topography. The set point of the AFM controls the force between the baseline and the maximum applied force F_{max} [25]. Data for adhesion map is obtained from (D) where the maximum adhesion occurs between the tip and the sample. After being detached from the sample and the subsequent free oscillation of the cantilever, the tip resumes to its equilibrium position at (E). For example, the baseline trigger determines the equilibrium position of the cantilever when it is not interacting with the sample. It is done by averaging the detected signals within the bandwidth of the trigger. By adjusting the trigger to mark the baseline on the oscilloscope trace, all other points-of-interest are in reference to the baseline [25].

3.2 Experimental

3.2.1 Chemicals

Octadecanethiol (ODT) and 11-mercaptoundecanoic acid (MUA) (Sigma-Aldrich) were used for cantilevers and tip arrays modification. Anhydrous ethanol (Commercial Alcohols Inc.) was used in all chemical ethanolic solution and for rinsing. Distilled and deionized 17.4 MΩ cm water from a water purificatoin system (Barnstead) was used throughout the experiment. 49% hydrofluoric acid aqueous solution (Fisher Scientific Company) was used for stripping off SiO_2 layer on the tip arrays. Sylgard 184 silicone elastomer and sylgard 184 curing agent (Dow Corning) were used for the fabrication of polydimethylsiloxane (PDMS) stamp. Hexane (EMD Chemicals Inc., Germany) was used for the cleaning and purification of the PDMS stamp. Purified N_2 gas for drying was used throughout the experiment. Piranha solution (1:3 H_2O_2/H_2SO_4, Fisher Scientific Company) was used for Si wafer cleaning.

3.2.2 Silicon chip, cantilevers and tip arrays

These experiments made use of 1 Si chip, 3 different kinds of cantilevers and 1 kind of tip array. The Si chip was diced from a 4" Si wafer and had dimensions of 1 cm x 1 cm. It was coated with ~5 nm of Cr and ~20 nm of Au and was chemically modified by μCP (details of the chemical modification of Si chip are covered in section 3.2.5). It was imaged in conventional friction force microscopy (FFM), FV and PFM. The assigned names for the cantilevers, their manufacturer specified characteristics, chemical modification and the types of experiments they were involved in this work are presented in Table 3.1. Cantilevers 1a was Au-coated and chemically modified by μCP (details of the chemical modification of cantilever 1a are covered in section 3.2.4). It was imaged in FFM in the conventional orientation and PFM in the inverted orientation. Cantilever 1b was also Au-coated and chemically modified by the immersion of the cantilever into 0.3 mM ethanolic solution of MUA. It was imaged in FV and PFM in the inverted design. Cantilever 2 was used as received from the manufacturer for the characterization of the patterned cantilever (cantilever 1a) and Si chip in conventional FFM. Cantilever 3 was also used as received for the adhesion mapping of the Au-coated chip in FV and PFM in the conventional orientation.

The tip arrays were microfabricated by Dr. J.-B. Green (as described in Ref. [26]) at the Cornell Nanofabrication Facility. The silicon dioxide (SiO_2) layer (~2 μm thick), which was remained on the tip arrays after the fabrication to protect the tips from being damaged, was removed by the immersion of the tip arrays in HF for more than 20 minutes, followed by rinsing with water and dried under a stream of N_2 before they were used.

Two tip arrays came from the same wafer of tip arrays were used for the adhesion mapping of the tipless cantilevers (cantilevers 1a and 1b) in the inverted design. Scanning electron micrograph (Figure 3.3, captured at 87° to the plane normal) of one of the tips from the tip array shows that the tip radius of curvature is ~30 nm and the tip height is ~7.8 μm. These tip arrays were coated with Au and

Assigned name[1,2]	Tipped or tipless	Material and shape	Length and thickness	Spring constant	Chemical modification	Experiment
1a	Tipless	Si Rectangular	110 μm 2 μm	0.95 N/m	Au-coated μCP	Conventional FFM and inverted PFM
1b	Tipless	Si Rectangular	250 μm 2 μm	0.65 N/m	Au-coated Immersion in MUA	Inverted FV and PFM
2	Tipped	Si_3N_4 V-shaped	90 μm 0.4 μm	0.08 N/m	N/A	Conventional FFM
3	Tipped	Si Rectangular	225 μm 3 μm	2.8 N/m	N/A	Conventional FV and PFM

Table 3.1. Characteristics of the cantilevers that were used in this project. Cantilever geometries were adapted from manufacturer's specification.

[1] Cantilevers 1a, 1b and 2 purchased from MicroMasch.
[2] Cantilever 3 purchased from Veeco Instrumentation Inc.

Figure 3.3. Scanning electron micrograph of a representative tip from a tip array. Image was taken at 87° from the plane normal.

one of them was chemically modified by immersion into a 0.3 mM ethanolic solution of MUA after it was cleaned in ozone (UVO-Cleaner®, Jélight Company Inc.) for 30 minutes. And then rinsed with water and dried under a stream of N_2 before they were used.

Ti and Au deposition on cantilevers 1a and the tip arrays was achieved by sputtering using Kurt J. Lesker Magnetron sputtering system (Nanofab, University of Alberta) under vacuum condition. The system was first pumped down to ~2 x 10^{-6} torr and then filled with Argon gas to ~7 x 10^{-3} torr. Ti worked as an adhesive layer between the substrate and Au. The deposition rates for Ti and Au are 0.03 nm/s and 0.14 nm/s, respectively. Approximately 14 nm Ti and 40 nm Au were deposited on the cantilever and the tip arrays. Cantilever 1b was Cr (worked as adhesive layer between the Si substrate and Au) and Au-coated by thermal evaporation deposition (FTM-2000, Torr International Inc.) under vacuum (5x10^{-6} mbar). The deposition rates were 0.05 nm/s for Cr and 0.03 nm/s for Au. Approximately 9 nm of Cr and 40 nm of Au were deposited on the cantilever.

3.2.3 Instrumentation

All topography and friction images for the Si chip, cantilevers 1a and 1b captured in the conventional orientation were obtained using Nanoscope IV controller equipped with Dimension 3100 scanning probe microscope (Veeco Instruments Inc.). Adhesion mapping in PFM were performed with a PFM Extension (WiTec Instruments Corp.) in combination with a digital storage oscilloscope (Tektronix, Inc.) and a Multimode SPM (Veeco Instruments Inc.) with a Nanoscope IIIa system controller. Adhesion mapping in FV was performed with a Multimode SPM (Veeco Instruments Inc.) with a Nanoscope IIIa system controller, and a digital storage oscilloscope was connected to the SPM.

Scanning electron micrographs were obtained from the scanning electron microscope (SEM) laboratory in the department of earth and atmospheric sciences in the University of Alberta (X-vision, JSM-6301 FXV, JEOL).

3.2.4 Microcontact printing of cantilever

The PDMS stamp used for the μCP of the cantilever was the same as the one that was used in section 2.2.4 and the same cleaning protocol for the PDMS as mentioned in section 2.2.4 was employed. Microcontact printing of the tipless cantilever was achieved in an identical manner as described in section 2.2.4.

3.2.5 Microcontact printing of Au-coated chip

The same PDMS stamp that was used in section 2.2.4 was used to pattern the Au-coated chip, and the same cleaning procedure for the PDMS as mentioned in that section also applied in this case. The patterning procedure was carried out as follows: vertical lines that were 1 mm apart were scratched on the chip. This chip was then cleaned by immersion into piranha solution for 15 minutes, followed by rinsing thoroughly with water and dried under a stream of N_2. The pattern on the stamp was aligned in between the vertical scratch lines. This allowed easy locating of the pattern when it was imaged in the AFM experiments. The stamp and the chip were placed in contact for 5 minutes, in which time the chip was immersed in a 1 mM ethanolic solution of MUA for 2 minutes. It was then rinsed by ethanol and dried under a stream of N_2.

3.2.6 Imaging

Note: all of the AFM images in the results and discussion section have been plane fitted and flattened by the Nanoscope software to remove imaging artifacts, care was taken not to introduce additional flattening artifacts. Flattening the images renders the average and the slope of each scan line equal to zero.

3.2.6.1 Conventional Orientation

Friction: Cantilever 2 was used in the FFM to verify the patterning on the Si chip and cantilever 1a in the conventional orientation (i.e. cantilever 2 on top and cantilever 1a on bottom). The tip was scanned at a rate of 5 Hz and the images were composed of 512 x 512 data points. The friction images of the tip scanned in the trace and retrace directions were captured for the patterned Si chip. The retrace image was subtracted from the trace image to obtain a more accurate friction image for the patterned Si chip.

FV: Cantilever 3 was used to probe the Si chip to obtain force-distance curves. The tip was scanned at a rate of 2 Hz and the topography and adhesion images were composed of 64 x 64 data points while the force-distance curves were also composed of 64 data points. Relative triggering at 0.03 mV was turned on.

PFM: Cantilever 3 was also used to probe the Si chip to obtain PFM adhesion and topographic images. The tip was scanned at a rate of 1 Hz and the images were composed of 512 x 512 data points. The z-piezo oscillation was ~1 kHz.

3.2.6.2 Inverted Orientation

FV: Cantilever 1b was probed by a chemically modified tip array to obtain force-distance curves in the inverted orientation. The scan rate was 2.5 Hz with topographic and adhesion images of 16 x 16 data points and 512 data points for the force-distance curves. Relative triggering at 0.2 V was turned on.

PFM: A tip array was used to probe cantilever 1a with a scan rate of 1 Hz and a chemically modified tip array was used to probe cantilever 1b with a scan rate of 0.8 Hz to obtain topographic and PFM adhesion images. These images were composed of 512 x 512 data points and the z-piezo oscillation was ~1 kHz in both sets of experiments.

3.3 Results and Discussion

This section will begin with an introduction and validation of pulsed force mode characterization of samples in a conventional AFM. This is followed with an experiment that demonstrates the use of PFM with the inverted AFM orientation.

As discussed in the experimental section above, a 1 cm square silicon sample was coated with Au and patterned via μCP. Verification of the μCP modified chip was performed with FFM, and the topographic and friction images are shown in Figure 3.4. Recall that the friction image is actually formed by taking the difference between two lateral force images (one that is the trace and the other that is the retrace). This trace minus retrace image is referred to as a friction image. Based on the pattern of the stamp, the low friction regions (dark

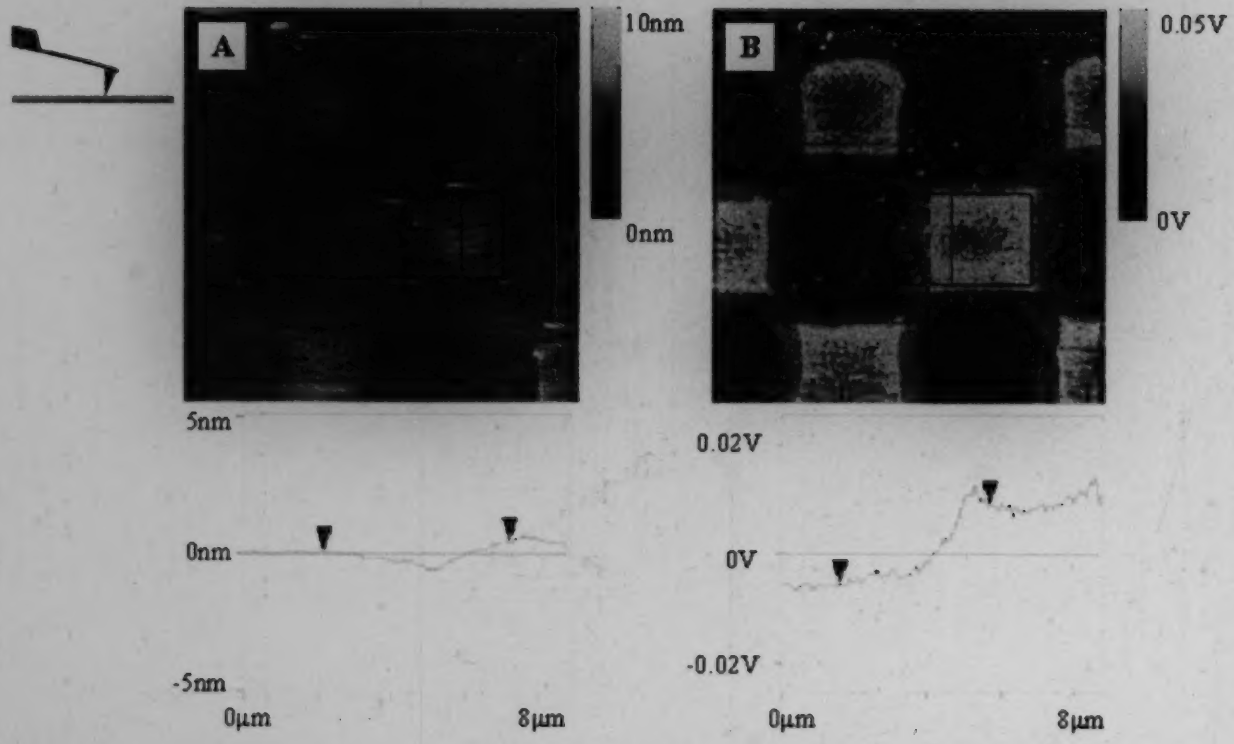

Figure 3.4. (A) Topography and (B) friction image of the patterned chip imaged by AFM in conventional orientation. Friction image was generated by trace minus retrace. Scan size is 15μm x 15μm. Dark contrast in (B) represents lower friction and bright contrast represents higher friction. Cross-sectional profiles correspond to the average (A) height and (B) friction calculated within the box shown in the images

correspond to the area that was stamped, and the high friction regions (bright) correspond to the area that was backfilled. Section analysis of the height data shows that on average the area in the backfilled region is 0.5 nm taller than the stamped region. An ODT monolayer should be ~1nm taller than a MUA monolayer. Thus while the assertion that the stamped region is covered with an ODT monolayer and that the backfilled region is covered with an MUA monolayer is supported by the frictional contrast, it is not supported by the height data. Instead the height data directly contradicts this assertion. In addition, the dark spots in the backfilled region (Figure 3.4B) suggest that the MUA or other contaminants did not form a uniform layer on the chip surface. This could be a result of the formation of multilayers on the backfilled region or some other form of surface contamination. In either case, the sample is heterogeneous, and that was the primary goal of the sample preparation. With this heterogeneous sample prepared, PFM data may be acquired and compared to the more traditional adhesion measurement methods.

The most common form of adhesion measurement with AFM is the force-distance curve. Force volume (FV) imaging involves making force-distance curve measurements at an array of xy locations, thus creating an image of adhesion measurements. The force measurements from the FV were used to compare with the PFM force measurements that were obtained afterward to determine the reliability of the PFM data. Figure 3.5 shows the topography and FV images of the same location, which was shown in Figure 3.4. The adhesion image consists of an array of 64 x 64 (or 4096) force-distance curves. Due to the data collection capabilities of the Nanoscope software, this lateral resolution (64 force-distance curves in 14.8 μm) limited the resolution of the force-distance curves to 64 data points. Higher resolution force-distance curves required sacrificing the lateral resolution, and thus the total number of force-distance curves per image. The force volume image, shown in Figure 3.5, required ~70 minutes to acquire. The force volume shown in Figure 3.5 is consistent with the friction image in Figure 3.4B in that a stronger adhesion between the tip and the surface corresponds to a friction.

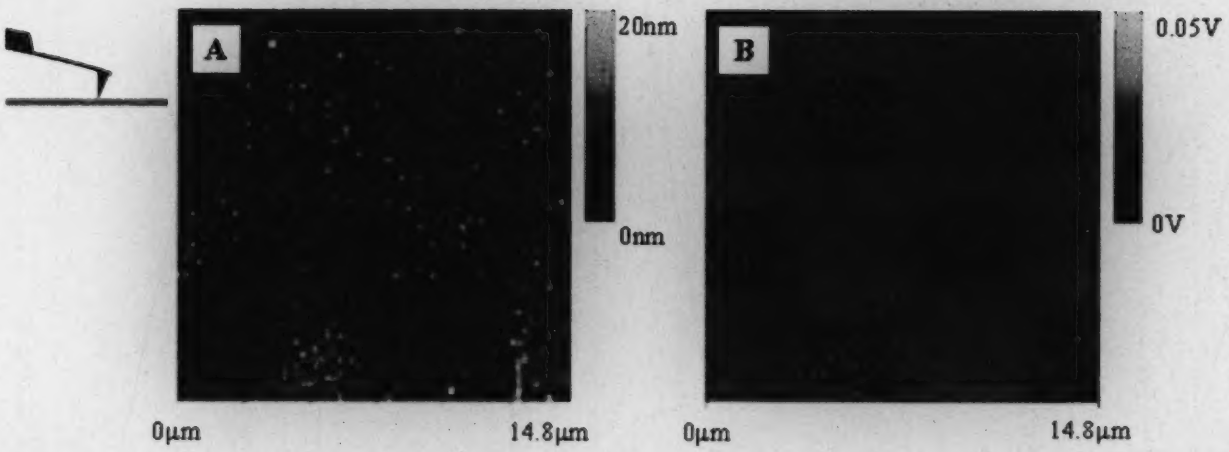

Figure 3.5. (A) Topography and (B) FV adhesion image of the patterned Au-coated Si chip imaged by AFM in conventional orientation. Scan size is 14.8μm x 14.8μm. Adhesion image is composed by 4096 force curves. Dark contrast in (B) represents higher adhesion and bright contrast represents lower adhesion.

Then two close-up FV images with scan size of 100 nm, one within the stamped region and the other inside the backfilled region, were obtained. Each image was composed of an array of 16 x 16 (256) force-distance curves and each force-distance curve had 512 data points. The units of the raw data in the force-distance curves were nanometer for the tip-sample distance and volt for the cantilever deflection. In order to convert the cantilever deflection into a useful unit, in this case the force, F (nN), the following equation was used,

$$F = V \times S \times k \tag{3.1}$$

where V is the measured deflection voltage in volts, S is the detector sensitivity in nm/volt and k is the cantilever spring or force constant in nN/nm. The cantilever sensitivity is defined as the ratio of the distance a cantilever bends to the volts detected by the split photodiodes. The sensitivity is determined from the slope of the force distance curve for the region where the cantilever was in contact with a rigid surface. To this end it was assumed that the chip substrate is a rigid substrate. The cantilever force constant was obtained from the manufacturer's specification. Figure 3.6 presents the force-distance curves measured within the stamped and the backfilled regions. The adhesive forces were determined by taking the difference between the force at the point where the tip broke free from the surface and the force when the tip is not interacting with the surface. In this way each force volume image which produced 256 force-distance curves, also produced 256 values for the adhesion force. Histograms of these adhesion force values are shown in Figure 3.7. As several histograms are presented in this chapter, diamonds will always correspond to data from stamped areas and triangles for data from backfilled areas, and the Gaussian curves are least square fitted Gaussian functions to the adhesion data. The fitting was done by Solver in Microsoft® Excel. It can be seen from the force-distance curves and the histograms that the adhesion distribution is fairly tight for both the stamped and backfilled areas. Furthermore, the results also show that the adhesion between the unmodified tip and the backfilled region is almost three times stronger than the adhesion between the same tip and the stamped region.

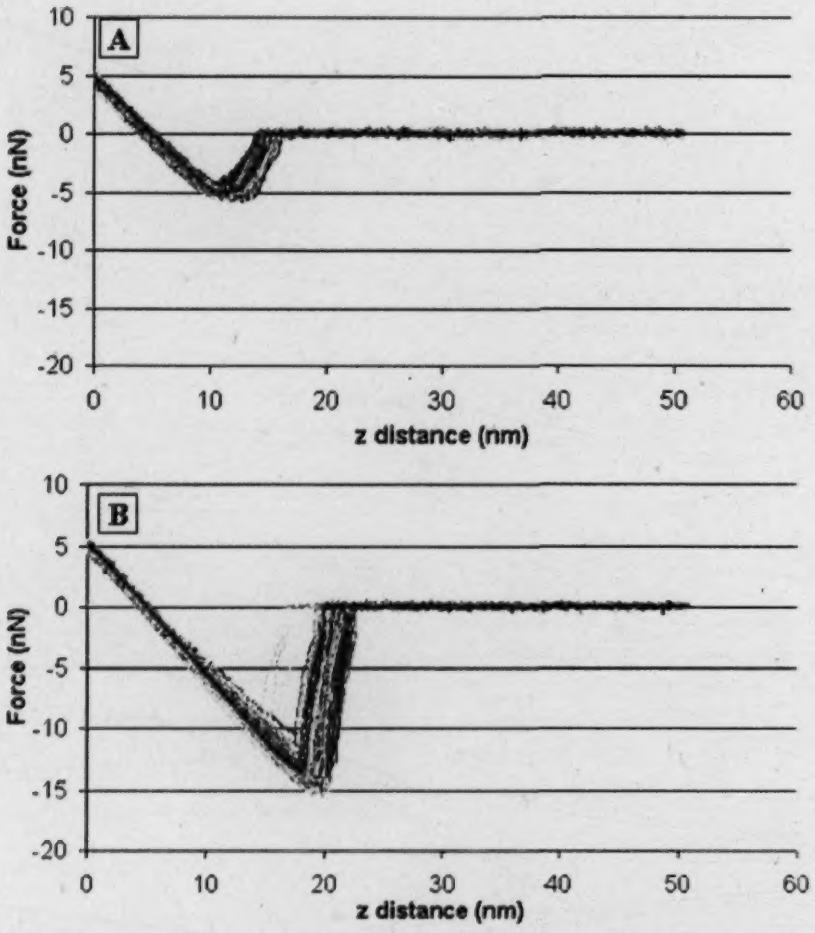

Figure 3.6. Force-distance curves obtained from FV adhesion measurements of the patterned Si chip inside (A) stamped region and (B) backfilled region with 100 nm scan area. Each plot is composed of 256 (retract) force curves and each force curve has 512 data points.

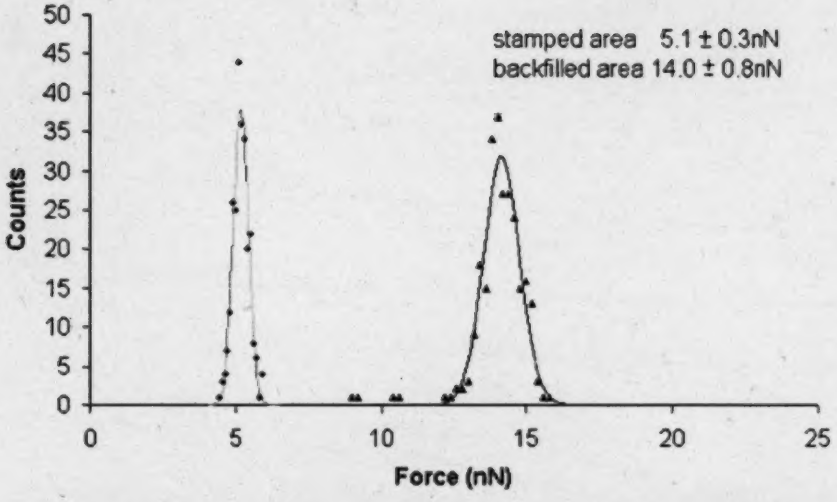

Figure 3.7. Histograms generated from FV measurements inside modified region (diamond) and backfilled region (triangle) of the patterned Si chip. Each histogram is composed of 256 force measurements. The measured average adhesion inside the modified region and the backfilled region are 5.1nN and 14.0nN, respectively.

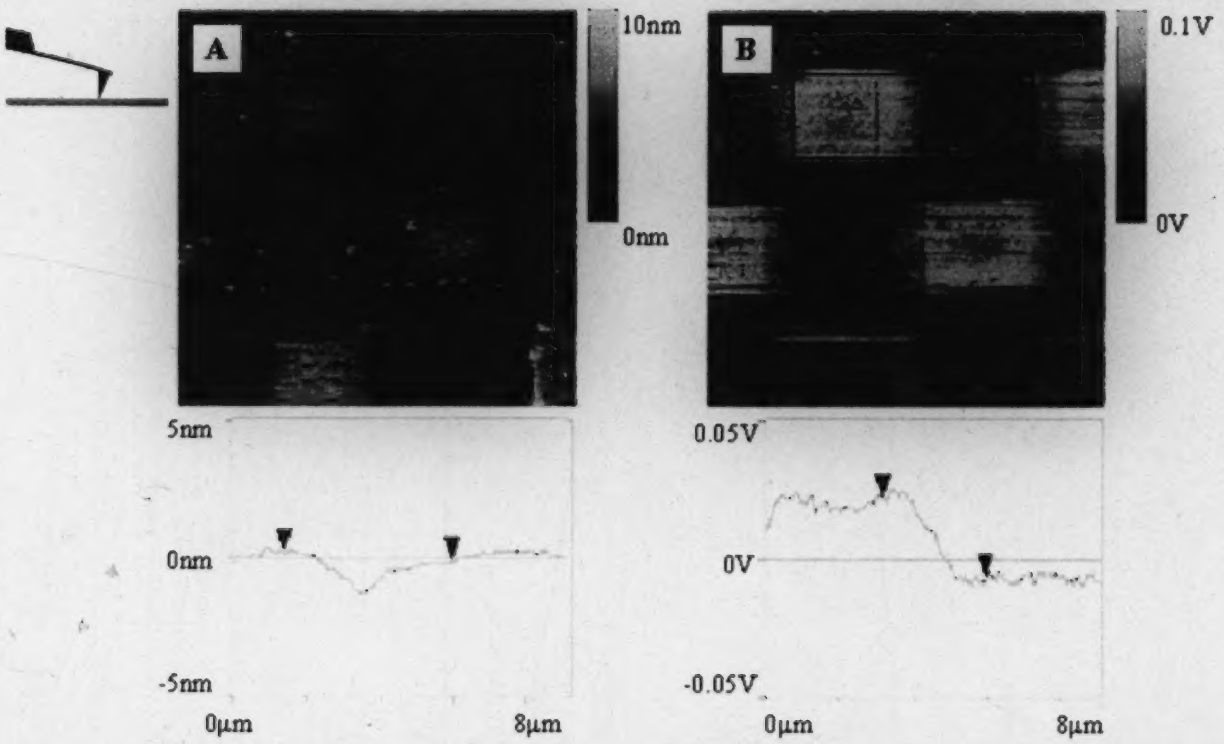

Figure 3.8. (A) Topography and (B) PFM adhesion image of the patterned Si chip imaged by AFM in conventional orientation. Scan size is 15μm x 15μm. Dark contrast in (B) represents lower adhesion and bright contrast represents higher adhesion. Cross-sectional profiles represent average (A) height and (B) adhesion calculated within the box shown in the images

The same area on the chip was then imaged by the PFM. Figure 3.8 which is a representative of many PFM images, was captured at a scan rate of 1 Hz and contains 512 x 512 data points. As a reminder, in PFM the electronics of the PFM module uses triggers to determine various values, such as the average value of the cantilever deflection when it is not interacting, and the minimum deflection of the cantilever during a force-distance curve. While the force-distance curve is not saved in normal operation of the PFM, the electronics are designed to extract the value for the adhesion from each force-distance curve. This deflection voltage is then sent to the Digital Instruments AFM electronics, which maps that voltage onto the xy coordinates, and creates a map of that voltage. The resulting image is called a PFM image, and corresponds to the PFM determined value for adhesion. Thus while each point in the image does not explicitly correspond to a particular force distance curve, in fact there are more force-distance curves than there are data points. The result is a high resolution technique.

The amount of time required to capture the PFM image was less than 10 minutes. Since the z-piezo oscillated at 1,000 Hz, ~600,000 force-distance curve measurements were performed during the time required to obtain this PFM image which is composed of 512 x 512 (262,144) data points. The PFM obtained topography (Figure 3.8A) looks similar to Figure 3.4A which is topography captured in contact mode, and the section analysis reveals that the average height in the stamped area is about 0.1 nm lower than the backfilled area. The dark contrast in PFM adhesion image represents low adhesion. The low adhesion area in the PFM image (Figure 3.8B) is consistent with the low friction in the friction image shown in Figure 3.4, and the low adhesion measured by FV as shown in Figure 3.5. The consistencies of the topographic images captured from PFM and CM, and the adhesion images captured from PFM and FV verified that the PFM is capable of producing reliable data from a normal patterned sample. However, the source of the horizontal bands in the PFM adhesion image remain something of a mystery. These bands occur more often when the scan size is greater than 1 μm. The reason for this occurrence could be that the tip picked up some particles during scanning, which changed its interaction with the sample surface, or that

there was a change in uniformity of the water meniscus between the tip and the surface, which alters the behavior of the cantilever.

In an analogous manner to the force volume experiment above, PFM images with smaller scan sizes were obtained inside the stamped and the backfilled regions. The scan size for these PFM images was also 100 nm and all of the experimental parameters were set to the same values as they were when capturing the 15 μm image. Figure 3.9 shows the topographic and PFM adhesion images captured within the backfilled region as well as their cross-sectional profiles. The section was performed by the dual section function provided by the Nanoscope software which allows one to examine exactly the same scan line on each of the images and to compare them on the same plot, as illustrated in the bottom part of Figure 3.9. These 100 nm images show a strong negative correlation between the topography and adhesion, i.e. high features in topography produce low adhesion. Supportive evidence can be drawn from the mirror image of the section lines where at taller topography (dashed line) the adhesion (solid line) is smaller. This is a well-known phenomenon that adhesion is directly proportional to the contact surface area. The contact area between the tip and the sample decreases when the tip scans over a tall, sharp feature, thus leading to an observed lower adhesion if the surface is homogeneous [18,20].

Figure 3.10 shows the histograms of the PFM adhesion measured inside the stamped and the backfilled areas. Notice that each of these histograms are composed of 262,144 data points, and that the data was offset by some unknown functions during output from the Nanoscope controller. In order to correct the offset adhesion, experiments to determine the unknown functions that cause the offset must be performed. This could be done by systematically correlating the PFM (Nanoscope) measured adhesion to the oscilloscope-displayed values. Unfortunately, this offset was not known at the time that these adhesion images were obtained, therefore, a reformulation of the data into raw data was not performed.

While the tip was scanning over the stamped and backfilled regions, part of the corresponding force-time curves shown on the digital oscilloscope were

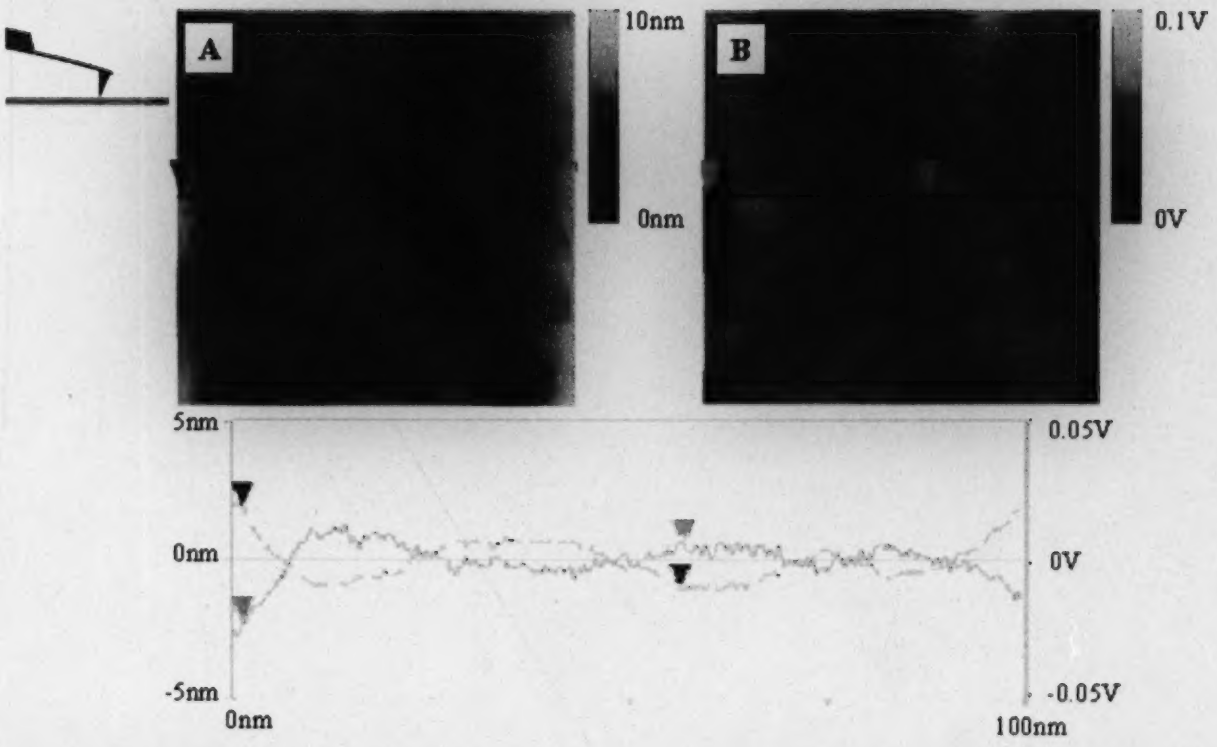

Figure 3.9. (A) Topography and (B) PFM adhesion image within the backfilled area of patterned Si chip by AFM in conventional orientation. The scan size is 100nm. The adhesion image (B) is composed of ~600,000 force measurements. Cross-sectional profiles correspond to the horizontal line shown on the topography (dashed line) and adhesion (solid line) image.

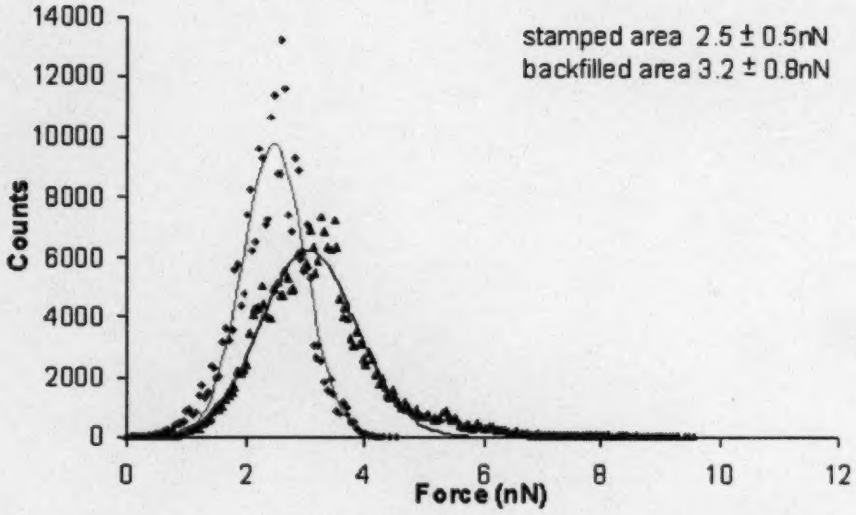

Figure 3.10. Histograms generated from PFM adhesion measurements inside modified region (diamond) and backfilled region (triangle) of the patterned Si chip. Each histogram is composed of ~600,000 force measurements. The measured average adhesion inside the modified region and the backfilled region are 2.5nN and 3.2nN, respectively.

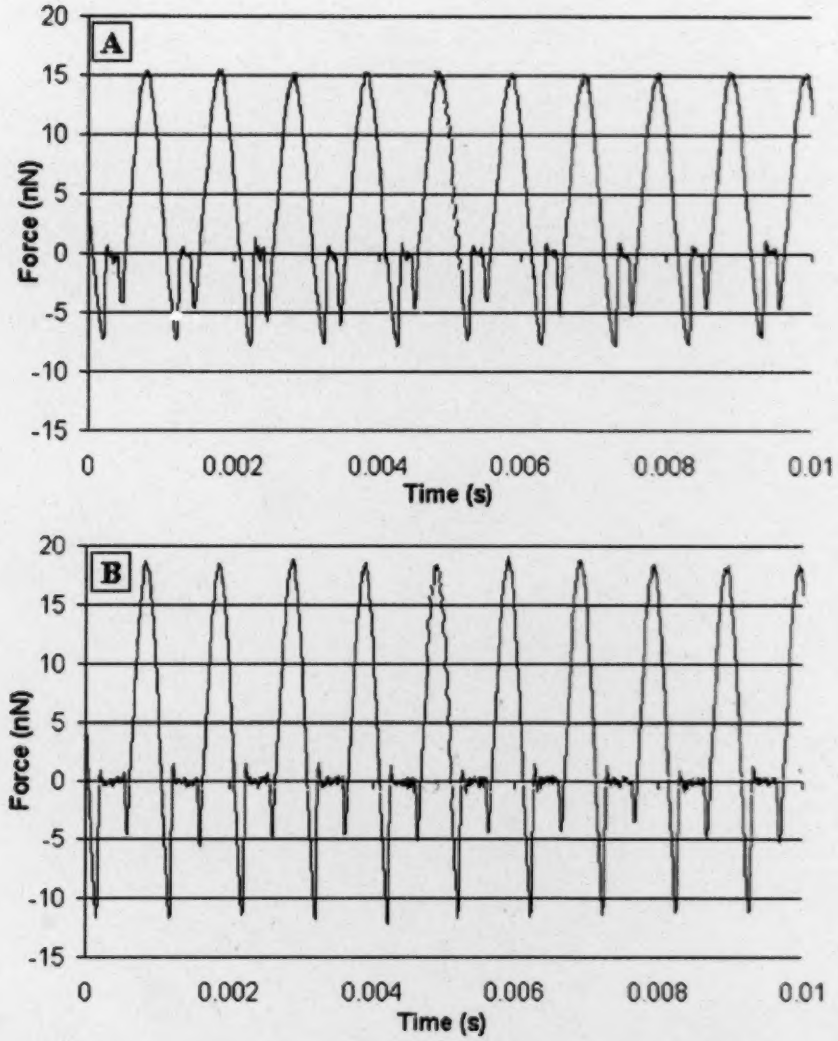

Figure 3.11. Force-time curves generated from oscilloscope during PFM adhesion measurements within 100nm scan area of the (A) modified region and (B) backfilled region of the patterned Si chip.

captured. A section of the curves is shown in Figure 3.11. There were 10,000 data points along the oscilloscope trace and 100 force-distance curves were captured within 0.1 s. Hence, each complete force-distance curve was composed of 100 data points. It is possible to capture all of the PFM force-distance curves in one complete scan, i.e., one image, in high resolution; however, this requires a device that can process extremely fast data throughput and is able to save a large amount of data. Nevertheless, such a device is not necessary in this experiment since the most useful data has already been collected by the PFM-AFM and used to generate the adhesion and topographic images.

The oscilloscope data was processed and the subsequent histograms of the force-distance curves were generated, as shown in Figure 3.12. Based on the histogram of the limited number of force-distance curves that were captured from the oscilloscope, the mean adhesions of the stamped area and the backfilled area with the unmodified Si tip were found to be 7 nN and 12 nN, respectively, and the discrepancies of these values with the ones measured in FV were 40 % and 14 %. The difference of the force volume and PFM measured adhesions could be a result of the small amount of data collected from the oscilloscope in PFM, which led to an inaccurate force representation. The difference in loading rate (the rate at which the tip jumps into contact with and detaches from the sample) could also contribute to the discrepancies [27-2829].

As the goal for this research project was to examine the plausibility of combining PFM with the inverted design of AFM to perform high-speed and high resolution force measurements, the i-AFM was set up to image the chemically modified Au-coated tipless cantilever in PFM. Verification of the μCP modified tipless cantilever was performed with FFM, and the topographic and trace friction images are shown in Figure 3.13. The friction image shown that this cantilever was heterogeneous. After the verification of the pattern, the tipless cantilever was mounted to the cantilever holder and was imaged by a substrate-supported Au-coated tip. Figure 3.14 shows the topography and PFM adhesion image of a 10 μm square within the 15 μm square shown in Figure 3.13. Note that Figure 3.14 is the mirror image of Figure 3.13 due to the inversion of the cantilever in i-AFM. A

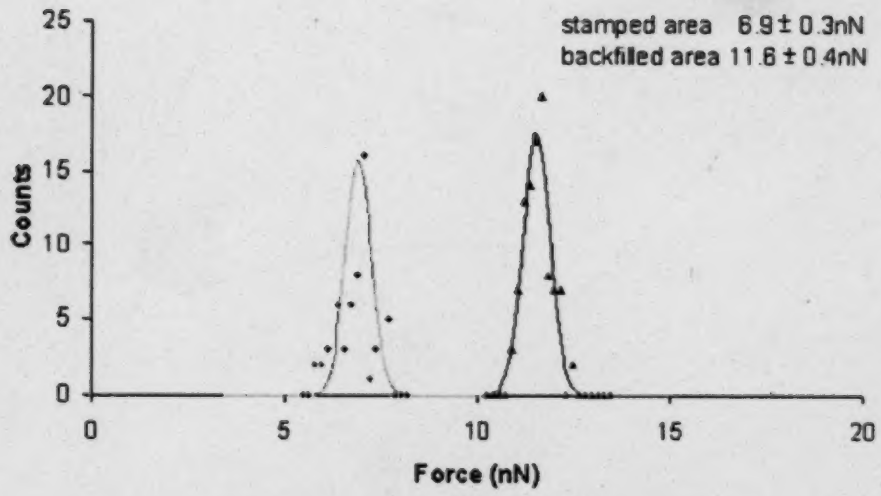

Figure 3.12. Histograms generated from oscilloscope captured PFM adhesion measurements inside modified region (diamond) and backfilled region (triangle) of the patterned Si chip. Each histogram is composed of 50 force measurements. The measured average adhesion inside the modified region and the backfilled region are 6.9nN and 11.6nN, respectively

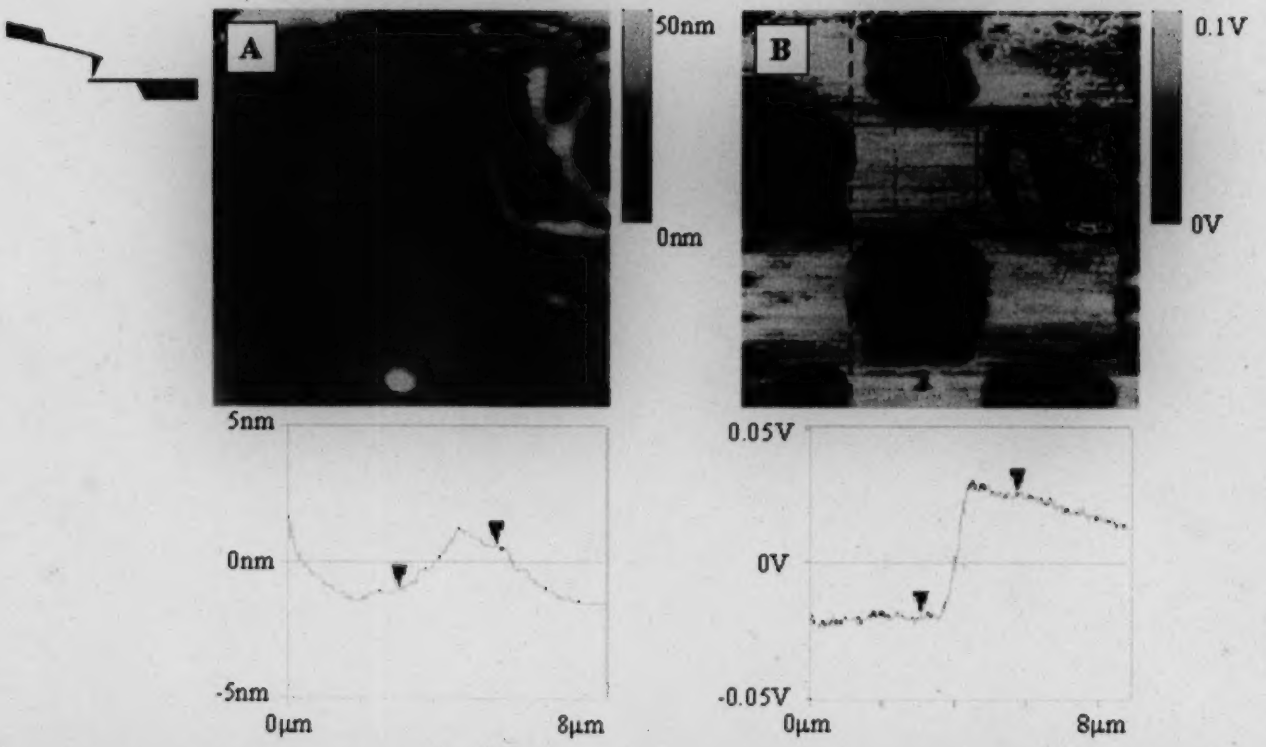

Figure 3.13. (A) Topography and (B) friction (trace) image of patterned cantilever by AFM in conventional orientation. Scan size is 15μm x 15μm. Dark contrast in (B) represents lower friction and bright contrast represents higher friction. Cross-sectional profiles correspond to the average (A) height and (B) friction calculated within the box shown in the images.difference indicate that PFM i-AFM is capable of differentiating surface compositions.

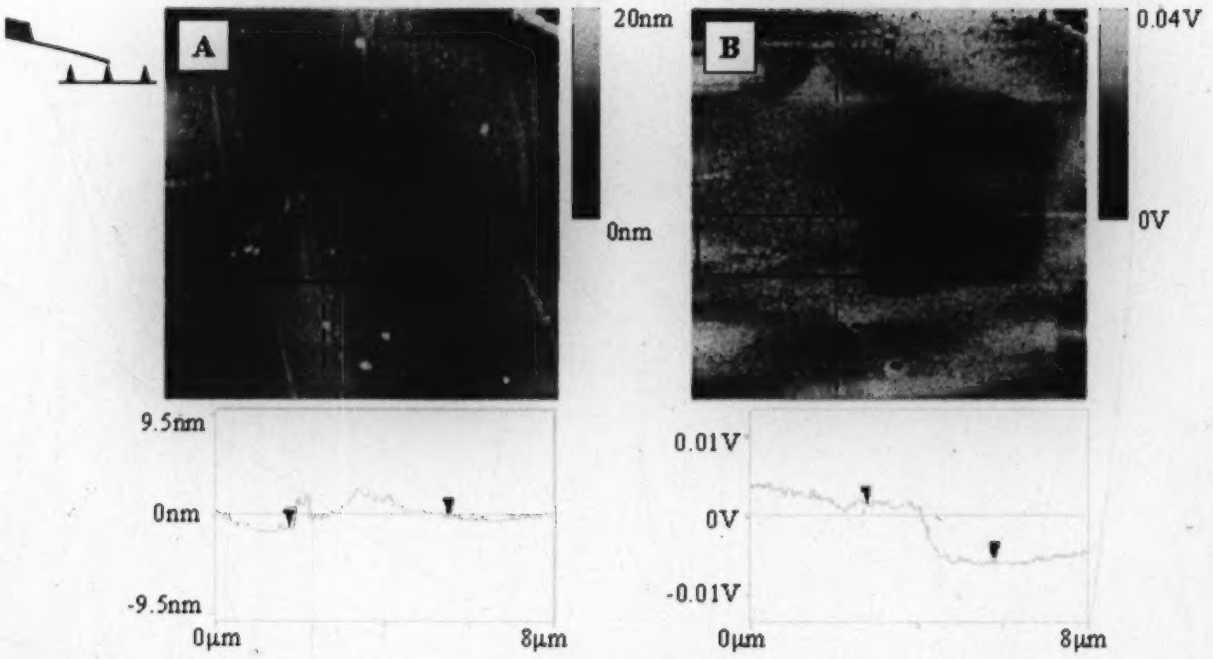

Figure 3.14. (A) Topography and (B) PFM adhesion image of patterned cantilever by AFM in inverted orientation. Scan size is 10μm x 10μm. The adhesion image is composed of ~600,000 force measurements. Dark contrast in (B) represents lower adhesion and bright contrast represents higher adhesion. Cross-sectional profiles correspond to average (A) height and (B) friction calculated within the box shown in images.

round-edge square can be seen in the adhesion image in Figure 3.14B which corresponds to the stamped region and the surrounding bright contrast corresponds to the backfilled region. Topographic effect on the PFM adhesion image can also be observed.

To further demonstrate that PFM could function in combination with the i-AFM, force measurements using a Au-coated tipless cantilever and a Au-coated tip array, both modified with MUA, were performed. The PFM adhesion was compared with the FV measured adhesion. Topography and PFM adhesion image with scan size of 1 μm are presented in Figure 3.15. Since this tipless cantilever was coated with thermally evaporated Au, the grain size of the Au atoms is larger than it is in sputtered-Au. Hence, the surface appears to be rougher than a sputtered-Au coated surface (Figure 3.14). The manufacturer specified spring constant of this cantilever was 0.65 N/m and the sensitivity of the cantilever was found to be 175 nm/V. The z-peizo oscillated at 1000 Hz with scan rate of 0.8 Hz in a 1 μm scan area with 512 x 512 data points. Therefore, the PFM adhesion image was composed of 640,000 force-distance curves. On the other hand, in FV, the resolution in the x and y plane was 16 x 16 and the FV scan rate was 0.0788 Hz, where each force-distance curve had 512 data points. That made up a FV image composed of 256 force-distance curves. The time it took to capture one PFM adhesion image and one FV image were about 11 minutes and 3.5 minutes, respectively. Although it took almost three times longer to capture the PFM image, it had 1,024 times better resolution on the x and y plane than the FV image, and the PFM adhesion map was composed of 2,500 times more force-distance curves than the FV image. Seventy curves captured in segments directly from the oscilloscope during the PFM measurement were processed and analyzed in Microsoft® Excel to generate force-distance curves (see Appendix B for a detail description for the conversion of the data to force-distance curves). Part of the curves captured from PFM and FV are shown in Figure 3.16. Since the loading rate was high (~1 kHz) in the PFM measurement, the subsequent free oscillation of the cantilever after detaching from the tip was very strong (Figure 3.16A), and this observation seemed to correlate to the magnitude of the adhesive force, i.e., a

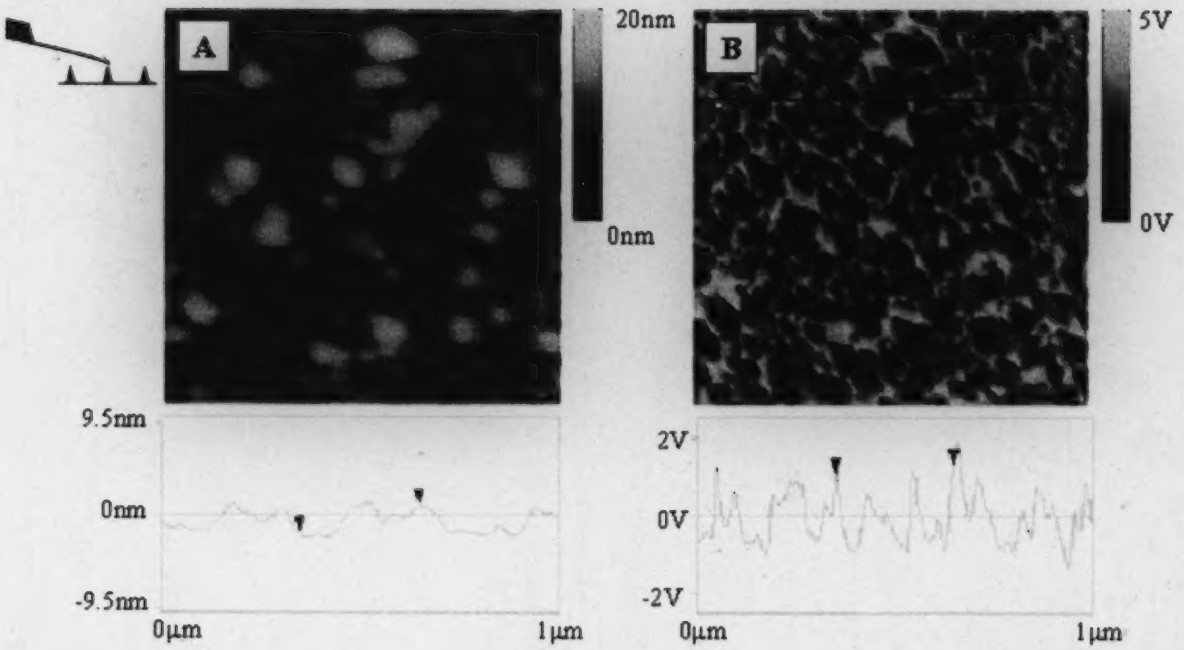

Figure 3.15. (a) Topography and (B) PFM adhesion image of modified cantilever by AFM in inverted orientation. Scan size is 1μm x 1μm. The adhesion image is composed of ~600,000 force measurements. Dark contrast in (B) represents lower adhesion and bright contrast represents higher adhesion.Cross-sectional profiles represent horizontal lines shown on images.

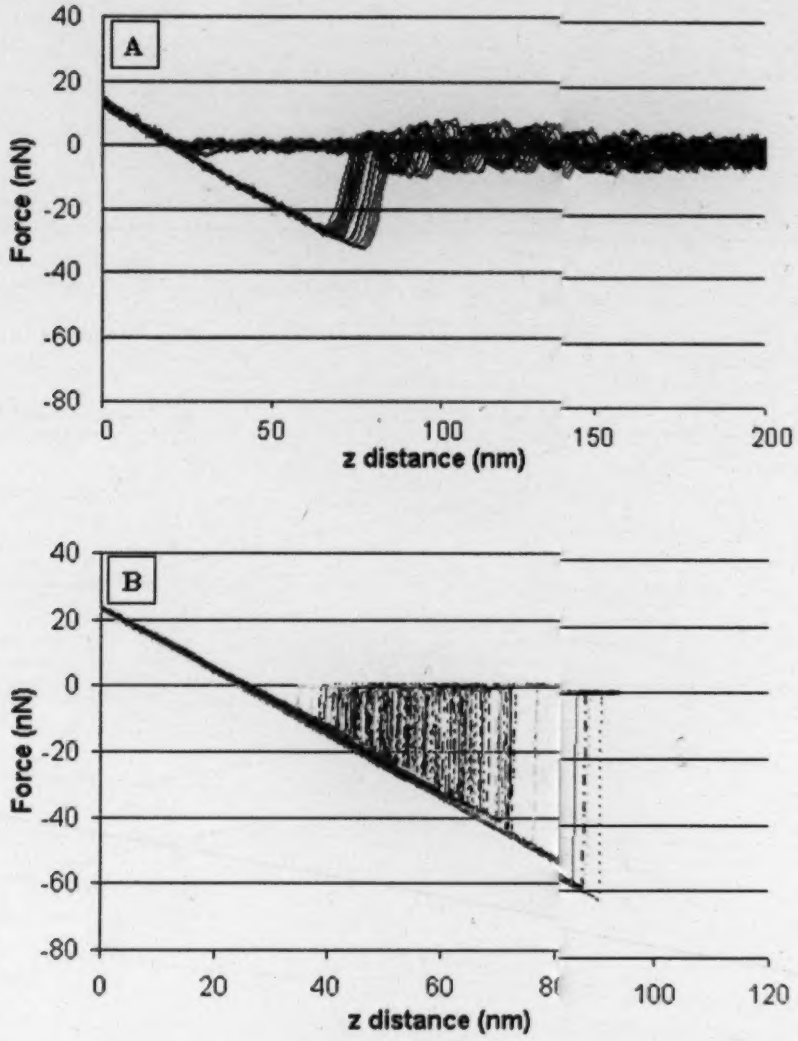

Figure 3.16. Force-distance curves generated from measurements of a modified cantilever

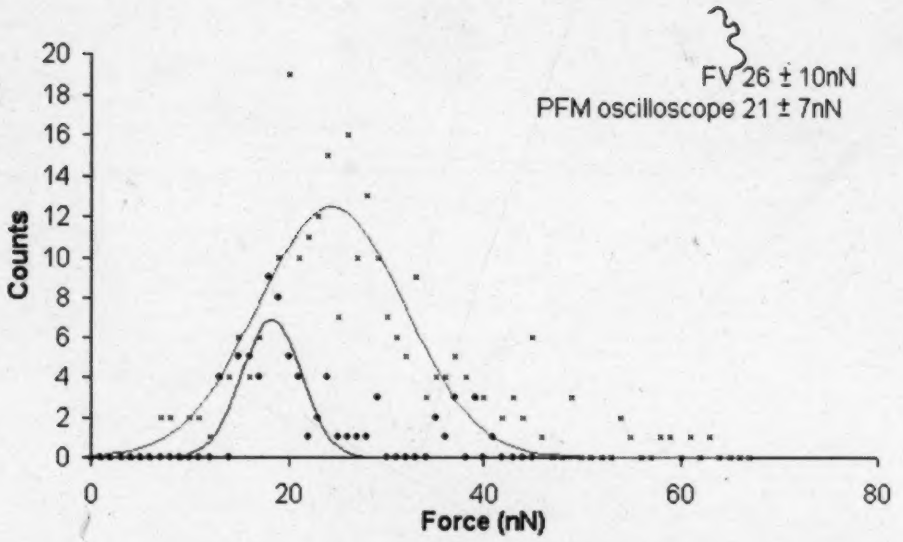

Figure 3.17. Histograms generated from FV (cross) and oscilloscope captured PFM (circle) adhesion measurements of modified cantilever by AFM in inverted orientation. FV generated histogram is composed of 256 force measurements and the PFM generated histogram is composed of 70 force measurements.

stronger adhesion between the tip and the cantilever produced a stronger oscillation. It can be seen from Figure 3.16B that the FV measured adhesion distribution is quite wide and mainly in between 10 nN to 40 nN. The histograms (Figure 3.17) show that the average adhesions for FV and PFM are 26 nN and 22 nN with the standard deviations of 10 nN and 7 nN, respectively. The average adhesions and their standard deviations measured in PFM and FV in 1 μm and 5 μm scan sizes are tabulated in Table 3.2. It is important to note that the PFM oscilloscope force-distance curves were captured in 7 random locations within the 1 μm and 5 μm scan areas. Adhesion divergence due to topographic effects could play a significant role in the measurements. Additionally, only 10 complete curves were captured in each segment which corresponded to 4 data points; thus, the PFM adhesion histogram only represents 28 data points (0.01%) of the 262,144 data points composing the image. Raw data is needed to generate accurate results; hence, it is desired to have the digital PFM and oscilloscope that can collect all the measured raw data. In spite of these problems, the results obtained in PFM and FV still showed a good agreement with each other within the standard deviation. Thus, it proves that PFMi-AFM has the ability to obtain reliable force measurements in high-speed and high lateral resolution.

3.4 Conclusion

The reliability of PFM in adhesive force measurement was studied. The results obtained from measurements of a μCP modified Au-coated Si chip using PFM and FV in conventional AFM were compared. The discrepancies of the measured adhesive forces in different modes might be due to topographic effects and different loading rates. Chemically modified tipless cantilevers and tip array were used to perform i-AFM in PFM. Adhesion data from PFM and FV operated in the inverted design were also collected and compared. The results obtained from each of these modes were consistent with one another within the standard deviations. Thus, this experiment has clearly demonstrated that it is practical to operate i-AFM in PFM. Moreover, the ability to measure accurate and precise adhesion in high-speed can be achieved by the usage of digital PFM and advanced digital oscilloscope.

	Adhesion (1μm)	Adhesion (5μm)
PFM	21.7 ± 7nN	20.3 ±14nN
FV	26.4 ± 10nN	23.4± 7nN

Table 3.2. Average adhesion measured by PFM (oscilloscope) and FV in 1μm and 5μm of modified cantilever in inverted orientation.

3.5 References

1 Rosa, A.,; Weilandt, E.; Hild, S.; Marti, O. *Meas. Sci. Technol.* **1997**, *8*, 1333.

2 Miyatani, T.; Horii, M.; Rosa, A.; Fujihira, M.; Marti, O. *Appl. Phys. Lett.* **1997**, *71*, 2632.

3 Pfrang, A.; Huttinger, J. K.; Schimmel, Th. *Surf. Interface Anal.* **2002**, *33*, 96.

4 Weisenhorn, A. L.; Maivald, P.; Butt, H-J.; Hansma, P. K.; *Phys. Rev. B* **1992**, *45*, 226.

5 Hoh, J. H.; Cleveland, J. P.; Prater, C. B.; Revel, J-P.; Hansma, P. K. *J. Am. Chem. Soc.* **1992**, *114*, 4917.

6 Radmacher, M.; Cleveland, J. P.; Fritz, M.; Hansma, H. G.; Hansma, P. K. *Biophys. J.* **1994**, *66*, 2169.

7 Radmacher, M.; Fritz, M.; Cleveland, J. P.; Walters, D. A.; Hansma, P. K. *Langmuir* **1994**, *10*, 3809.

8 Van der Werf, K. O,; Putman, C. A. J.; Groth, B. G.; Greve, J. *Appl. Phys. Lett.* **1994**, *65*, 1195.

9 Mizes, H. A.; Loh, K-G.; Miller, R. J. D,; Ahujy, S. K.; Grabowski, E. F. *Appl. Phys. Lett.* **1991**, *59*, 2901.

10 Magonov, S. N.; Elings, V. B.; Whangbo, M-H. *Surf. Sci.* **1997**, *375*, L385.

11 Whangbo, M-H.; Bar, G.; Brandsch, R. *Surf. Sci.* **1998**, *411*, L801.

12 Marti, O.; Stifter, T.; Waschipky, H.; Quintus, M.; Hild, S. *Colloid Surface* **1999**, *154*, 65.

13 Hinder, S. J.; Connell, S. D.; Davie, M. C.; Roberts, C. J.; Tendler, S. J. B.; Williams, P. M. *Langmuir* **2002**, *18*, 3151.

14 Dickson, L. E.; Berg, J. C. *J. Adhesion Sci. Technol.* **2001**, *15*, 171.

15 Zhang, H.; Grim, P. C. M.; Foubert, P.; Vosch, T.; Vanoppen, P.; Wiesler, U.-M.; Berresheim, A. J.; Mullen, K.; De Schryver, F. C. *Langmuir* **2000**, *16*, 9009.

16 Miyatani, T.; Okamoto, S.; Rosa, A.; Marti, O.; Fujihira, M. *Appl. Phys. A* **1998**, *66*, S349.

17 Okabe, Y.; Furugori, M.; Tani, Y.; Akiba, U. Fujihira, M. *Ultramicroscopy* **2000**, *82*, 203.

18 Okabe, Y. Akiba, U. Fujihira, M. *Applied Surface Science* **2000**, *157*, 398.

19 Fujihira, M.; Tani, Y.; Furugori, M.; Akiba, U.; Okabe, Y. *Ultramicroscopy* **2001**, *86*, 67.

20 Sato, F.; Okui, H.; Akiba, U.; Suga, K.; Fujihira, M. *Ultramicroscopy* **2003**, *97*, 303.

21 Kwak, K. J.; Kudo, H.; Fijihira, M *Ultramicroscopy* **2003**, *97*, 249.

22 Kwak, K. J.; Kudo, H.; Yoda, S.; Fijihira, M *Ultramicroscopy* **2004**, *100*, 179.

23 Akimoto, K.; Sato, F.; Morikawa, T.; Fujihira, M. *Jpn. Appl. Phys. 1* **2004**, *43*, 4492.

24 Green, J.-B. D.; Novoradovsky, A.; Park, D.; Lee, G. U. *Appl. Phys. Lett.* **1999**, *74*, 10.

25 Krotil, H.-U.; Stifter, T.; Waschipky, H; Klaus, W.; Hild, S; Marti, O. *Surf. Interface Anal.* **1999**, *27*, 336.

26 Mabry, J. C.; Yau, T.; Yap, H.-W.; Green, J.-B. ultramicroscopy 2002, 91, 73.

27 Grandbois, M.; Beyer, M.; Rief, M.; Clausen-Schaumann, H.; Gaub, H. E. *Science* **1999**, *283*, 1727.

28 Lo, Y.-S.; Zhu, Y.-J.; Beebe, Jr. T. P. *Langmuir* **2001**, *17*, 3741.

29 Evans, E. *Annu. Rev. Biophys. Biomol. Struct.* **2001**, *30*, 105.

CHAPTER 4

CONCLUSIONS AND FUTURE

4.1 Conclusions

The experimental results presented in the preceding chapters have demonstrated that the hypotheses stated in the beginning of this thesis are valid. Various types of surface characterization techniques were mentioned and used. DPN and μCP modified surfaces were verified by frictional force microscopy (FFM) [1]. Surface properties such as inhomogeneity of material, chemical composition and topography lead to the lateral deflection of a cantilever in contact mode (CM) atomic force microscopy (AFM) [2]; thus, producing friction images.

Phase imaging in tapping mode (TM) [3] on the modified surface was performed in both conventional and inverted AFM. Inverted AFM (i-AFM) [4] is a newly developed technique where a cantilever-supported sample is probed by one of thousands substrate-supported tips. Agreement of the phase imaging results obtained by conventional AFM and i-AFM proved that i-AFM is able to operate in TM. The power to resolve topography and surface inhomogeneity in conventional TM-AFM can also be applied to iTM-AFM.

Reduction of the amplitude of an oscillating cantilever as far as 20 μm above the substrate-supported tip was observed in the iTM-AFM experiment. The magnitude of the amplitude reduction increases when the tip height decreases and the cantilever-tip distance decreases. Fitting over the experimental force-distance curve with equation (2.7) showed that the amplitude is proportional to the separation between the tip and the cantilever to the power of one and a half, while the theory of squeeze-film damping [5-8] states that the amplitude is proportional to the third power of the separation. This discrepancy indicated that the observed damping of the cantilever was not due to the squeeze-film damping, and we believed that it was atmosphere-related. Increasing the tip height by fabrication of taller tips or modifying the existence tips could most likely avoid or at least minimize the damping effect.

The capability of pulsed-force mode (PFM) [9-,12] to perform high-speed force measurement with high lateral resolution while simultaneously collecting topographical data was demonstrated in chapter 3. The periodic contact and detachment between the tip and the sample at high frequency, i.e. 1 kHz, allowed a 15 μm adhesion image, composed of ~600,000 force curves and 512 x 512 points, be captured within 10 minutes (Figure 3.8). More than 70 minutes were required to image the same location with lateral resolution of 64 x 64 points and 64 force curves (Figure 3.5) in force volume (FV) measurements [13-15]. Force measurements from the PFM and FV in the i-AFM design were also performed. Adhesion data acquired between chemically modified cantilevers and tip array in PFM and FV (Table 3.2) shows a consistency with one another within error. In this experiment, we have shown that PFM could be combined with i-AFM to obtain topography and adhesion measurements. Use of digital PFM for force measurement is considered to be superior as the most useful raw data can be collected and stored, and in turn provide more accurate and precise results.

4.2 Future Prospects

The benefit of having multiple tip selection and the possibility to modify each of the tip with different chemistries or biomolecules in i-AFM makes this technique a powerful surface characterization tool. Since i-AFM is still in its early stage of development, it needs to go through a long way of method development and optimization. We have demonstrated that i-AFM was functional in TM, FV and PFM, and the work presenting i-AFM operating in CM has been published [16]. Studies on operating i-AFM in all of the modes mentioned above in fluids will be useful since much of the interest is focused on cell-cell and cell-drug interactions nowadays. Being able to conduct measurements in physiological condition is definitely an advantage. Besides, a well-controlled, contamination-free and high reproductive surface modification method on micro scale surface, i.e. tipless cantilever, needs to be developed. Currently, some the members in our group are studying the plausibility of applying DPN on i-AFM in CM and TM. Advanced robotic spotting technology [17] is employed to modify tips on tip arrays, with different chemistries, which are then used to "write" on tipless

cantilever. If the optimal conditions for this surface modification technique are well understood then the cantilever and tips on tip array can be modified with thousands of different kinds of chemistries and\or biomolecules, and thousands combinations of interactions can be measured. Furthermore, chemical identification techniques such as spectroscopy may be combined with the i-AFM to improve the validity of force measurements.

4.3 References

1 Mate, C.M; McClelland, G. M.; Erlandsson, R.; Chiang, S. *Phys. Rev. Lett.* **1987**, *59*, 1942.

2 Binnig, G.; Quate, C. F.; Gerber, C. *Phys. Rev. Lett.* **1986**, *56*, 930.

3 Zhong, Q.; Inniss, D.; Kjoller, K.; Elings, V. B. *Surf. Sci.* **1993**, *290*, L688.

4 Green, J.-B. D.; Novoradovsky, A.; Park, D.; Lee, G. U. *Appl. Phys. Lett.* **1999**, *74*, 10.

5 Sherry, F. M.; Neuzil, P.; Viasuso, R.; Maclay, G. J. *Electrochem. Soc. Pro.* **1995**, *83*, 95.

6 Cleveland, J. P.; Anczykowski, B.; Schmid, A.E.; Elings, V. B. *Appl. Phys. Lett.* **1998**, *72*, 2613.

7 Andrews, M.; Harris, I.; Turner, G. *Sensor Actuat. A-Phys.* **1993**, *36*, 79.

8 Nnebe, I.; Schneider, W. *Langmuir* **2004**, *20*, 3195.

9 Rosa, A,; Weilandt, E.; Hild, S.; Marti, O. *Meas. Sci. Technol.* **1997**, *8*, 1.

10 Miyatani, T.; Horii, M.; Rosa, A.; Fujihira, M.; Marti, O. *Appl. Phys. Lett.* **1997**, *71*, 2632.

11 Hild, S.; Rosa, A.; Volswinkler, V.; Marti, O. *Bull. Mic. Soc. Can.* **1998**, *26*, 24.

12 Stifter, T.; Weilandt, E.; Marti, O.; Hild, S. *Appl. Phys. A* **1998**, *66*, 597.

13 Mizes, H. A.; Loh, K-G.; Miller, R. J. D,; Ahujy, S. K.; Grabowski, E. F. *Appl. Phys. Lett.* **1991**, *59*, 2901.

14 Radmacher, M.; Fritz, M.; Cleveland, J. P.; Walters, D. A.; Hansma, P. K. *Langmuir* **1994**, *10*, 3809.

15 Van der Werf, K. O,; Putman, C. A. J.; Groth, B. G.; Greve, J. *Appl. Phys. Lett.* **1994**, *65*, 1195.

16 Mabry, J. C.; Yau, T.; Yap, H. W.; Green, J. B. D. *Ultramicroscopy* **2002**, *91*, 73.

17 Zubritsky, E. *Anal. Chem.* **2000**, *72*, 761A.

Appendix A

Automate 5 Professional macro for amplitude-distance experiment (section 2.2.8)

```
1.  <AMLOOP TOTALLOOPS="20">
2.  <AMWINDOWFOCUS WINDOWTITLE="NanoScope Control">
3.  <AMSENDKEY>{ALT}ms</AMSENDKEY>
4.  <AMSENDKEY>{TAB}{TAB}{ENTER}</AMSENDKEY>
5.  <AMPAUSE SCALAR="1">
6.  <AMSENDKEY>{TAB}{TAB}{TAB}{ENTER}</AMSENDKEY>
7.  <AMPAUSE SCALAR="1">
8.  <AMSENDKEY>{CTRL}c</AMSENDKEY>
9.  <AMPAUSE SCALAR="1">
10. </AMLOOP>
```

1. Loop the following steps 20 times
2. Focus window "Nanoscope Control"
3. Click on step motor
4. Click "tip up", where the step is pre-set to 3.95um
5. Pause for 1sec
6. Close the step motor window
7. Pause for 1sec
8. Click capture
9. Pause for 1 sec
10. Endloop

Appendix B

Conversion of cantilever deflection from volts to newtons

Conversion of cantilever deflection (volts) vs. time curve captured from oscilloscope in PFM adhesion measurement into force vs. distance curve.

1. Plot cantilever deflection (volts) vs. time
2. Insert a wave function into the plot

   $f(t) = A\cos[2\pi(\omega t) + \phi]$, where

   A = coefficient relating the calculated distance to actual distance travel by z-piezo

   ω = true z-piezo oscillation frequency

   t = time at each data point

   ϕ = phase shift of the calculated wave function
3. Adjust ω and ϕ so that the calculated wave function is in phase with the oscilloscope captured PFM adhesion curve
4. Convert the cantilever deflection signal from volts into force using the following equation

   $F = V \times S \times k$, where

   V = raw voltage

   k = cantilever spring constant

   S = sensitivity obtained from oscilloscope trace captured during FV measurement. Since the distance traveled by the tip is known in FV, sensitivity of the cantilever can be calculated from the slope of the retract force curve
5. Plot force vs. calculated wave function and adjust A so that the slope at the contact regime is equal to 1.